Nanoscale Advances

REVIEW

View Article Online
View Journal | View Issue

Cite this: *Nanoscale Adv.*, 2020, **2**, 70

Progress in supercapacitors: roles of two dimensional nanotubular materials

Pritam Kumar Panda, [a] Anton Grigoriev, [a] Yogendra Kumar Mishra [b] and Rajeev Ahuja *[c]

Received 16th May 2019
Accepted 28th October 2019

DOI: 10.1039/c9na00307j

rsc.li/nanoscale-advances

Overcoming the global energy crisis due to vast economic expansion with the advent of human reliance on energy-consuming labor-saving devices necessitates the demand for next-generation technologies in the form of cleaner energy storage devices. The technology accelerates with the pace of developing energy storage devices to meet the requirements wherever an unanticipated burst of power is indeed needed in a very short time. Supercapacitors are predicted to be future power vehicles because they promise faster charging times and do not rely on rare elements such as lithium. At the same time, they are key nanoscale device elements for high-frequency noise filtering with the capability of storing and releasing energy by electrostatic interactions between the ions in the electrolyte and the charge accumulated at the active electrode during the charge/discharge process. There have been several developments to

[a]*Department of Physics and Astronomy, Uppsala University, Box 516, SE-75120, Uppsala, Sweden. E-mail: rajeev.ahuja@physics.uu.se*
[b]*Mads Clausen Institute, NanoSYD, University of Southern Denmark, Alsion 2, DK-6400, Denmark. E-mail: mishra@mci.sdu.dk*
[c]*Department of Materials and Engineering, Royal Institute of Technology (KTH), SE-10044, Stockholm, Sweden*

Pritam Kumar Panda is pursuing a Ph.D. in the Department of Physics and Astronomy, Uppsala University, Sweden under the supervision of Prof. Rajeev Ahuja and Priv.-Doz. Dr habil. Yogendra Kumar Mishra from Mads Clausen Institute, NanoSYD, University of Southern Denmark, Sønderborg, Denmark. He has a double Master's in Bioinformatics from Utkal University & D.Y. Patil University in 2014 and 2016 respectively. He has worked as a junior research fellow in the Infection Biology lab, KIIT University, India and later joined as a graduate scientist in the Division of Pediatric Haematology and Oncology, University of Freiburg, Germany. He has published more than 30 papers including many in top ranked journals, such as Leukemia (Nature), Nanomedicine, Scientific Reports (Nature), Toxicological Sciences, Materials Science and Engineering C, Gut Pathogens (BMC), etc. and also serves as a referee for various reputed journals. His expertise includes bioinformatics, computational biology, biophysics, 2D material modelling of electron transport in nanoscale devices, and computational modelling of bio-nanoparticles. His primary topic of research is computational modelling of 2D materials for biosensing applications.

Dr Anton Grigoriev is a researcher and member of the Condensed Matter Theory group (CMT) and Uppsala University UniMolecular Electronics Centre (U3MEC). His primary research area focuses on surface physics, surface chemistry and electron transport properties of nanosystems. He uses computer simulations to study surface structures, for understanding molecular adsorption and intermolecular interactions. The major application area considered is molecular electronics. He is an expert in modelling of electron transport in metal–molecule–metal systems.

increase the functionality of electrodes or finding a new electrolyte for higher energy density, but this field is still open to witness the developments in reliable materials-based energy technologies. Nanoscale materials have emerged as promising candidates for the electrode choice, especially in 2D sheet and folded tubular network forms. Due to their unique hierarchical architecture, excellent electrical and mechanical properties, and high specific surface area, nanotubular networks have been widely investigated as efficient electrode materials in supercapacitors, while maintaining their inherent characteristics of high power and long cycling life. In this review, we briefly present the evolution, classification, functionality, and application of supercapacitors from the viewpoint of nanostructured materials to apprehend the mechanism and construction of advanced supercapacitors for next-generation storage devices.

Introduction

State-of-the-art technology has revolutionized the energy industry on a large scale and has led to many discoveries thereafter. A lot has been achieved in this direction, although achieving longer cycle life and high energy density is still a challenge. A primary challenge in this scientific era has been imposed by us (human population) due to high energy consumption and a high pollution generation rate to reduce the energy consumption that led many researchers to develop efficient supercapacitors. The key issues, *e.g.*, high production cost, low energy density, and short cycle life, have been the major concerns in the supercapacitor industry to date and to overcome these aforementioned problems, various critical approaches have been explored as follows: (a) developing aqueous electrolytes to reduce high cost, (b) hybrid supercapacitor, solid-state supercapacitor and nonporous electrode materials production to overcome the low energy density problem, and (c) introduction of novel electrode materials (ionic liquids) to overcome the problem of short cycle life. Above all, the understanding of fundamental and basic science, *e.g.*, surface chemistry, dielectric properties, and materials properties, may help overcome the major challenges and the vision of achieving low-cost production, high energy density, longer cycle

Yogendra Kumar Mishra is a professor with special responsibilities in nanomaterials at Mads Clausen Institute, NanoSYD, University of Southern Denmark, Sønderborg, Denmark. Prior to moving Denmark, he was leading a scientifically independent group (2011–2019) and Alexander von Humboldt Fellow (2009–2011) at Functional Nanomaterials Chair, Institute for Material Science, Kiel University, Kiel, Germany. In Kiel, he introduced a new fabrication technique, the "Flame Transport Synthesis FTS Approach", allowing versatile nanostructuring of metal oxides and their 3D interconnected networks as "Flexible Ceramics". The developed tetrapodal 3D shaped ZnO nanostructures by him found many applications in engineering and biomedical fields. The sacrificial nature of ZnO tetrapods enables them to be used as templates for the growth of various new materials (inorganic, organic, polymer, ZIFs, MOFs, etc.) which offered a wide range of multifunctional applications. He has published more than 150 papers (total citations >6200; H index of 44) including many in top-ranked journals, such as Materials Today, Advanced Materials, Nature Communications, Advanced Functional Materials, Nanoscale, and many others. He is an editorial board member for several journals, e.g., Scientific Reports (Nature), Materials Today Chemistry, Nanomaterials, etc. and also serves as a referee for various prestigious journals, funding agencies, faculty promotions, etc. At NanoSYD, his main research focus is Hybrid and Smart 3D Materials for Sustainable Technologies.

Rajeev Ahuja is a full time Professor in the Department of physics and astronomy at Uppsala University, Sweden, and heads a research group of 17 theoretical physicists. He is one of the most highly cited researchers in Sweden. In his research career, he has supervised 30 graduate students and 35 postdoctoral research associates. At present he has a group of 12 people, which include 5 PhD students and 5 post-doctoral fellows. He has published over 825 papers (citations more than 30000; H-index 80) in his research career in leading international journals. Ahuja has been awarded the Wallmark prize for 2011 by the Royal Swedish Academy of Sciences, Stockholm. This award is presented to young scientists by the King of Sweden. He has been awarded the Beller Lectureship for the APS March Meeting, 13–17 March 2017, in New Orleans, Louisiana. Ahuja is a member of the Royal Research Society, Uppsala and is on the executive board of the European High-Pressure Research Group (EHPRG). He is the editor in chief of Cogent Physics (Taylor & Francis Group) and an editorial board member at Nature Scientific Reports.

life, and high efficiency can be fulfilled. Over the past three decades, intensive research has been carried out to meet the demand for next-generation technologies to overcome the global energy crisis with the advent of human reliance on energy-consuming labor-saving devices in which supercapacitors play a pivotal role. They have been known for many decades under colloquial terms, *e.g.*, "supercapacitors", "double-layer capacitors, "ultracapacitors", "power capacitors", "gold capacitors", "power cache" *etc.* and it's still a very rapidly emerging topic with the hope to fulfill the criteria of energy storage and hence avert future energy crises.[1] In the early 1950s, the design of fuel cells and rechargeable batteries came into action with the usage of carbon electrodes with a high specific surface area and thus the era of designing capacitors to achieve high energy storage was initiated. A low voltage electrolytic capacitor with porous carbon electrodes was developed by H. Becker in 1957, which led to the design of a capacitor with high capacitance.[2] Extending the concept of Becker, in the period of 1966–1970, Standard Oil (Ohio) developed electrical energy storage apparatus which was further documented by Donald L. Boos in 1970 as an electrolytic capacitor with activated carbon electrodes. In 1971, SOHIO did not commercialize their invention rather they licensed their technology to a Japanese multinational information technology and electronics company that finally marketed "Supercapacitors" with the purpose to provide backup power for computer memory. The actual term "supercapacitor" was introduced by Brian Evans Conway in 1999 illustrating fundamental experiments on ruthenium oxide electrochemical capacitors to explain the increased capacitance due to surface redox reactions with faradaic charge transfer between electrodes and ions ultimately leading to increased electrochemical energy storage.[3,4] The evolution of supercapacitors caused a boost in power applications that led to the introduction of "ultracapacitors" in 1992 by Maxwell laboratories which further concentrated on the increase in the electrolyte's breakdown voltage. In 1994, an "Electrolytic-Hybrid Electrochemical Capacitor" was introduced by David A. Evans which combined a high dielectric strength anode with a high pseudo-capacitance metal oxide cathode yielding a hybrid capacitor. Eventually the previous developments led to the emergence of lithium-ion capacitors in 2007, which took the industry to the next level in terms of power storage and applications. The phase of 1957–2007 has marked the evolution of supercapacitors in a drastic manner but they have some limitations, for instance, high production cost, low energy density and short cycle life (Fig. 1). Several projects were initiated after the introduction of lithium-ion supercapacitors that offered the highest gravimetric specific energy (15 W h kg^{-1}, 54 kJ kg^{-1}). Their limitations were greater than their advantages up to 2013, but the focus has been on improving specific energy, reducing internal resistance, increasing lifetimes and reducing costs.[5] Graphene[6] based supercapacitors were introduced in 2010 by Belle Dumé; more specifically, curved graphene sheets that could store high energy with a specific charge density of 85.6 W h kg^{-1} at room temperature and 136 W h kg^{-1} at 80 °C.[6] The technology marked the beginning of the developmental phase of supercapacitors that are comparable to nickel-metal hydride batteries . Researchers around the world have made strides in improving the specific capacitance of graphene-based supercapacitor electrodes but they have some major drawbacks in terms of capacitance which did not meet the criteria of the theoretical capacitance of 550 F g^{-1} despite the high specific surface area of single-layered graphene sheets (~3000 m^2 g^{-1}).[7]

Several modifications have been made towards improving the specific capacitance, longer cycle life, and particular materials used for electrodes and electrolytes. The discovery of carbon-based supercapacitors by the activation of graphene marked the progress of supercapacitors in energy technology and introduced new materials for use as electrode materials to achieve high energy density, high charge density, higher surface area, longer cycle life, and high capacitance.[8] Table 1 demonstrates the developments made thereafter by the introduction of carbon-based supercapacitors.

Taxonomic classification

A typical Ragone plot[9] (Fig. 3(a)) shows that supercapacitors play a pivotal role in bridging the gap between traditional capacitors and batteries and occupy a prominent position in developing energy storage devices. Despite intensive research in energy storage mechanisms, lithium battery technologies are still lagging behind the increasingly punitive performance stipulated by industries. To overcome this problem supercapacitors have been widely used extensively, ranging from portable devices to industrial power and energy applications to induce a long-overdue change towards a sustainable generation, management and consumption of energy without relying explicitly on renewable resources. The combination of high specific energy with high power density demands specific energy storage mechanisms in which supercapacitors are best in the aspects of performance and delivery from small scale energy consumption to industrial scale. The taxonomy of supercapacitors' broad classification based on electrolytes, materials, and configurations draws significant attention in terms of energy storage capacity and their application,[10] as shown in Fig. 2.

Further divisions in electrolytes consist of organic, aqueous and ionic liquids in which a longer cycle life can be achieved in the order of ionic liquids ≫ aqueous ≫ organic in terms of high potential difference, high specific energy, and maximum power density.[11–21] Materials-based supercapacitors are subdivided into electric double-layer capacitors (EDLCs), pseudocapacitors, and hybrid capacitors.[22] The unique storage mechanism of the materials based classification involves two significant concepts mainly; one utilizes the charge transfer concept between electrodes and electrolytes (faradaic) and the other is without any chemical reaction/mechanism (non-faradaic).[23] Material-based subdivisions and mechanisms are listed in Fig. 2 and Table 2. As far as the configurations are concerned, the classification is based on the type of symmetry, *e.g.*, symmetric (two equal electrodes), asymmetric (two different electrodes with the same mechanism) and hybrid (two different electrodes and different mechanisms) among which to achieve better

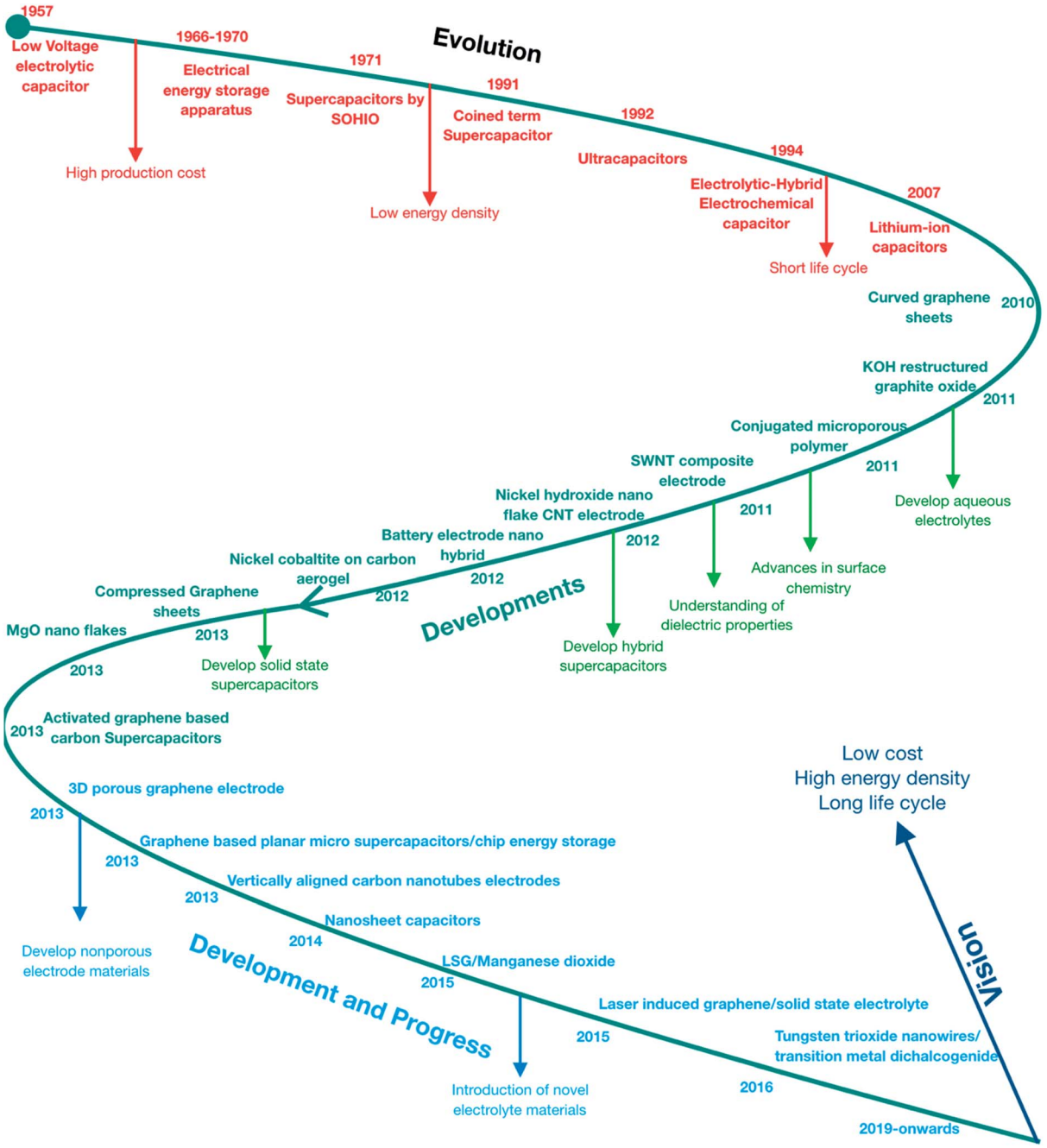

Fig. 1 Roadmap of the evolution, progress, and developments in supercapacitors.

efficiency, hybrid-based supercapacitors are mainly used nowadays.[24,25]

They are preferred because of their improved performance in energy density without altering the power density , which delivers higher specific capacitance due to their asymmetric behaviour.[26] The asymmetric behavior of hybrid-supercapacitors gives enhanced characteristics such as intrinsic shell area, atomic charge partition length, rapid and repeatable redox reactions, *etc.*, which has the combined characteristics of both EDLC and pseudocapacitors respectively.[25,27–29] Fig. 3(b) shows the specific power–energy plot illustrating the storage capacity of asymmetrical capacitors occupying the specific region with an aqueous electrolyte, compared to other power devices such as EDLCs, conventional capacitors, asymmetric capacitors with organic electrolytes, and fuel cells. They have been proven to be one of the best energy storage devices in terms of specific power which is 100 times higher than that of batteries. In Fig. 3(c), out of all the conventional supercapacitors, hybrid-based supercapacitors exhibit an attainable performance focusing on characteristic features as shown in the plot. There has been less exploration of hybrid supercapacitors compared to the other two types, and researchers hypothesize that they may

Table 1 Developmental progress of supercapacitors after 2010

Year	Material	Development	Specific energy	Capacitance	Cycles	Specific power
2011	Potassium hydroxide[434]	Restructured-graphite oxide	85 W h kg^{-1}	200 F g^{-1}	>10 000	
2011	Aza-fused-π-conjugated microporous[435]	Conjugated microporous polymer	53 W h kg^{-1}	270 F g^{-1}	10 000	
2011	Single-walled-carbon nanohorn/ nanotube composite[436]	Composite electrode				990 W kg^{-1}
2012	Nickel hydroxide[437]	Nanoflake-CNT composite electrode	50.6 W h kg^{-1}	3300 F g^{-1}	—	—
2012	$Li_4Ti_5O_{12}$ (LTO)[438]	Battery-electrode nanohybrid	40 W h l^{-1}		10 000	7.5 W l^{-1}
2012	Nickel cobaltite[439]	Carbon-aerogels composites	53 W h kg^{-1}	1700 F g^{-1}		2.25 W kg^{-1}
2013	Graphene sheets[440]	Liquid-mediated transport network	60 W h l^{-1}			
2013	Activated graphene[210]	Macro- and meso-porous electrodes	74 W h kg^{-1}			
2013	Na_xMnO_2 (ref. 441)	Nanoflakes	110 W h kg^{-1}	1000 F g^{-1}		
2013	Graphene electrodes[442]	3D porous graphene electrodes	98 W h kg^{-1}	231 F g^{-1}		
2013	Graphene[443]	Chip-based energy storage	2.42 W h l^{-1}			
2013	Carbon nanotubes[444]	Vertically aligned CNTs	13.50 W h kg^{-1}		300 000	37.12 W g^{-1}
2014	$Ru_{0.95}O_2^{0.2-}/Ca_2Nb_3O_{10}^{-}/Ru_{0.95}O_2^{0.2-}$ nanosheet ultrathin capacitors[445]	Room temperature solution-based capacitors		27.5 μF cm^{-2}		
2015	Laser-scribed graphene/MnO_2 (ref. 446)	Hybrid capacitor	42 W h l^{-1}		10 000	10 kW l^{-1}
2015	Graphene[447]	Flexible and stackable laser-induced supercapacitors		9 mF cm^{-2}		0.02 mA cm^{-2}
2016	WO_3/2D WS_2 layers[448]	Transition-metal dichalcogenides	100 W h l^{-1}		30 000	1 kW l^{-1}

outperform the most promising class of supercapacitors available today in the near future and further developments have continued in order to tune the design and flexibility[22] which is discussed further.

The merging of battery type faradaic or pseudocapacitive electrodes with a capacitive electrochemical double layer (EDL) electrode gives rise to hybrid supercapacitors that allow a reinforcing combination of properties of different components synergetically.[30] This combination can reinforce the need for charge storage mechanisms in order to improve the overall performance. In consideration of the combinatorial strategy to develop hybrid supercapacitors, an optimal configuration is thus required for the mixing approach (composite electrodes). The mixing approach denotes the use of different electrodes in appropriate proportions concerning relative concentrations and particle sizes as are necessary for percolation paths keeping their chemical nature, crystal structure, and physiochemical properties stable. A growing number of hybrid materials for electrodes have been developed with improved power and energy densities. One such study by Dubal *et al.*[30] proposed hybrid combinations of electroactive and conductive materials including a wide variety of inorganic species from oxides to polyoxometalate clusters, conducting organic materials and carbon-based electrodes, as depicted in Fig. 3(d). Also they provided a list of cathode and anode electrode materials used to optimize the performance, *e.g.*, for the cathode, $Li_{1-x}Ni_{1-y-z}Co_yM_zO_4$, $Li_xMn_2O_4$, $LiMnO_2$, MnO_2, V_2O_5, LiV_3O_8, $Li_{1-x}VOPO_4$, and Li_xFePO_4 specifically focusing on Li_xFePO_4 and for the anode, a wide variety of materials as well as approaches have been investigated from lithium metal to graphite and carbons to alloys and recently metal nanocomposites have attracted great interest, of which core–shell $LiMnPO_4$–$LiFePO_4$ nanoparticles are an interesting example of hybrid supercapacitors. Revisiting all the materials aforementioned is beyond the scope of this review. However, in this review we will discuss some major advancements in two-dimensional nanotubular material based hybrid supercapacitors.

Fig. 2 An overview of the taxonomical classification of supercapacitors. The lightning bolt symbol represents energy and the cylindrical stack represents the storage.

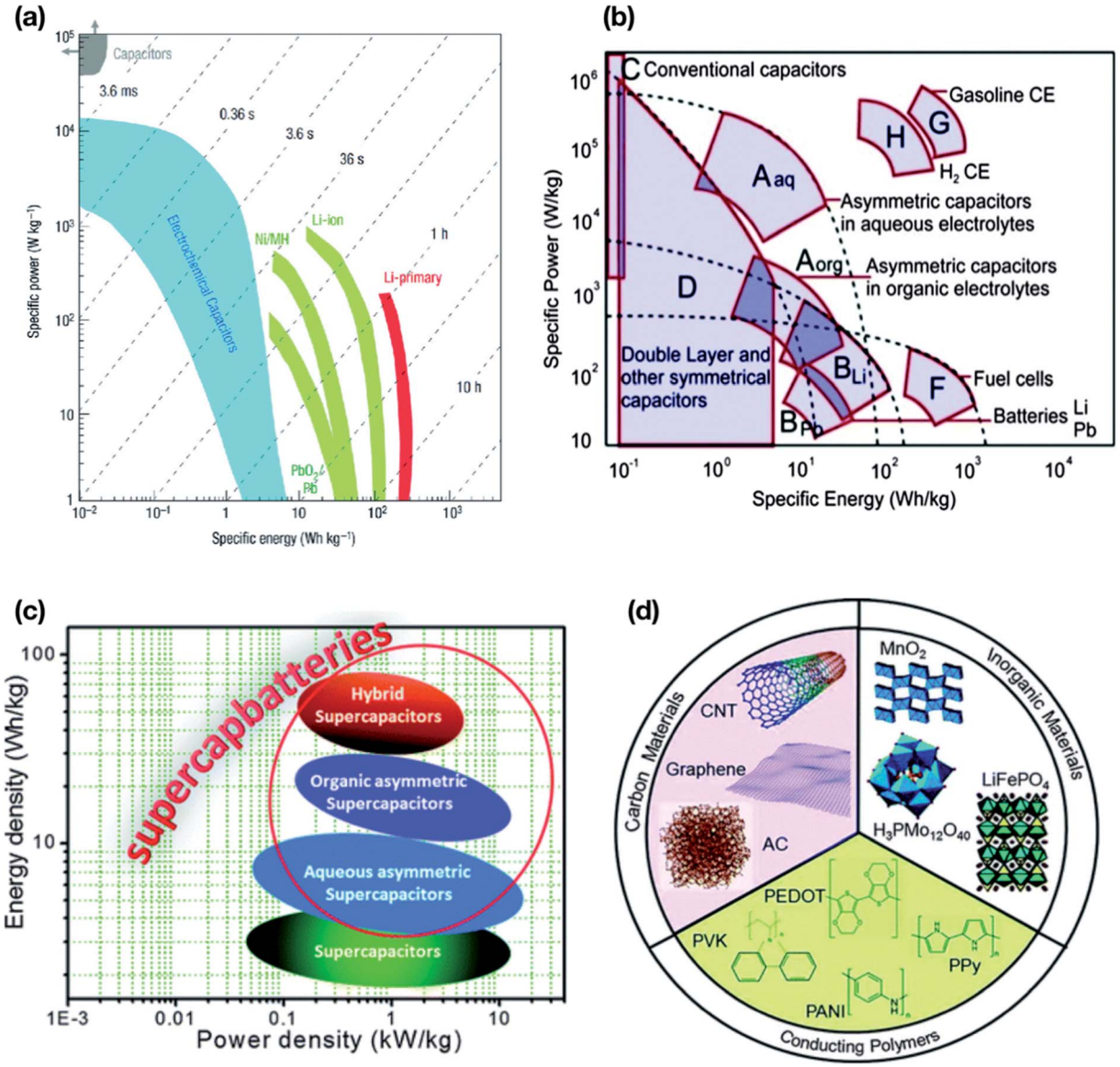

Fig. 3 (a) Typical Ragone plot showing power against energy density.[473] (b) Specific energy/power performance for different energy storage devices.[30] (c) Ragone plot showing the recent status of supercapacitors, asymmetric supercapacitors, and hybrid supercapacitors.[30] (d) Illustration of various components used in the design of hybrid materials for energy storage.[30] (a) has been adapted/reproduced from ref. 473 with permission from Nature Materials, Springer Nature.[473] (c–e) have been adapted/reproduced from ref. 30 with permission from Chemical Society Reviews, Royal Society of Chemistry.[30]

A general overview of the construction and mechanism of supercapacitors

Supercapacitors are devices that bridge the gap between capacitor elements and rechargeable batteries and are capable of storing charge/energy electrostatically by the help of two porous electrodes (usually made up of porous activated carbon)[31] immersed in an electrolyte solution. They have been evolved to boost high energy storage capacity in terms of peak power demands or recapturing energy for which they are considered to be more effective than batteries. The three key elements of a supercapacitor are the separator, electrolyte, and electrodes, and their properties uniquely complement its overall performance. The dielectric strength, chemical inertness, porosity (ion-permeable) and shallow thickness are the most important requirements for a separator for effective working of the supercapacitor. The electrodes must also be highly porous, with the highest possible specific surface area, low electrical resistivity, high chemical stability, *etc.* The porous electrodes are separated by a small distance, liquid, or wet dielectric material. The electrodes and separator are impregnated within a liquid electrolyte (aqueous or organic)[32–35] that allows the transfer of ions while providing insulation between the electrodes[36,37] driven by the electrode surface area and separation between the electrodes which in-turn gives rise to double-layer (Helmholtz layer) capacitance. The positive and negative ionic charges within the electrolyte utilize the high surface area of

Table 2 Taxonomical classification of material-based supercapacitors[a,b]

Types	Mechanism	Energy storage	Performance	Common materials
EDLCs	Chemical transfer	Non-faradaic	0.335 kW kg^{-1} average specific power and 5 kW kg^{-1} maximum specific power in the potential range of 0.0–2.8 V (ref. 449)	Carbon-based
Pseudocapacitors	Chemical transfer (quick)	Faradaic	Average specific capacitance range of 200–500 μF cm^{-2} 1–2 orders of magnitude higher than that of EDLCs[8]	Metal oxide-based
Hybrid	Physical transfer	Faradaic + non-faradaic	Average specific power (0.5 kW kg^{-1}) and maximum specific power (9 kW kg^{-1}) at 5 mA cm^{-2} in the potential region of 1.0–3.0 V (ref. 449)	Both carbon and conducting polymer or metal oxide-based composites[1]

[a] Chemical transfer: Charge transfer between electrodes and electrolytes through electrosorption, redox reactions, and intercalation processes.[8] [b] Physical transfer: Charges are distributed on the surface without making or breaking chemical bonds.

electrodes and accumulate at the surface and compensate for the electric charge[1,8,38–40] as shown in Fig. 4(a). As depicted by Chen *et al.*,[41] a supercapacitor is composed of a multilayered structure including an inner compact layer, an outer compact layer and a diffuse layer which consists of solvated cations and anions. The electrode as shown in Fig. 4(b) is a porous carbon negative electrode that involves chemical bonding which in general is not purely physical nor chemical. The unsolvated anions and partially solvated cations in the compact layers are in the form of closely packed ions on the electrode surface and give rise to linear potential distributions with different gradients. For instance, in the diffuse layer, ion concentration and potential distribution deviate from linearity and reach a plateau towards the end of bulk electrolyte solution as shown in Fig. 4(b). The potential profile of the whole cell is given by eqn (1)

$$U = E_P - E_N, \quad (1)$$

where U is the voltage, and E_P and E_N represent positive and negative electrodes. As shown in Fig. 4(c), the potential in the electrolyte solution (E_s) remains constant due to the mobility of ions. The ions from the electrolyte were adsorbed on the maximal surface area of the electrode in which electrodes make use of electrostatic attraction between ions and electrolyte that allows the formation of oppositely charged layers at the interface.[42] Due to the high surface area of the electrodes, the charge storage mechanism and the performance on the basis of specific capacitance and energy density are better than those of conventional electrochemical capacitors.[43] Supercapacitors can be classified into EDLCs and pseudocapacitors based on their energy storage mechanism, as shown in Fig. 4(d). The two main storage mechanisms in supercapacitors involve electric double-layer charge storage at the interface between the electrolyte and electrodes, and the pseudocapacitance, involving reversible fast faradaic redox reactions at the electrodes' surfaces. EDLCs are the most common commercially available supercapacitors where the charge is stored electrostatically or non-faradaically using a double layer (Helmholtz layer) in which the charge accumulates on the electrode surface by following the natural attraction of unlike charges diffused across the separator into the pores of the electrodes in the electrolyte medium Fig. 4(e).[1,44] The mechanism is followed by the generation of two layers of polarized ions at the electrode interface due to the applied voltage. The two layers *i.e.*, one layer within the solid electrode and the other with opposite polarity generated from dissolved and solvated ions distributed in the electrolyte move towards the polarized electrode which is separated by a monolayer of solvent molecules forming a molecular monolayer called the inner Helmholtz plane that adheres by physical adsorption on the electrode surface and separates the oppositely polarized ions from each other, forming a molecular dielectric. In pseudocapacitors, the charge is stored faradaically or electrochemically through the transfer of charge across the interface. This phenomenon is achieved through electrosorption, reduction–oxidation reactions, and an intercalation process as shown in Fig. 4(f).[4,45] When voltage is applied at the capacitor terminals, the polarized ions in the electrolyte move to the opposite polarized electrode. The interface between the surfaces of the electrodes and the adjacent electrolyte forms an electric double-layer. The movement of one layer of ions at the electrode surface and the second layer of adjacent and solvated ions to the polarized electrode forms a static electric field which gives rise to double-layer capacitance. Accompanied by the electric double-layer, some de-solvated electrolyte ions also act as electron donors, permeate the separating solvent layer and are absorbed by the electrode's surface atoms that deliver their charge to the electrode resulting in a faradaic current. This faradaic charge transfer phenomenon gives rise to pseudocapacitance which is originated from a sequence of fast reversible redox reactions, electrosorption or an intercalation process between the electrode surface and electrolytes. The later devices are often misunderstood with a battery-type electrode storage mechanism: as per the definition, the pseudocapacitor's

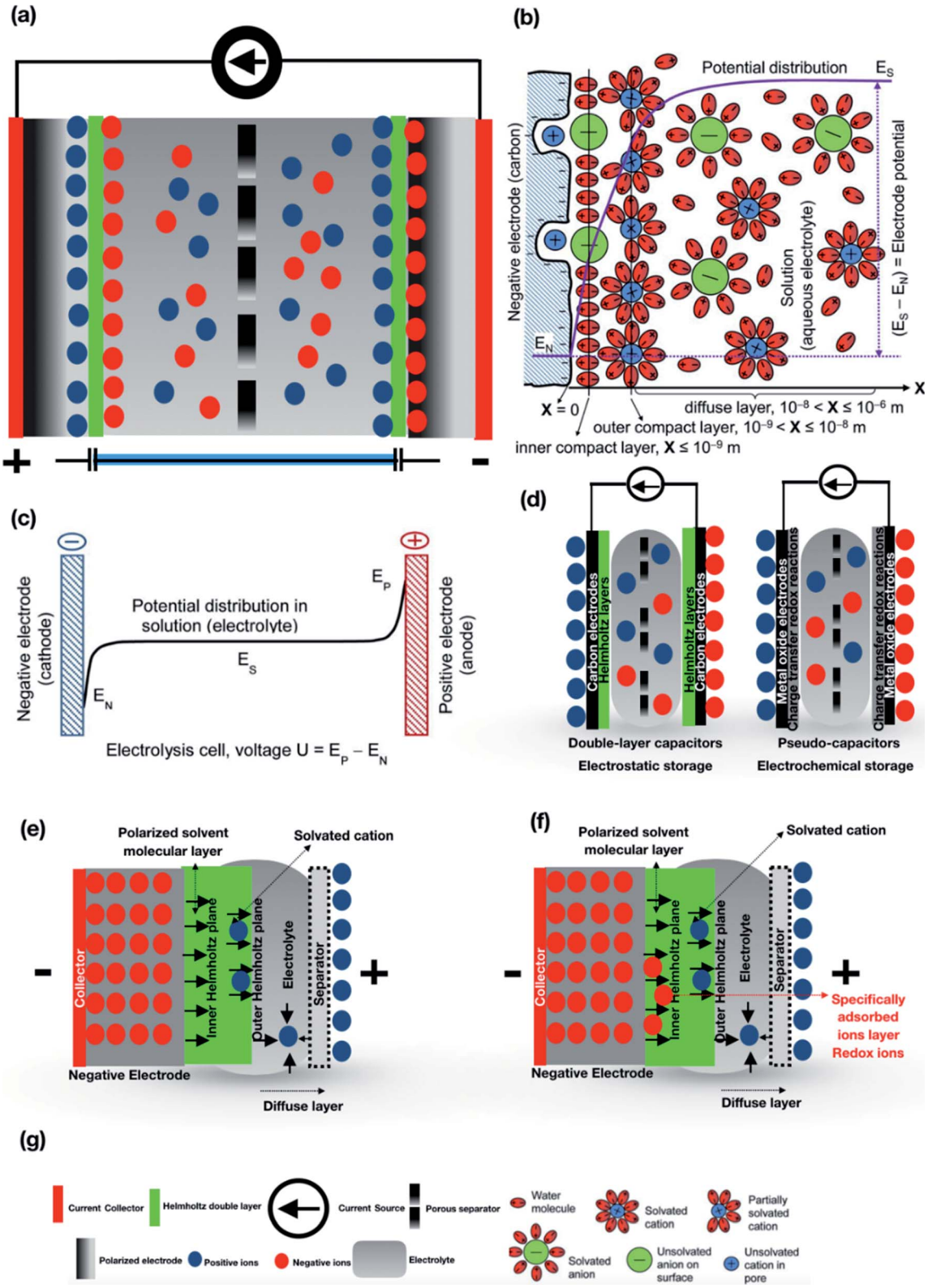

Fig. 4 (a) Schematic representation of basic construction of a supercapacitor. (b) Cross-sectional interface of the electrochemical double layer structure between a porous carbon negative electrode and an aqueous electrolyte. E_N, E_P, and E_s are respectively the potentials of the negative and positive electrodes, and the electrolyte. (c) Potential distribution in the electrolyte solution between the negative and positive electrodes. (d) Energy storage mechanisms in supercapacitors *e.g.* electrostatic storage mechanism in double-layer capacitors & electrochemical storage mechanism in pseudo-capacitors. (e) The charge is stored electrostatically or non-faradaically using a double layer (Helmholtz layer) in which the charge accumulates on the electrode surface by following the natural attraction of unlike charges diffused across the separator into the pores of the electrodes in the electrolyte medium. The arrows represent the polarized solvent molecular layer in the inner Helmholtz plane and the arrows

electrodes must be capacitive, that is the storage should be proportional to the applied voltage, while, in batteries, a flat discharge plateau is often observed. This behavior is characteristic of the electrode and cannot be applied in case of the asymmetric or hybrid device performance.[46] In both, the storage mechanisms are synergetic between electrode and electrolyte materials.[47] Generally, when the voltage is applied to a supercapacitor, ions in the electrolyte solution diffuse into the pores of the electrode of opposite charge and charge accumulates at the interface between the electrodes and the electrolyte, forming two charged layers (double layer) with an extremely small separation distance. The capacitance value C is proportional to the surface area A and is the reciprocal of the distance d between the two layers[48,49] as depicted in eqn (2).

$$C/A = \varepsilon_0\varepsilon_r/d, \quad (2)$$

where ε_r is the relative dielectric constant, and d is the thickness of the double layer with surface area A. The thickness of the double layer depends on the concentration of electrolytes and the size of ions. To achieve a higher capacitance, porous electrodes have been used to increase the surface area with an extremely large internal effective surface. Carbon technology is often used in these capacitors because it creates a very large surface area with a separation distance of just a few angstroms (0.1 nm), due to its porosity which is discussed further in this review.

Charge–discharge mechanism

Although supercapacitors have many advantages over batteries, they still lag due to some limiting factors, *e.g.*, high cost per watt, low specific energy, high self-discharge, low cell voltage, *etc.* (Source: Maxwell Technologies, Inc.[50]). But in consideration of a sudden surge of energy, supercapacitors are slightly better than batteries due to their relatively fast charge–discharge cycle (Fig. 5(a)). They exhibit the capability to store more energy than conventional capacitors and are also capable of delivering it faster than rechargeable batteries along with a high tolerance towards charging and discharging cycles. Fig. 5(a) demonstrates a typical charge–discharge profile where supercapacitors supersede conventional batteries in terms of time taken to charge and discharge, respectively. According to the pie charts depicted in the figure, batteries take almost 80% of time to charge (light green color in recharge time) as well as to discharge (pink color in discharge time) in comparison to supercapacitors whereas the time to charge and discharge is comparatively shorter (less than 20%) in supercapacitors. In addition to having a limited number of charge–discharge cycles in batteries, the performance of the batteries' cycle life significantly deteriorated and shortened when a large pulsed discharging current with a peak greatly exceeding the average power consumption occurs. To reduce the peak current draw in battery-powered electronics with a highly fluctuating load, supercapacitors are widely exploited to mitigate such load current fluctuations in batteries.[51] Fig. 5(b) depicts a typical charge/discharge cycle of supercapacitors and batteries. Compared to hundreds of cycles for batteries, supercapacitors have the ability to withstand thousands of cycles before degrading and also have the ability to be deeply discharged when compared to batteries. The self-discharge rate of supercapacitors due to their composition is significantly higher than that of batteries. Fig. 5(c) illustrates the cyclic voltammograms of positive and negative electrodes in a three-electrode cell and galvanostatic charging and discharging plots for a two electrode cell for rechargeable batteries and supercapacitors respectively. Eqn (3) expresses the energy density of a supercapacitor as:

$$E = \frac{1}{2}CV^2 \quad (3)$$

E is the energy provided by the supercapacitor, C is the capacitance of the supercapacitor, and V is the voltage of the supercapacitor. The potential for positive electrodes (Fig. 5(c)) tends towards positive in the graph and is always higher than that of negative electrodes due to electrical polarities. The electrical polarities generated are due to the fact that current always flows from positive to negative electrodes *via* an external circuit and the electrons flow from negative to positive electrodes. Generally, faradaic reactions that are generated from the interface of electrode|electrolyte are always present in rechargeable batteries but not in supercapacitors and because of this difference, the minimum cell voltage can decrease to zero in supercapacitors as shown in Fig. 5(c).

The voltage and current characteristics upon charge and discharge of a supercapacitor are depicted in Fig. 5(d). During charge, the voltage linearly increases and the current drops when the capacitor is fully charged without any full-charge detection circuit and when the condition of a constant current supply is applied during discharge, the voltage drops linearly and the current increases. The charge/discharge process is unlimited in the case of supercapacitors but not in the case of rechargeable batteries which have a defined cycle life. A comparison can thus be established between batteries *vs.* supercapacitors in terms of charge time; supercapacitors take only 1–10 seconds to charge whereas batteries (lithium-ion) take 10–60 minutes. Likewise, the cycle life is around 1 million hours in comparison to 500 h in batteries. The optimum cell voltage is around 2.3 to 2.75 V in supercapacitors and 3.6 V in batteries (referred from Battery University™ sponsored by Cadex Electronics Inc.).

Efficient charge storage mechanisms: electrodes

To improve the specific capacitance and charge storage, supercapacitors rely on electrode materials that are theoretically and experimentally supported. Mostly carbon-based materials

with positive ions represent solvated cations. (f) The charge is stored faradaically or electrochemically through the transfer of charge across the interface. This phenomenon is achieved through electrosorption, reduction–oxidation reactions, and an intercalation process. The arrows with negative ions represent redox ions and arrows with positive ions depict solvated cations. (g) Depiction of symbols in (a and b). (b, c and g) have been adapted/reproduced from ref. 41 with permission from Taylor & Francis.[41]

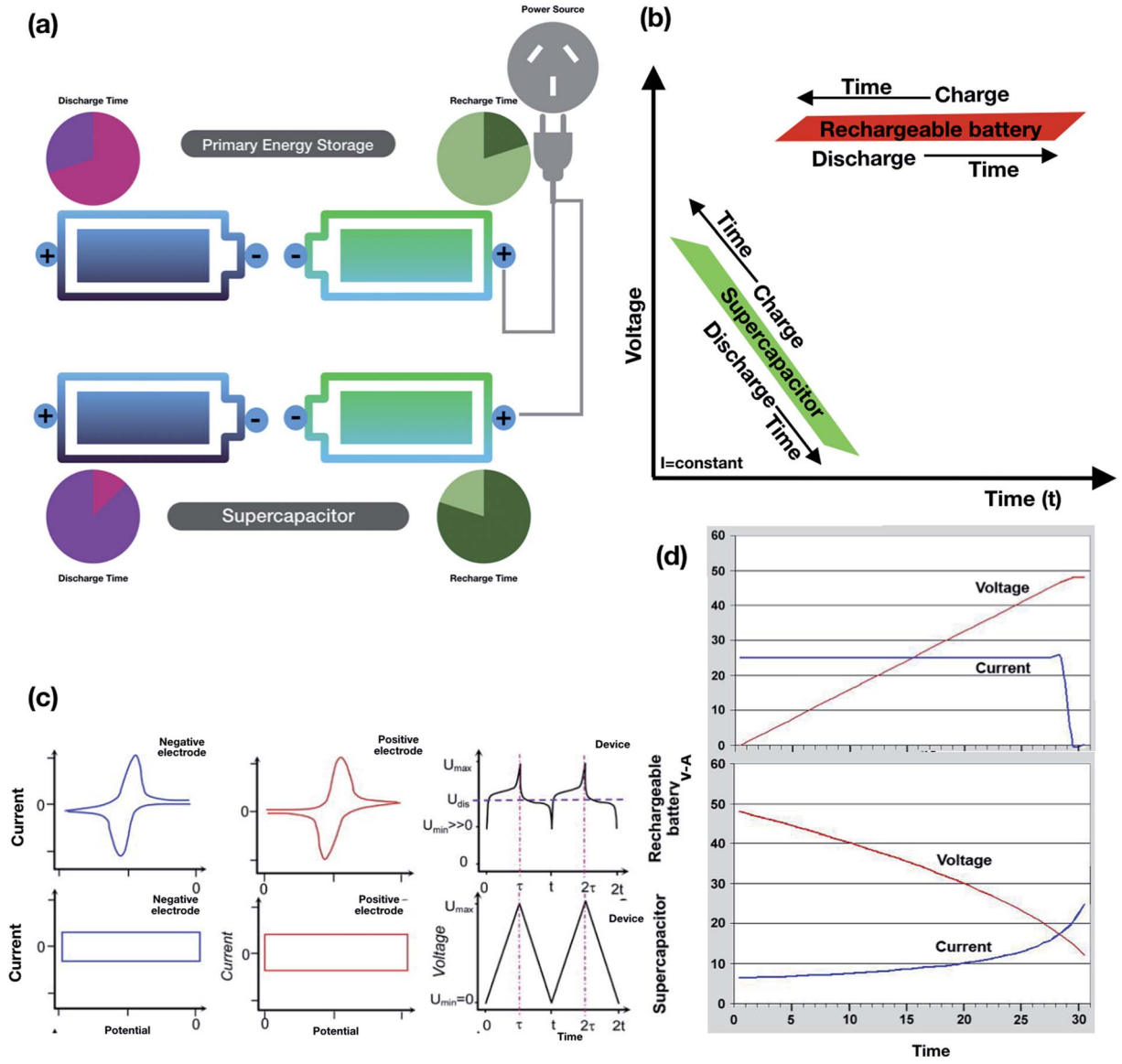

Fig. 5 (a). Comparison of the charge and discharge cycles of batteries *vs.* supercapacitors. Pink color signifies the discharge time cycle and light green represents recharge timing (b). (c) The cyclic voltammograms of positive and negative electrodes in a three-electrode cell and galvanostatic charge and discharge plots for a two-electrode cell for rechargeable batteries and supercapacitors respectively. U_{max} and U_{min} are the maximum and minimum cell voltages; U_{dis} is the average discharge voltage; τ and t: end times of the first charge and discharge cycle, $\tau \geq (t - \tau)$. 2τ and $2t$: end times of the second charge and discharge cycle. (d) Charge–discharge voltage curves (referred from Battery University™ sponsored by Cadex Electronics Inc.[474]). (c and d) have been adapted/reproduced from ref. 41 and 474 with permission from Taylor & Francis[41] and Battery University™ Copyright ©2003–2018 Cadex Electronics Inc. (Cadex)[474] respectively.

are used in the fabrication of supercapacitors due to their high surface area, low cost, availability, and technologies supporting the production of carbon-based electrodes. Mostly EDLCs use carbon-based electrodes as the charge transfer mechanism strongly relies on the surface area accessible to electrolytic ions. The nature of the electrode material depends on various properties, *e.g.*, carbon, is primarily focused on subclasses of EDLCs that is of great importance as they have a higher surface area, easy fabrication, and low-cost material. Various forms such as activated carbon, carbon nanotubes, and carbon aerogels can be used to store charges in EDLCs out of which we have mainly focused on nanotube structural conformations. There is an increasing demand in the usage of carbon nanotubes in EDLC electrode materials in the form of mesopores which are grown as entangled mat that allows continuous charge distribution on the available surface area. Physical mechanisms play a pivotal role in charge transfer where the surface area is utilized more efficiently to achieve higher capacitance.[52,53] The diffusion of electrolytes is more facile in mesoporous networks resulting in low ESR (equivalent series resistance)[54] and high power densities[55] compared to other types of carbon-based electrodes.[56–58] Influential parameters such as the pore sizes, pore shape, structure, surface functionality and electrical conductivity play a pivotal role in increasing the specific capacitance,[59,60] for

example, when using activated carbon, single and multiwalled carbon nanotubes, graphene, graphene oxide, *etc.*. One can further discuss the other influential parameters, *e.g.*, pore size, in inducing an effect on the specific capacitance and performance of supercapacitors. Illustrative examples of carbon-based nanoporous materials are shown in Fig. 6(a–d).

Effect of pore sizes on specific capacitance and performance

Gogotsi *et al.*[61] made a major discovery on pore size effects on specific capacitance based on the contribution of unsolvated ions to capacity in purely double-layer electrodes using carbide-derived carbons with pore sizes smaller than 1 nm. They demonstrated the diffusion of ions through these pores upon desolvation, which contributes to increasing capacitance. Generally, the material used for electrodes is nowadays based on porous carbon that uses ion adsorption on the surface. The effect of pore size on capacitance may potentially improve the performance by maximizing the electrode surface area. As shown in Fig. 7(a), a detrimental effect on capacitance can be observed with the increase in pore size while the specific capacitance is normalized by the surface area of the electrodes.[62–64] Fig. 7(b) shows the optimization of electrodes to potentially improve the performance based on pore size. The specific capacitance is inversely proportional to the pore size, and one can easily note the difference in pore sizes leading to increased or decreased performance and specific capacitance. When the pore size is larger than the size of the ions, the contribution to capacitance is from the adjacent pore walls but having reduced specific capacitance,[65] whereas the decrease in the size of the pores approximate to the crystallographic diameter of the ions led to increased capacitance as the solvation shell/pore is highly distorted and squeezes the ions allowing a closer approach of the ion center to the electrode surface.[66–69]

By assuming that the carbon electrodes are cylindrical, the specific capacitance with respect to the specific surface area (SSA) can be depicted as given in eqn (4)

$$\frac{C}{A} = \frac{\varepsilon_0\, \varepsilon_r}{b \ln\left(\frac{b}{b-d}\right)} \tag{4}$$

where ε_r is the electrolyte dielectric constant, ε_0 is the dielectric constant in a vacuum, b is the pore radius and d is the distance between approaching electrolyte ions and the carbon surface.[70] One such theory has been experimentally demonstrated by Gamby *et al.*,[71] who has shown that the specific capacitance of porous carbon electrodes showed a peculiar dependence on pore size. When the pore size is above 2 nm, the surface-specific capacitance decreases as the pore size decreases due to less accessibility for ions. But this pore dependence theory has been contradicted by Kiyohara *et al.*,[72]

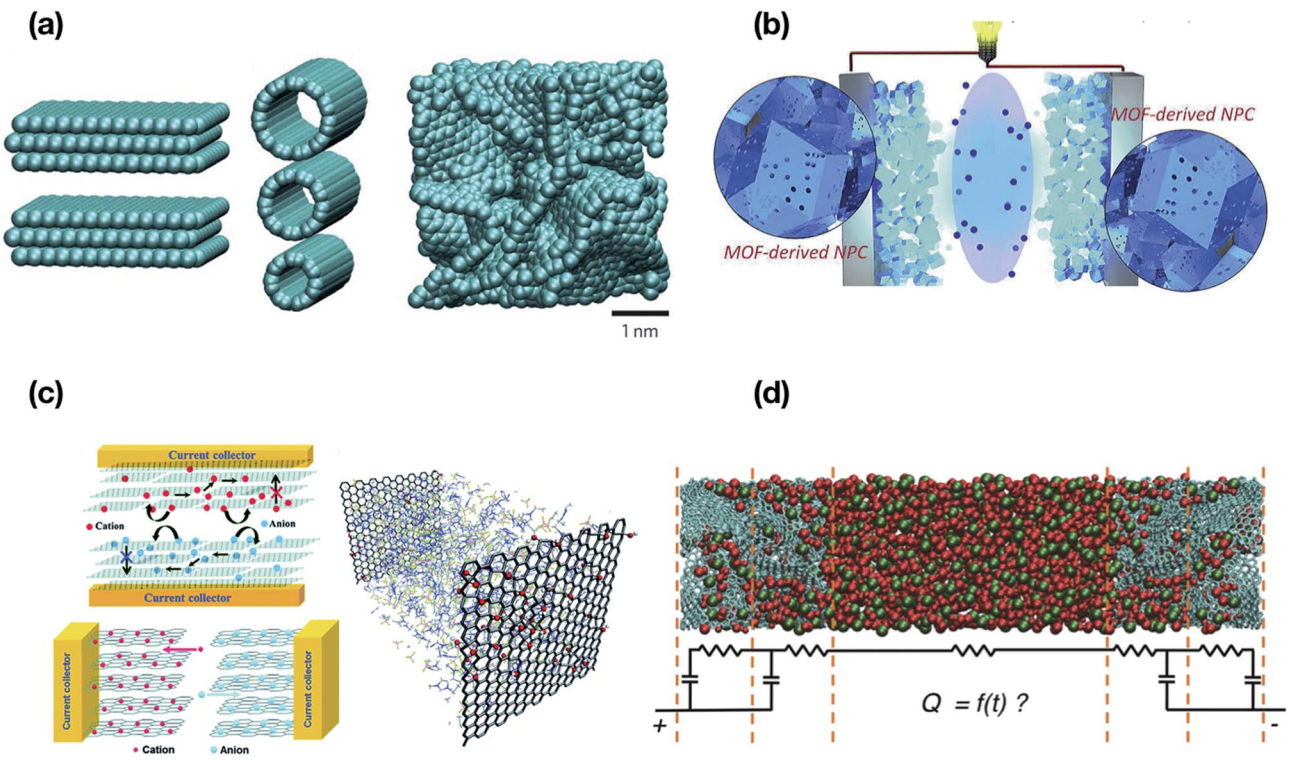

Fig. 6 (a) Ordered structures with slit pores, nanotubes and asymmetric nanoporous carbons.[42] (b) Symmetric supercapacitor based on metal oxide framework derived nanoporous carbon.[475] (c) Stacked geometry model for a carbon-based electrode material consisting of GO electrodes with pure EMI + BF_4−.[476] (d) Porous electrodes made of carbide derived carbon immersed in a BMI-PF_6 ionic liquid electrolyte.[477] (a) has been adapted/reproduced from ref. 42 with permission from Springer Nature.[42] (b) has been adapted/reproduced from ref. 475 with permission from the Royal Society of Chemistry.[475] (c) has been adapted/reproduced from ref. 476 with permission from the Royal Society of Chemistry.[476] (d) has been adapted/reproduced from ref. 477 with permission from American Chemical Society.[476]

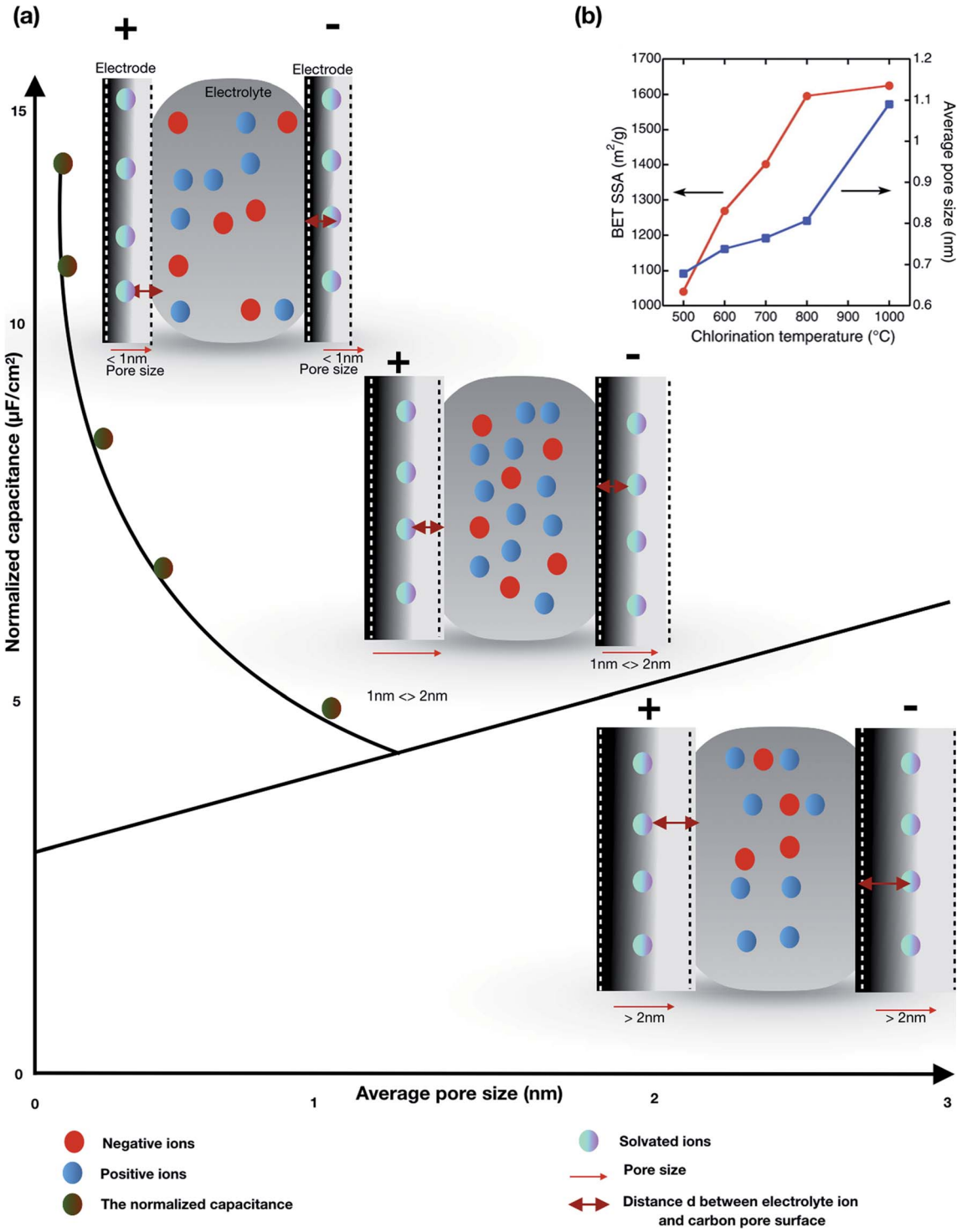

Fig. 7 (a) Solvated ions residing in pores with varying adjacent pore walls. A decrease in the pore size leads to high or improved capacitance with the efficient approach of ion mobility towards the pore walls. The detrimental effect on capacitance can be observed with the increase in pore size as per Chmiola *et al.*[62] (b) The plot depicts effect of synthesis temperature on the SSA, and the average pore size of CDC. Redline illustrates the SSA values and Blue line depicts the pore size. (b) has been adapted/reproduced from ref. 62 with permission from the American Association for the Advancement of Science.[62]

stating that when the pore size is smaller than 2 nm the surface-specific capacitance increases as long as the pore size is larger than the ions which was illustrated by Monte Carlo simulations. The enhanced understanding of ionic transport in porous media can be demonstrated by the charge storage mechanism in ionic pores smaller than the size of solvated

electrolyte ions. Furthermore, these findings also allow the design of specific capacitors for several applications such as hybrid electric vehicles. Further tuning the carbon porosity and designing carbon materials with a large volume of narrow but short pores may allow both energy and power characteristics to be improved. Kornyshev *et al.*[73] (Fig. 8(a)) showed the accumulation of only one row of ions in a narrow nanopore in an unpolarised electrode using the two state ising model. Speaking about the pore radius, a tiny change in the pore radius might affect the voltage dependence on capacitance showing a smeared resonance as shown in Fig. 8(b). The standard way of increasing the capacitance is to decrease the pore size of the electrodes as well as the thickness of pore walls. The model that they presented was based on several assumptions: (i) the propensity of cations and anions to occupy the pores in the electrode even in the unpolarized state of the electrode; (ii) during the polarisation of electrodes, co-ions tend to replace the counter ions; (iii) the ions are densely packed with no voids in between them; (iv) electrostatic interaction of ions in the pore is screened by polarization of pore walls.

To gain an insight into the intrinsic effects of nanopores on the electrochemical capacitive behavior, several experiments and hypotheses have been proposed. Itoi *et al.* proposed that heteroatom doping into porous carbon materials would potentially change the behavior of pore structures and sizes which in turn give noticeable pseudocapacitance in microporous carbon, *e.g.*, ZTC (zeolite-template carbon).[74] To increase the charge efficiency, the pore size distribution of electrode materials should be optimized for the removal of targeted ions by capacitive deionization through entrapment in EDLCs where the porous electrodes are polarized.[75] Design and optimization of nanopores in graphene are critically important due to tunable porous channels which could potentially enhance the electrochemical storage capacity.[76] Jung *et al.* showed that graphene aerogel supercapacitors exhibit a specific capacitance of 325 F g^{-1} at 1 A g^{-1} and an energy density of 45 W h kg^{-1} in a 0.5 M H_2SO_4 aqueous electrolyte with high electrochemical stability and electrode uniformity. Urita *et al.* proposed an ideal porous structure of carbon electrodes for EDLCs where the gravimetric capacitance was above ~200 F g^{-1} even in an organic electrolyte by utilizing the carbon nanopore surface more effectively.[77] For enhanced capacitive deionization (CDI), Gao *et al.* proposed that the usage of carbon electrodes with optimized chemical surface charge could extend the CDI working voltage window

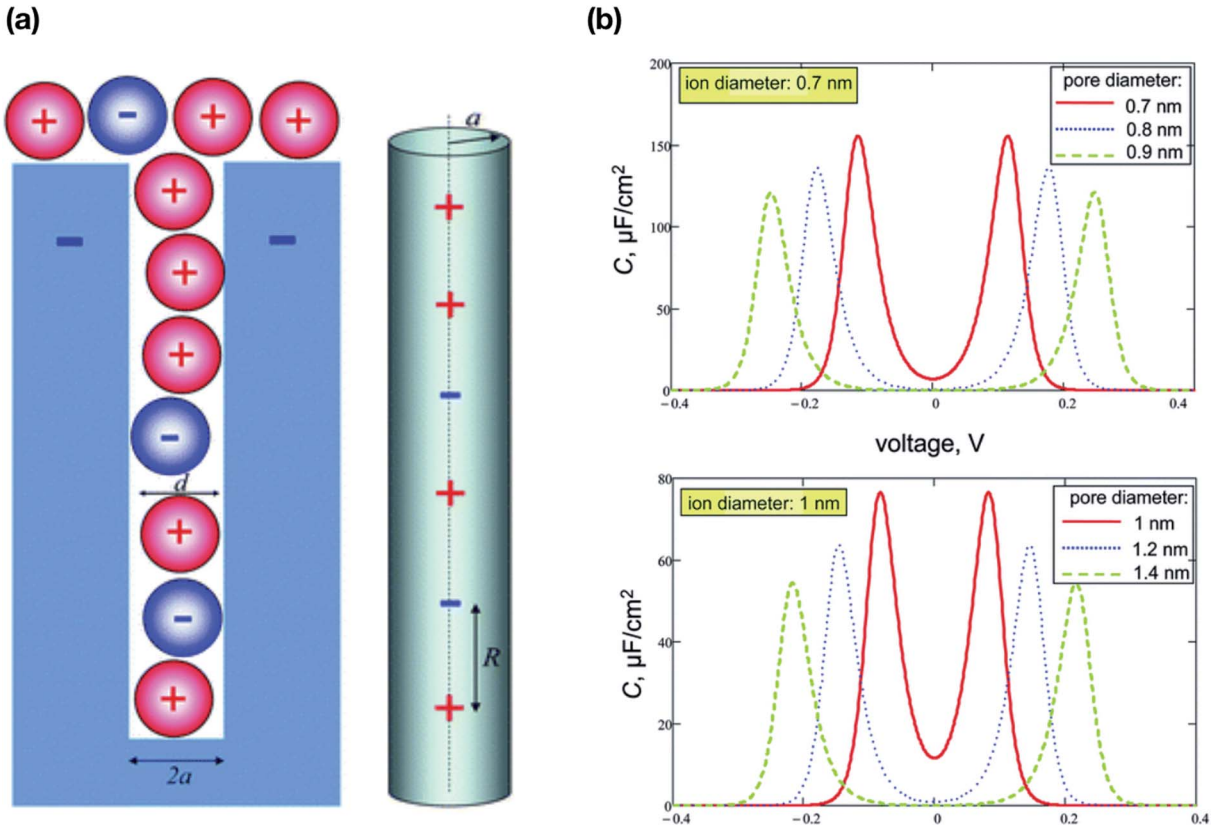

Fig. 8 (a) Schematic cross section of a negatively polarized electrode pore showing accommodation of one line of ions in the order of $d < 2a < 2d$. One dimensional lattice representation of distribution of ions. Reprinted with permission from Royal Society Publishing.[73] (b) The specific voltage-dependent differential capacitance of a single pore per unit surface area. The effect of the diameter of the pore, shown for an ion diameter of 0.7 nm (upper panel) and 1 nm (lower panel); the effective dielectric constant of the pore interior, $\varepsilon = 2$. Due to saturation of charge density, the capacitance vanishes very quickly with voltage. (a and b) have been adapted/reproduced from ref. 73 with permission from the Royal Society of Chemistry.[73]

through discharge voltage which in turn increases the salt adsorption capacity.[78] Several other studies proposed the characterization and effects of porous electrodes to meet the demands of three basic requirements: (i) increase the capacitance values, (ii) low resistance, and (iii) stability.[77–90] Interesting work by Kalluri *et al.*[91] reported atomistic simulations to study the effect of pore size and surface charge density on the capacitance of graphitic nanoporous carbon electrodes. They showed that through molecular dynamics (MD) simulations of pore-size dependent accumulation of aqueous electrolytes in slit-shaped graphitic carbon pores of different widths (0.65 nm to 1.6 nm), the capacitance of wider pores does not depend significantly on the applied potential window. Rather, the penetration of ions into pores becomes more difficult with decreasing pore width and increasing strength of the hydration shell which is in contrast to previously reported pore size effects. Another study by Song *et al.*[92] reported the intrinsic ion selectivity effects of narrow hydrophobic pores using single-walled carbon nanotube membranes. They performed MD simulation studies with a pore radius of 3.4–6.1 Å, to show that Na^+, K^+, and Cl^- face different free energy barriers when entering hydrophobic pores which gave consistent results with the work of Tai *et al.*[93] MD simulations proposed earlier have been consistent with experimental results.[94–120] Seminal studies by Kornyshev *et al.*[73,121] proposed superionic states in EDLCs with nanoporous electrodes which are in agreement with the studies of Chmiola *et al.* & Largeot *et al.*,[63,122] where they have explained the effect of an anomalous increase in capacitance with the decrease of pore size using image forces that exponentially screen out the electrostatic interaction of ions in the interior of pores. Also, basic assumptions for a nanopore model made by Kornyshev *et al.*[73] led to future theoretical and experimental developments which may be useful for understanding what, in principle, nanoporous electrodes could deliver for energy storage. Apart from experimental and molecular atomistic observations, several first principles-based DFT (Density Functional Theory) theories have been proposed to exhibit the supercapacitor capacitance based on nanopore networks.[123–136] The state of the art DFT methods have been proposed to calculate pore size distribution in various nanoporous materials.[132,137–158] For instance, in the seminal studies of Seaton *et al.*,[159] the pore size distribution from adsorption isotherms has been determined by DFT based methods in which they have suggested a method for modeling nitrogen adsorption on porous carbon by local mean-field approximations. Lastoskie *et al.*[160] used non-local DFT within Tarazona smooth density approximation for modeling nitrogen adsorption on carbons. The pore size distribution range has been depicted below in the figure to understand the mechanism of how electrode porosity has a direct effect on particle to particle contact between the active material and the conductive diluent. By controlling porosity, higher intra-electrode conductivity can be achieved to ensure adequate electron exchange as well as sufficient void space for electrolyte access/transport.

Electrolyte materials and their applications

Apart from the most influential components such as electrodes, electrolytes have a greater impact on the performance of supercapacitors on the basis of ionic type, size, ion mobility, ionic conductivity, viscosity, thermal stability, and voltage window. We will cover some aspects of electrolyte materials to enable the readers to understand the importance of this in designing supercapacitors. The equivalent series resistance (ESR) is an important parameter for determining the power density of supercapacitors where the type of electrolyte used generally governs the charge/discharge rate. The electrolyte is usually the primary limiting operating voltage of the supercapacitor with its chemical stability issues.[161] A schematic overview of the classification of electrolytes is illustrated in Fig. 9, comprising liquid electrolytes which include aqueous, non-aqueous, organic, ionic liquid, neutral, alkaline, mixed and acidic electrolytes; redox-active electrolytes that include gel polymers; solid-state/quasi-solid-state electrolytes which include inorganic solid-state electrolytes, solid polymer electrolytes, and gel polymer electrolytes.[162] Considering the effects of electrolytes on increasing capacitance and power density, widening the potential window of the solution is one of the effective solutions. Higher priority must be given to the potential window in a range of working voltages for which the other parameters, *e.g.*, power density, temperature range, salt solubility, material interaction, ion pore size, and electrochemical stability, under various conditions cannot be overlooked.[163] Great efforts and multiple research activities are currently driven towards the development of advanced materials and configurations for enhanced energy densities, as well as cheaper preparation and processing methods. The aforementioned materials (electrodes and electrolytes) are widely fabricated, which in turn enables researchers to design novel material based supercapacitors. We will discuss the many efforts and approaches taken by researchers to design advanced electroactive materials and electrodes (specifically nanotubular materials) which is the main objective of this review.

Nanotubular networks

Since miniaturization of electronic components enables faster and more energy-efficient devices, micro- and nano-sized supercapacitors play a crucial role in the filtering of high-frequency noise in such systems. As capacitance is connected to physical size, any other technology would simply take too much space in microelectronic assemblies. Following these requirements, nanotube networks were found to be excellent candidates for supercapacitor materials (Fig. 10).

They can be made flexible (and even stretchable), are intrinsically porous and, being wrapped 2D sheets, possess an exceptional surface-to-volume ratio. Materials possessing tunable electronic properties can be used as electrodes within a wide range from insulating boron nitride nanotubes (BNNTs) to highly conductive carbon nanotubes (CNTs).[164,165] One of the important discoveries made in 1991 by Sumio Iijima is of particular importance as the discovery of hollow, nanometer-

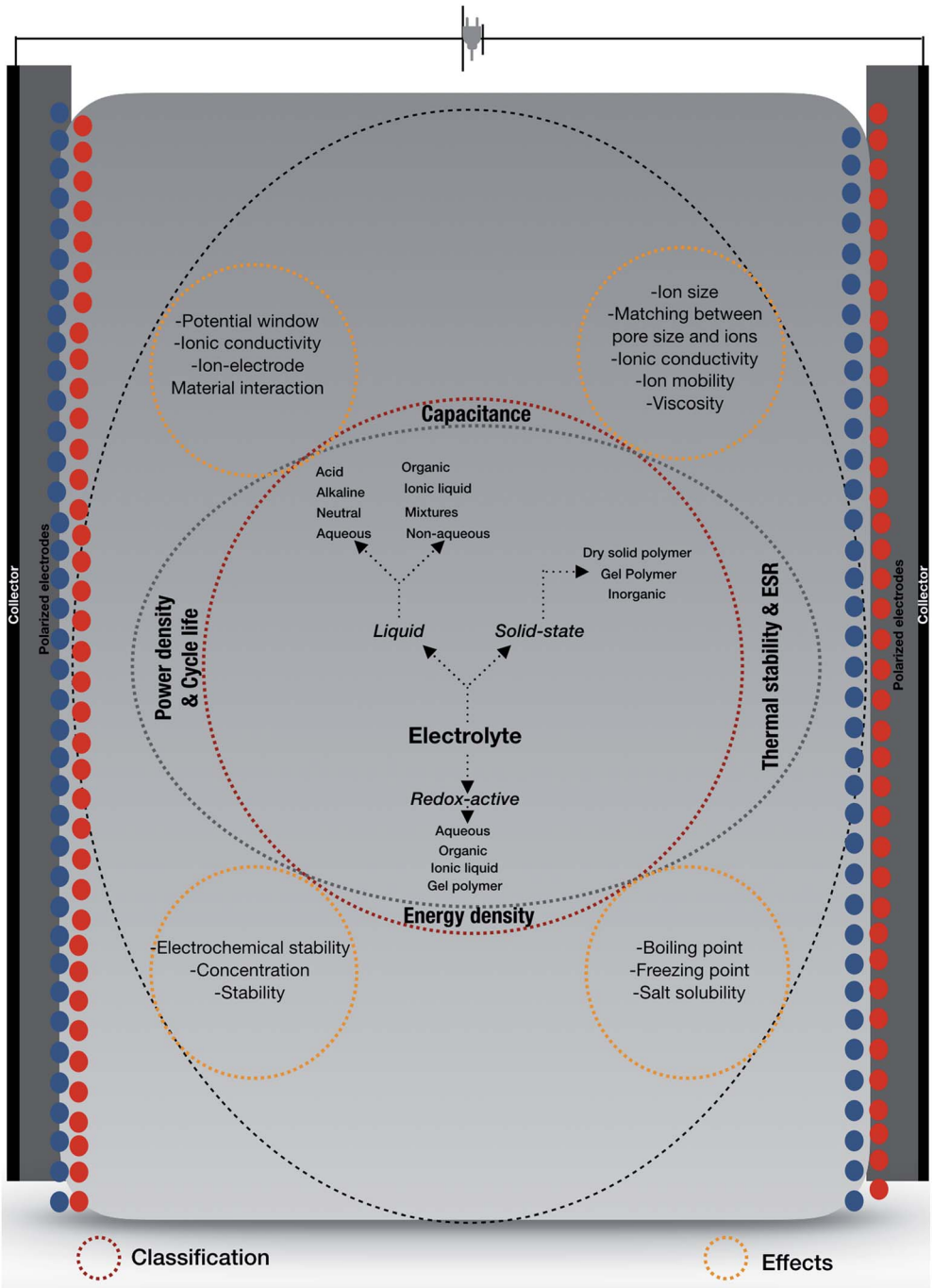

Fig. 9 Classification of electrolytes with electrochemical supercapacitor effects based on electrolytes.

sized tubes composed of graphitic carbon marked the beginning of an era in carbon nanotubes (Fig. 11).

Nanotubular materials are classified into three types: single-walled type (SW-type), multi-walled type (MW-type) and scrolled type (S-type) which are rectangular sheets rolled into single and concentric cylindrical forms with no edge atoms. S-type are generated from a single straight sheet keeping both ends free [166] (Fig. 12(a–d)). In SW-type nanotubes, due to rolling of sheets they undergo displacement of atoms which causes strain energy which is given by the following eqn (5) and (6):

$$E_s = N_{i\varepsilon_0} + N_{i\varepsilon_e} \quad (5)$$

$$E_t = N_{\varepsilon_0} + N_{\varepsilon_s} \quad (6)$$

where $N = N_i + N_e$, and N_i and N_e are the numbers of internal and edge atoms respectively. ε_0 is the energy per atom of a periodic large sheet. ε_e is the energy per one atom associated with edge atoms and ε_s is the energy per atom due to strain. Also the strain energy is correlated with the diameter of the tube through eqn (7)

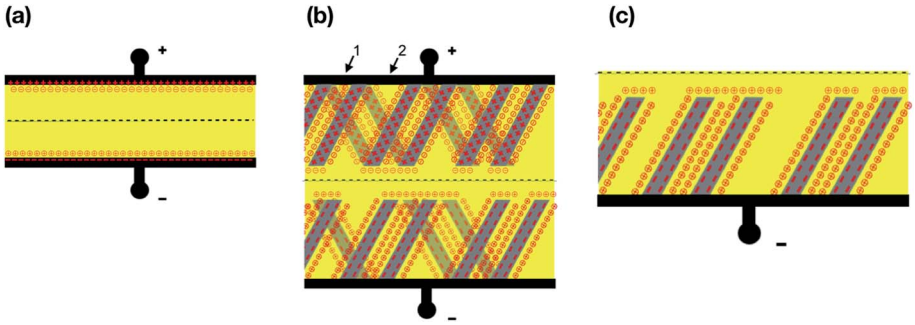

Fig. 10 (a) Schematic view of a charged capacitor (left) and (b) supercapacitor (right): solid black—electrodes; dashed—separator; yellow—electrolyte; nanotubes schematically shown in shades of gray; numbers indicate the hierarchical system of pores 1—small pores and 2 big ones; " +"—positive charge; " ⊖"—negative ion; " −"—negative charge (electrons); " ⊕"—positive ion. (c) Illustration of a part of a supercapacitor consisting of monolayers of nanotubes.[167]

$$\varepsilon_s \sim 1/D^2, \quad (7)$$

Among the structural types of nanotubes, SW-type nanotubes are energetically more stable due to their topological configuration and excess energy due to strain unless the diameter of tubes is beyond a critical value *e.g.* $N_{\varepsilon_s} < N_{\varepsilon_0}$. Their unique topological and self-healing properties make these tubes very stable, which, however, require certain efforts for surface functionalization (Fig. 13), often a necessary

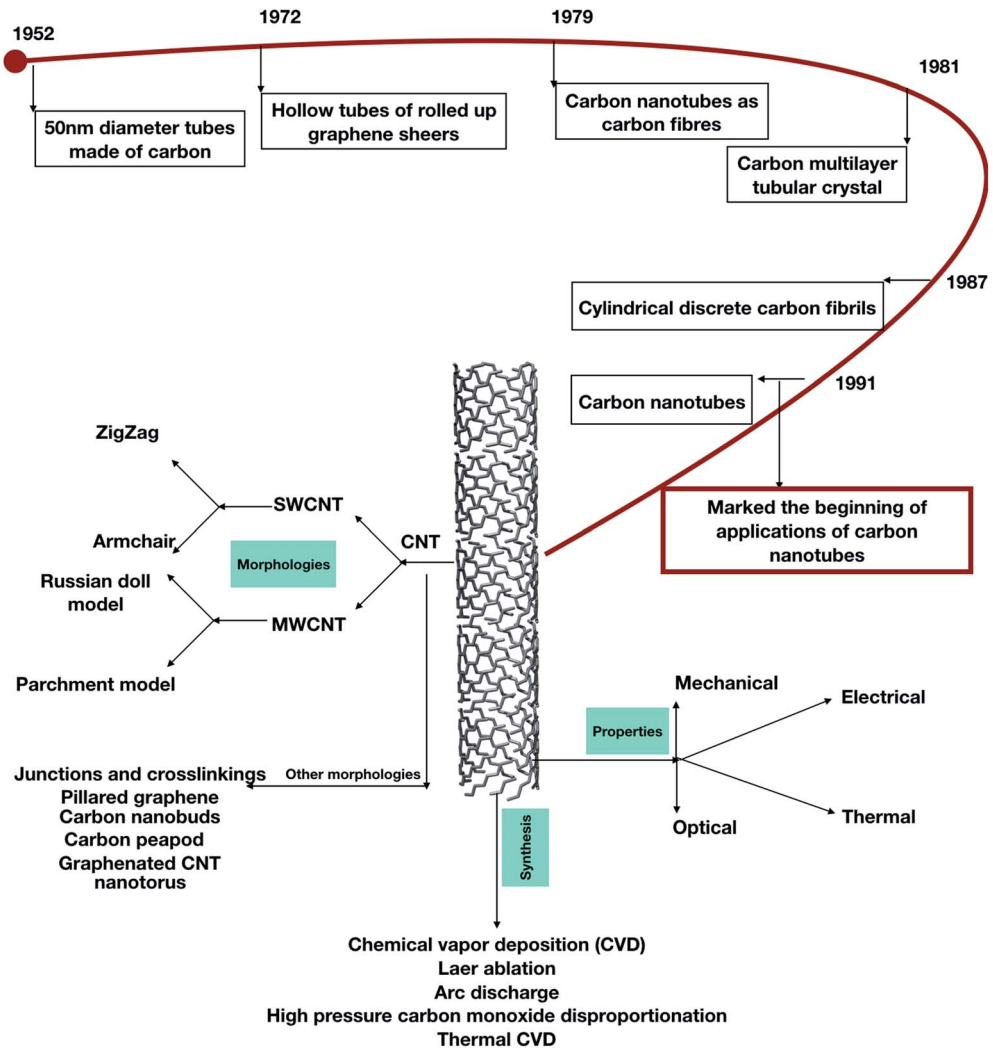

Fig. 11 A schematic diagram showing the discovery, morphologies, properties, and synthesis of carbon nanotubes.

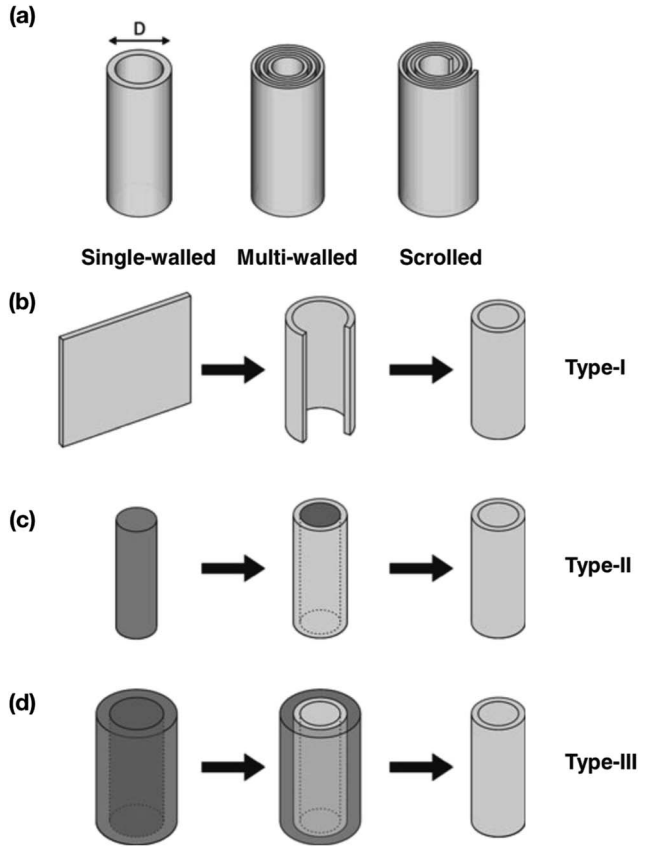

Fig. 12 (a). Type of nanotube. (b) Pathways of obtaining nanotubes, *e.g.*, rolling of the sheet, (c) the surface of a core-type template, and (d) the internal surface of a sheath-type template. Reprinted with permission from Springer.[478] (a–d) have been adapted/reproduced from ref. 478 with permission from Springer Nature.[478]

requirement for tuning the electrode properties as well as matching the redox potential to that of the electrolyte. This is achieved either by aggressive surface treatments[167] or wrapping CNTs with or around a polymer.[168] Some polymers can form nanotubes on their own or around templates, with the notable example of the oldest known conducting polymer, polyaniline (PANI) nanotubes. It is worth mentioning that most of these materials are environment-friendly and/or are easy to dispose of. The discovery of fullerenes envisage a new horizon in synthesizing CNTs by rolling up graphene sheets into SWNTs and MWNTs that exhibit high stiffness and chirality[169–171] which can be used in electronic devices as electrodes in supercapacitor applications[172] due to their high electrical conductivity and flexibility. To facilitate the flow of electrons in CNTs, the fabrication and functionalization of the CNT networks is required. Generally, CNTs have an electron mean free path of ~1 μm, an order of magnitude greater than conventional 2D materials. To allow the electrons to move freely and to obtain a better transport regime, the CNT networks present in the channel area (between the source and drain contacts) in conjunction with the electrodes require fabrication to observe the change in electrical signals which is the key factor in elucidating the mechanism of sensing. One such example has been reported by Gui *et al.*,[173] where CNT van der Waals networks have been used to sense DNA nucleotides that showed sensing capabilities. The 3D networks with a high surface area and good electrical conductivity enable their use in various applications where the storage of gaseous species or ions is important. For instance, CNT networks in conjunction with metal oxides constitute efficient electrodes for electrochemical batteries and supercapacitors, in which the electrical conductivity and the large surface area of the CNT network are the key parameters for the battery performance.[174,175] Considering lightweight supercapacitors, 3D nanotube networks with high electrical conductivity can be used as electrical conductors; CNT aerogels with densities of a few mg cm^{-3} could provide excellent substitutes for metal wires.[176] A schematic view of CNT structures, effects and their application in supercapacitors is depicted in Fig. 13 with the conception of building CNTs from graphene[177] *via* van der Waals forces providing ultra-high-strength and light weight dimensions with conductive electrical and thermal properties.

Various factors such as surface functionalization, heating, and structural effects with modified shape engineering influence the multiple applications of CNTs.[178] For the first time, Niu *et al.*[54] suggested that CNTs can be used as supercapacitors from the viewpoint of surface functionalization effects using nitric acid with functional groups on MWCNTs with a specific area of 430 $m^2 g^{-1}$, a gravimetric capacitance of 102 F g^{-1} and an energy density of 0.5 W h kg^{-1} obtained at 1 Hz on a single-cell device, using 38 wt% sulfuric acid as the electrolyte. Structural effects include the electrical charge accumulated due to electrostatic attraction on the surface of the electrode/electrolyte interface accessible by ions in the electrolyte. As CNTs possess a high surface area, the specific capacitance is always high in most cases; however, it also depends on the pore size distribution and conductivity. To explain the structural effects, Zhang *et al.*[179] that CNTs with a diameter of about 25 nm and a specific area of 69.5 $m^2 g^{-1}$ had a specific capacitance of 14.1 F g^{-1} and showed excellent rate capability, better than those of entangled CNTs. To improve the graphitization of CNTs, heating is one of the major criteria to remove amorphous carbon and depends on the heating temperature and oxidization.[180,181] With increasing temperature, the specific surface area increases, whereas the average pore diameter decreases and saturates at high temperatures. Chemical activation at surfaces of CNTs also enhances specific capacitance by surface functionalization.[53,182,183] For instance, specific capacitance increased by almost seven times after chemical activation because of the microporosity of pure MWCNTs using chemical KOH activation.[182] Another example of functionalization has been explained by Xiao *et al.*,[184] in which the electrochemical performance was enhanced by the effect of annealing on different functional groups *e.g.*, >CO, >COH and COOH at different temperatures to adjust the redox active functional groups on freestanding CNT films which was achieved at 200 °C that provides long term stability. Higher power density is another characteristic feature that enhances supercapacitor performance and can be achieved by shape engineering of CNTs. Highly densely packed SWCNTs showed higher capacitance and better performance for thick electrodes.[185,186]

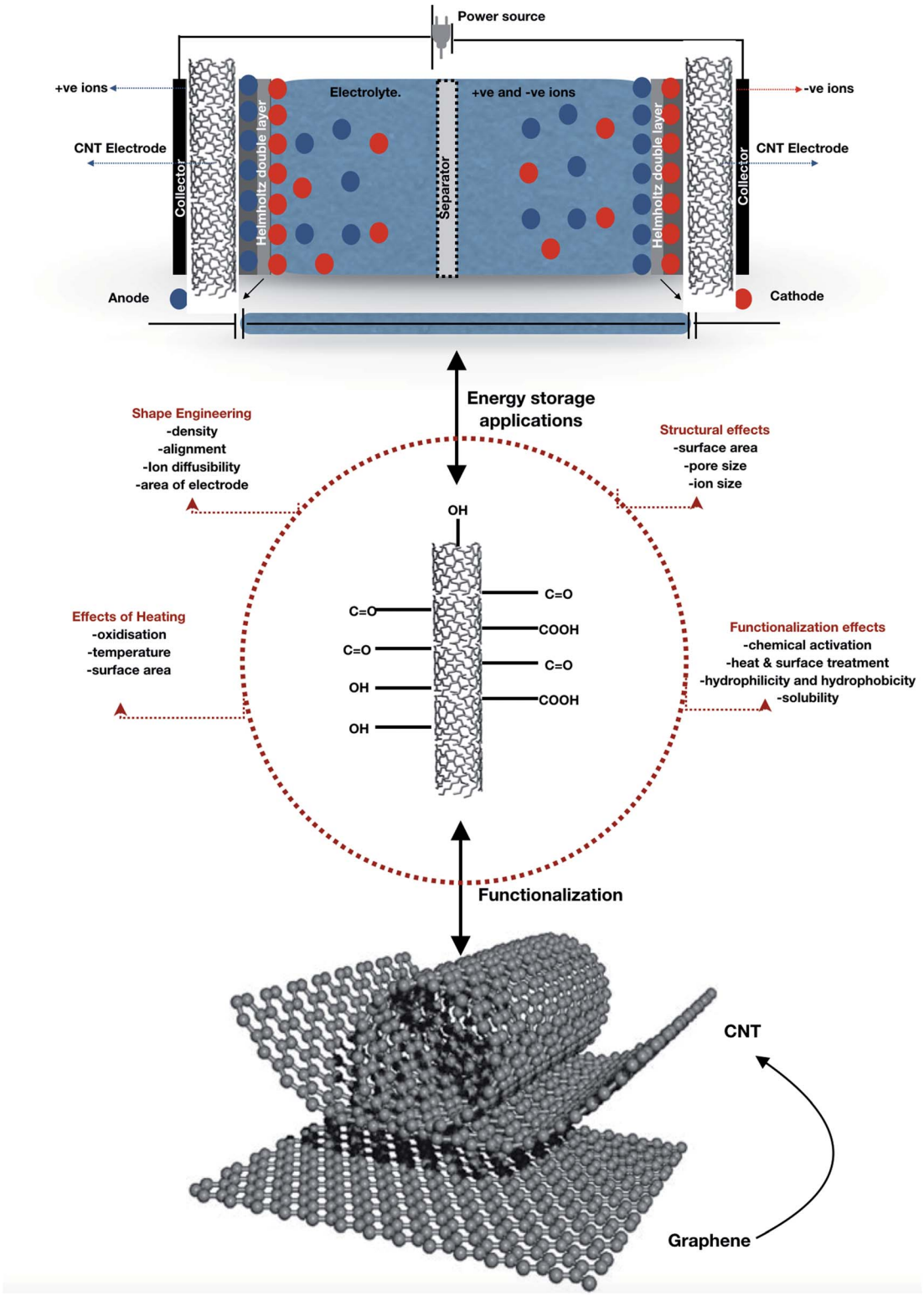

Fig. 13 CNT network for supercapacitor applications and its effects.

Systematical investigations of the aforementioned factors can optimize CNTs for better performance and long-term stability. A new horizon for application of CNTs came into the limelight when Pankratov *et al.*[187] reported on the first self-charging biosupercapacitor based on C*t*CDH/BOD (*Corynascus thermophilus* cellobiose dehydrogenase (C*t*CDH)/bilirubine oxidase (BOD) electrodes for direct electron transfer (DET) communication as shown in Fig. 14.

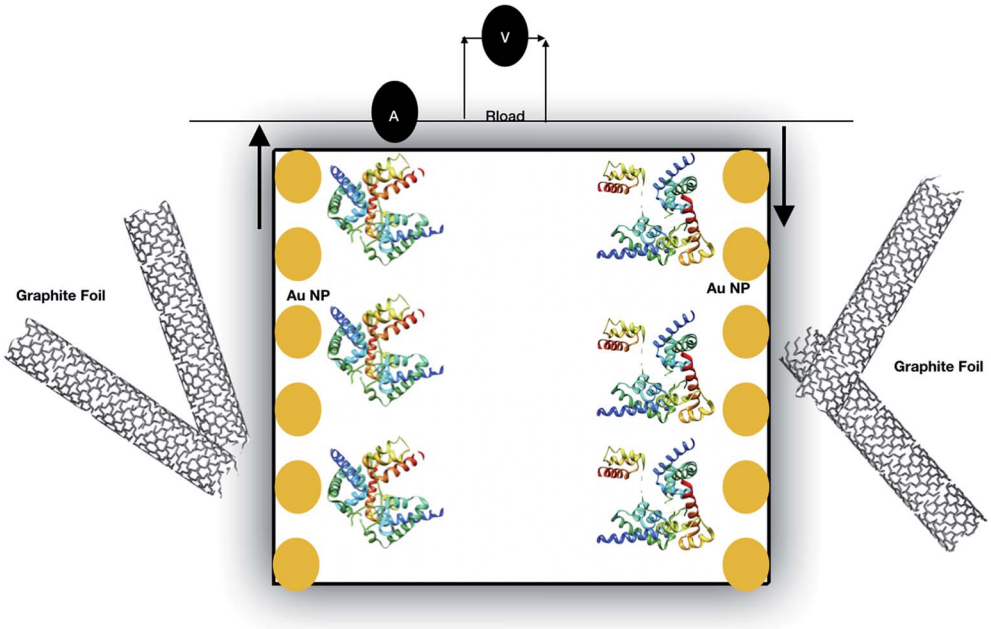

Fig. 14 Self-charging biological supercapacitor; capacitive side was built using graphite foil modified with a polyaniline/CNT composite and the charging side was prepared using an enzymatic fuel cell designed from 3D gold NP (yellow color) based nanobiostructures.[190,479]

The capacitive part of the supercapacitor polyaniline/CNT composite was prepared by drop casting a suspension of nanotubes and electrodepositing a polyaniline film on the electrode surface.[188] The charging part was comprised of CtCDH and *Myrothecium verrucaria* bilirubin oxidase ($MvBO_x$), used as anodic and cathodic bio-elements, respectively, immobilized on gold electrodes modified with 20 nm AuNPs.[189] The self-charging bio-supercapacitor provided a maximum power density of 1.2 mW cm^{-2} at 0.38 V improved by a factor of 170 in comparison to that of state-of-the-art EFCs albeit operating in a pulsed power mode.[190] Carbon-based nanotube networks used for supercapacitors have been proven as promising candidates for energy storage applications. To get an overview of the specific capacitances of CNT based supercapacitors, we used a graphical illustration that is depicted in Fig. 15.

The plot was developed based on the relationship between specific capacitance (F g^{-1} on the *y*-axis) and energy density (W h kg^{-1} on the *x*-axis). The color bar scale represents the specific capacitance, and the category division was done based on energy density values obtained from the references as depicted

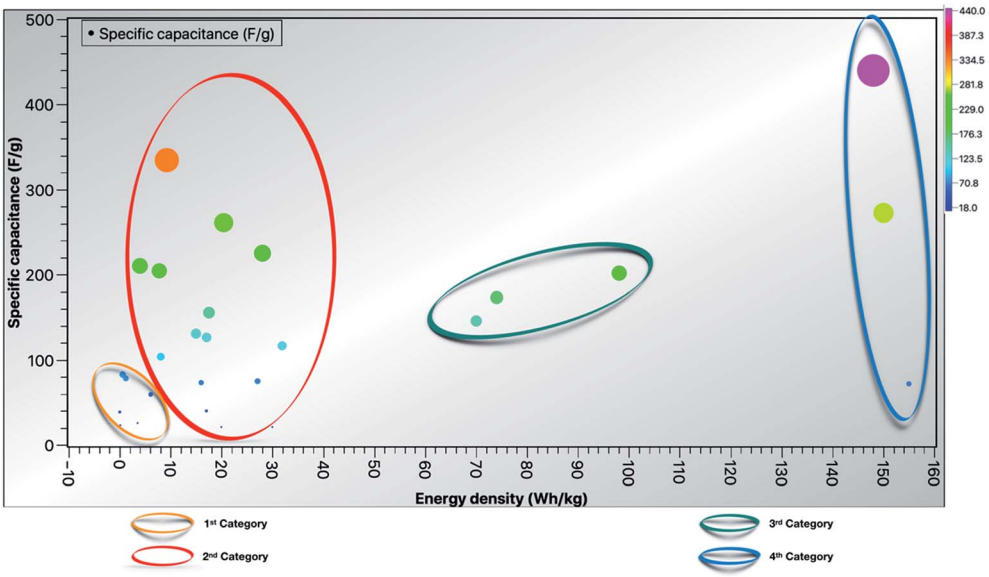

Fig. 15 Relational graph depicting specific capacitance *vs.* energy density in various nanotube network-based supercapacitors.

Table 3 Relationship between specific capacitance (F g^{-1} on the *y*-axis) and energy density (W h kg^{-1} on the *x*-axis) in different materials as shown in Fig. 15

Material	Energy density (W h kg^{-1})	Specific capacitance (F g^{-1})
CNTs	0.02	39
SWCNTs with transferred Cu	0.13	23
AMWCNTS	0.55	83
MWCNTs	1.1	79
CNTs	3.56	25.6
PAN based CNFs	6	60
MWCNTs	7	18
CNF-PAN + Nafion	4	210
CNF bacterial cellulose N, P-codoped	7.76	205
MWCNT catalyst removed by HNO_3	8	104
CNFs and PANI on PAN N_2 doped	9.2	335
PAN/pitch base CNFs	15	130.7
VASWCNTs	16	73
CNF PAN + (PMHS) in DMF	17	127
Nanodiamond	17	40
Graphene sheet thermally reduced in water + IL solution which becomes gel in the end	17.5	156
MWCNTs transferred on Ni foil	20	21
CNF-bridged porous carbon by carbonization activation	20.4	261
VADWCNTs on CP	27	75
Carbon cloth/CNTs	28	225
Purified MWCNTs	30	21
(EG) exfoliated graphene	31.9	117
PAN-CNF + CNTS activation in KOH	70	146
Graphene sphere activated	74	174
CNFs@Ppy annealed at 900 °C	98	202
VAMWCNTs	148	440
Graphene water as a spacer	150	273
Graphene + CNTs on Ti	155	72

in Fig. 15. The 1st category[191–197] consists of supercapacitors with low energy density (0–10 W h kg^{-1}) and specific capacitance below 100 F g^{-1}, the 2nd category[54,56,196,198–208] consists of supercapacitors with energy density in the range of 10–40 W h kg^{-1}, the 3rd category[209–211] consists of supercapacitors with an energy density range of 70–100 W h kg^{-1}, and the 4th category[212–214] consists of supercapacitors with energy density from 140–160 W h kg^{-1} and the description of the materials is tabulated in Table 3. Recent progress in CNT based high-performance supercapacitors has been immensely investigated using various techniques[215–230] and more systematic investigations are needed to achieve high capacitance. However, using composite CNTs, *e.g.* with oxides, polymers or both, as electrodes for the stability of hybrid supercapacitor is still questionable.

Horizons of nanotube networks

Nanotube networks can be used as ultrathin separators made of BNNTs, where 0.5 m thickness is reported,[231] but the most developed role of nanotube-based materials is in constituting supercapacitor electrodes. The reason why nanotubes perform better than, *e.g.*, amorphous carbon (which is a cheaper solution) is believed to be nanotube organization in the hierarchical porous structure, with both micro- and mesopores.[178,232] This nanoscale order especially contributes to improved volumetric capacity, so that smaller devices can be created for microelectronic applications. Currently, CNT-based electrodes are the only ones where volumetric capacity (per cm^3) can be twice the gravimetric capacity (per gram) and over 300 F cm^{-3}, which means they can be relatively heavy in terms of weight but with small dimension. The theoretical limit for the capacitance of carbon-based materials in double-layer charge storage supercapacitors is just below 600 F g^{-1}, as calculated from the specific capacitance of about 20 F cm^{-2} and specific surface area 3000 m^2 g^{-1},[43] and even smaller values were reported.[164] Finite conductivity and geometrically limited full access to the whole surface area limit the specific capacitance of pure carbon-based double-layer charge storage supercapacitors to about 250 F g^{-1} and the practical energy storage limit is then below 10 W h kg^{-1}. In the following, we will first discuss nanotube networks, and then review ways to overcome these limitations. One of the straightforward ways is to use pseudocapacitive or hybrid storage mechanisms, where template-made MgO_2 nanotubes[233] and similar arrangements hold a sort of a record.[43] Another is to employ different (asymmetric) electrode materials to extend the operating voltage window beyond the electrolyte decomposition limit when different potential windows of the electrodes are used to maximize the operating voltage of the full device. In view of the requirements imposed on superconductor electrode materials, especially a hierarchical porous morphology, nanotube networks for such applications are grown in a controlled way. Different kinds of templates are used, like

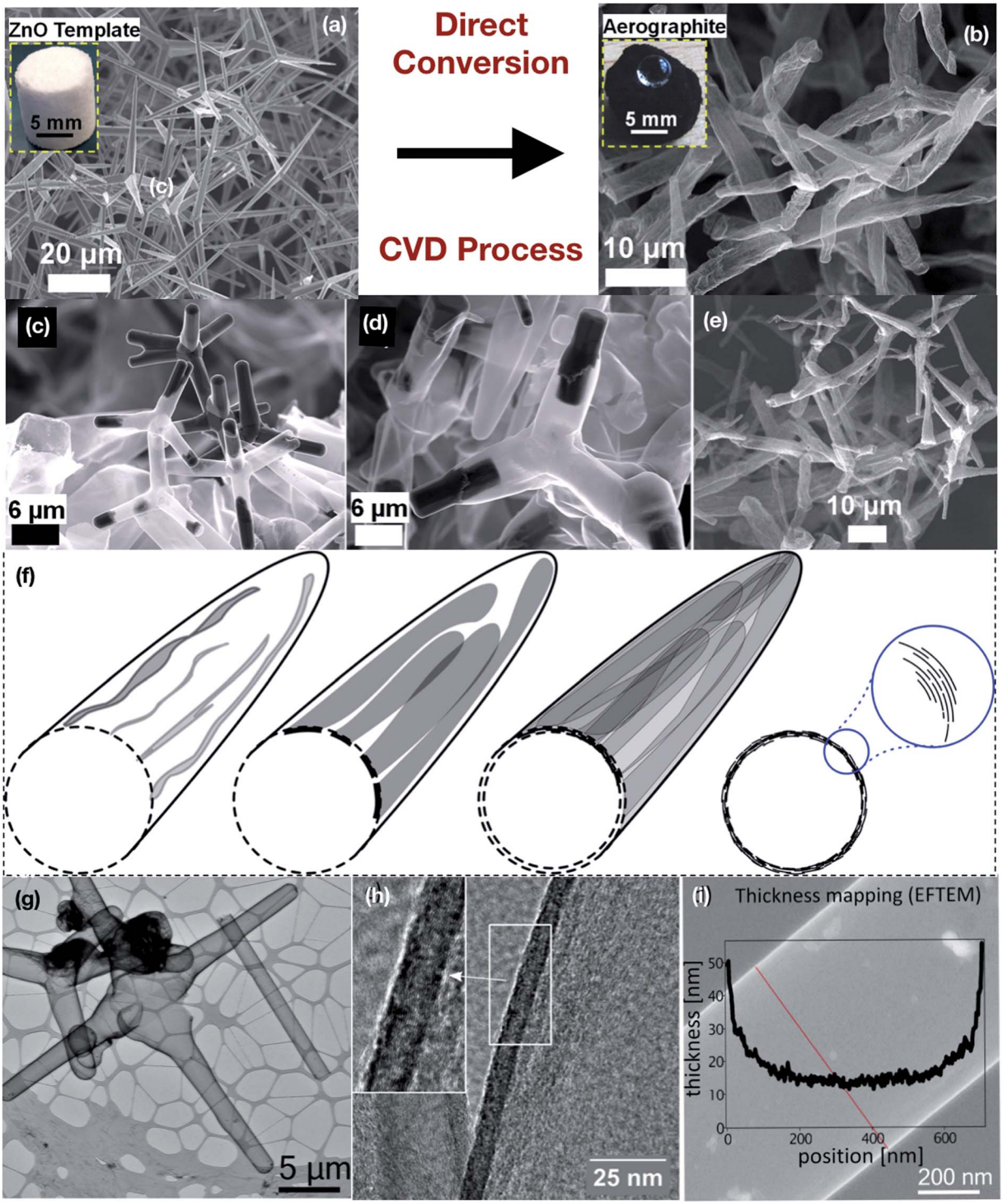

Fig. 16 (a and b) Highly porous ZnO tetrapodal network template transformed into a nano-microtubular carbon based aerographite tetrapod network through the CVD process. Hydrogen gas molecules selectively etch ZnO and toluene gas simultaneously deposits carbon at high temperatures inside the CVD chamber. (a) The SEM image demonstrates the tetrapodal geometry of ZnO structures. (b) Converted carbon based network tetrapodal morphology of the aerographite network. The conversion process takes place *via* selective removal of ZnO.[385] SEM images of aerographite conversion from ZnO: (c) partially converted, (d) almost converted, and (e) completely converted (crumbled aerographite network).[385,480,481] (f) Schematic of sacrificial growth of aerographite tubular carbon arms over ZnO arms through a belt-like growth process. Aerographite structures retain the initial ZnO template architecture which is mainly tetrapodal. The aerographite tetrapods are hollow from inside with a nano-microtubular arm morphology[480,481] in contrast to the initial ZnO template which is solid. (g) TEM image of typical aerographite particles in the 'normal' hollow, closed graphitic shell modification on a lacey carbon grid. (h) HR-TEM image with the parallel view of an aerographite closed shell with a low curvature (diameter of the tubular ligament ≈ 2000 nm). (i) EFTEM was used to investigate the thickness of the intact hollow closed shell aerographite ligament (red line indicates the locations where the thickness measurement was performed). (a–i) have been adapted/reproduced from ref. 385 with permission from Elsevier.[385]

ZnO tetrapods, alumina porous templates, MgO_4, or templates of catalyst particles deposited on a surface to facilitate the growth of a" forest" of nanotubes, often guided with an external field. Later followed strategies have often called on template-free growth methods.[214,234] PANI nanotubes are synthesized using a sodium dodecyl sulfate template. Hierarchical carbon nanotube tube networks created by a direct wet chemical infiltration of dispersed CNTs into a porous ceramic network[235] form self-entangled networks surrounding the ceramic network in the form of a nano-felt assembly, resulting in a double-hierarchical CNTT (CNT tube) architecture.[165] Tubes form an open pore structure with pores in the range of several micrometers, which is beneficial for supercapacitor applications due to the ease of surface accessibility. Also, CNTT–polymer composites were built over these networks. In 2017, a lightweight material aerographite was introduced (Fig. 16). Aerographite[236] is a 3D interconnected carbon foam with a hollow tetrapodal morphology. The electrical conductivity of aerographite is strongly dependent on the wall thickness, the degree of graphitization and the ambient temperature. The wall thickness of aerographite, in turn, can be controlled by a stepwise reduction of solid arms of the sacrificial ZnO template with respect to synthesis time, in which wall thicknesses between 3 and 22 nm can be easily achieved (Fig. 16(a–f)).

The decrease of the wall thickness leads to a reduced electrical conductivity of untreated aerographite (Fig. 16(b)). In contrast, the conductivity of annealed aerographite increased with reducing the wall thicknesses.[236] Aerographite shows a metallic conductive behavior that can be changed to semiconducting by further high-temperature treatment[236] due to the surface defects, charge carrier density and graphitization that increases the electrical conductivity in thin-walled structures and shows low bandgap energies as the bandgap energy is dependent on the wall thickness of aerographite. The unique combination of a high surface area, light weight, large porosity, tunable conductivity, *etc.*, of aerographite makes it a suitable candidate with high potential in the direction of supercapacitor and other energy-related applications.

Nanostructured materials for advanced supercapacitors

Nanotechnology has undoubtedly opened a new avenue enabling new materials and technology for energy storage applications. Out of all the new materials proposed to date for

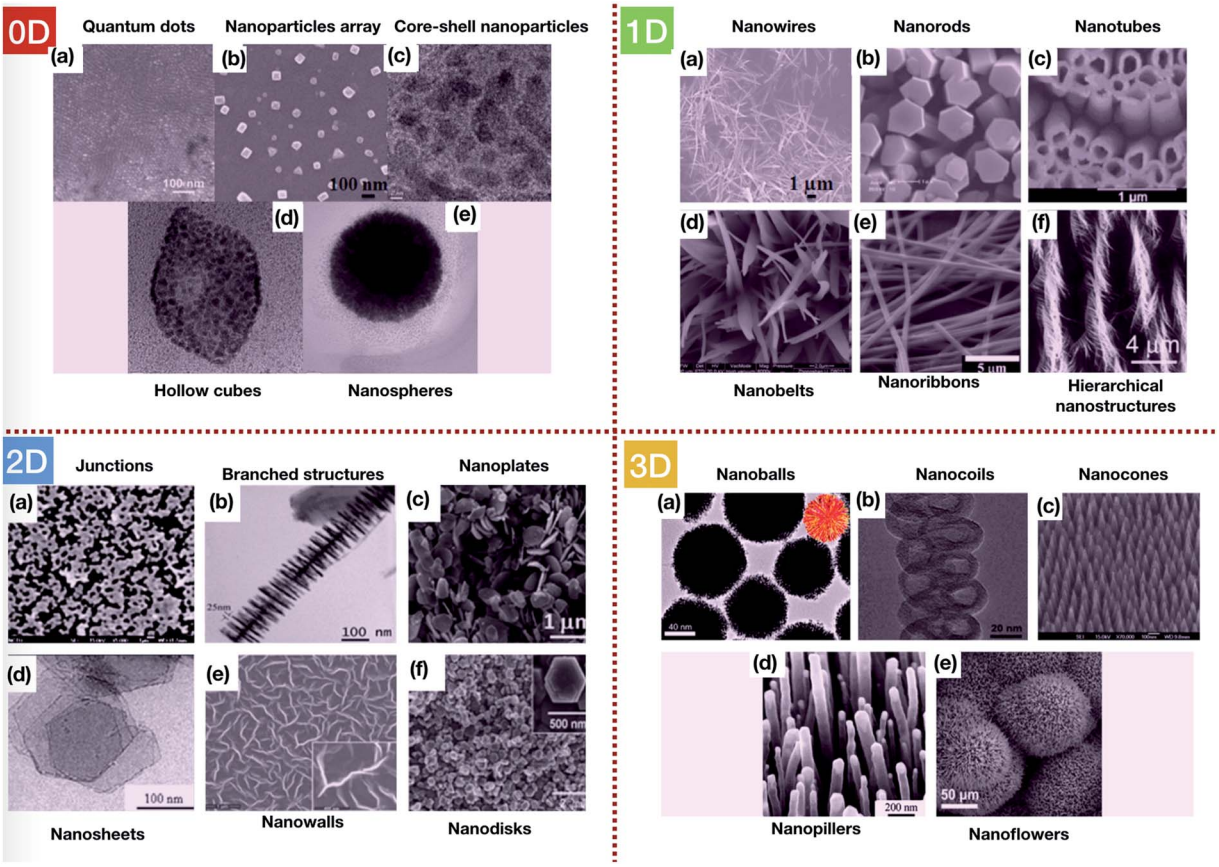

Fig. 17 Typical SEM and TEM images of NSMs, *e.g.* 0D: (a) quantum dots, (b) nanoparticle arrays, (c) core–shell nanoparticles, (d) hollow cubes, and (e) nanospheres. 1D: (a) nanowires, (b) nanorods, (c) nanotubes, (d) nanobelts, (e) nanoribbons, and (f) hierarchical nanostructures. 2D: (a) junctions (continuous islands), (b) branched structures, (c) nanoplates, (d) nanosheets, (e) nanowalls and (f) nanodisks. 3D: (a) nanoballs (dendritic structures), (b) nanocoils, (c) nanocones, (d) nanopillars and (e) nanoflowers. This figure has been adapted/reproduced from ref. 243 with permission from Elsevier.[243]

energy storage applications, graphene has proven to be the mother of all graphitic forms because of its capacity to be wrapped into 0D buckyballs, a roll of 1D nanotubes and a stacked 3D graphite form.[237] These materials continuously spur the development of high capacitive, cost-effective, and highly efficient energy storage. To mitigate the deficiencies imposed by lithium-ion batteries due to the lack of lithium resources,[238–241] nanostructured electrodes play a pivotal role as they possess structure-dependent advantages accelerating the reaction kinetics in the diffusion process as well as achieving good cycling stability. The diversified advantages of various nanostructures for high performance energy storage applications have attracted many researchers to delve into designing electrode materials in many forms such as *e.g.* low dimensional architectures (0D, 1D, 2D, and 3D), and hierarchical & hollow nanostructures which include single-shelled hollow spheres, tubular nanostructures, hollow polyhedrons, yolk-shelled nanostructures, multi-shelled nanostructures and frame like nanostructures.[242] The characteristics of all the diversified nanostructures can be summarized as follows: 0D nanostructures can be amorphous or crystalline and exhibit various shapes and forms being single or polycrystalline, composed of single or multiple chemical elements respectively, generally nanomaterials. 1D nanostructures comprise nanotubes, nanorods, and nanowires being a standalone material or embedded within another medium. 2D nanostructures exhibit plate-like shapes including nanofilms, nanolayers and nanocoatings being single or multi-layered structures deposited on a substrate. 3D nanostructures are not confined within the range of nanoscale in any dimension arbitrarily characterized above 100 nm, composed of multiple arrangements of nanosized crystals in different orientations which contain the dispersion of nanoparticles, bundles of nanowires and multiple nanolayers. Nanostructured materials (NSMs) have been characterized on the basis of dimensionality.[243] 0D NSMs comprise uniform particle arrays, *e.g.* quantum dots,[244] heterogeneous particle arrays, core–shell quantum dots, onions, hollow spheres, and nanolenses. 1D NSMs are ideal systems having a large number of novel phenomena at the nanoscale level. The size and dimensionality of 1D NSMs depends on the structural and functional properties such as nanowires, nanorods,[245] nanotubes,[246] nanobelts,[247] nanoribbons,[248] and hierarchical nanostructures.[249] 2D nanostructures have two dimensions outside of the nanometric size range and comprise junctions, branched structures,[250] nanoprisms, nanoplates,[251] nanosheets,[252] nanowalls[253] and nanodisks.[254] 3D NSMs have a large specific surface area and other superior properties over their bulk counterparts arising from the quantum size effect, *e.g.* nanoballs,[255] nanocoils,[256] nanocones, nanopillars[257] and nanoflowers[258] (Fig. 17). Particular importance has been given to design heterogeneous nanostructures both theoretically and experimentally for energy storage applications. A schema devised by Liu *et al.*[259] (Fig. 18) shows the nanostructured materials used as electrodes acquire high energy densities at high rate capabilities which can be dramatically enhanced if optimal configured nanostructured materials can be chosen. They have classified them into 4 major divisions such as 0-D consisting of core–shell nanoparticles, nanospheres and composite nanoparticles, 1-D consisting of CNTs and nanowire arrays, 2-D consisting of graphene based composites and carbon coated nanobelts and finally 3-D nanostructures

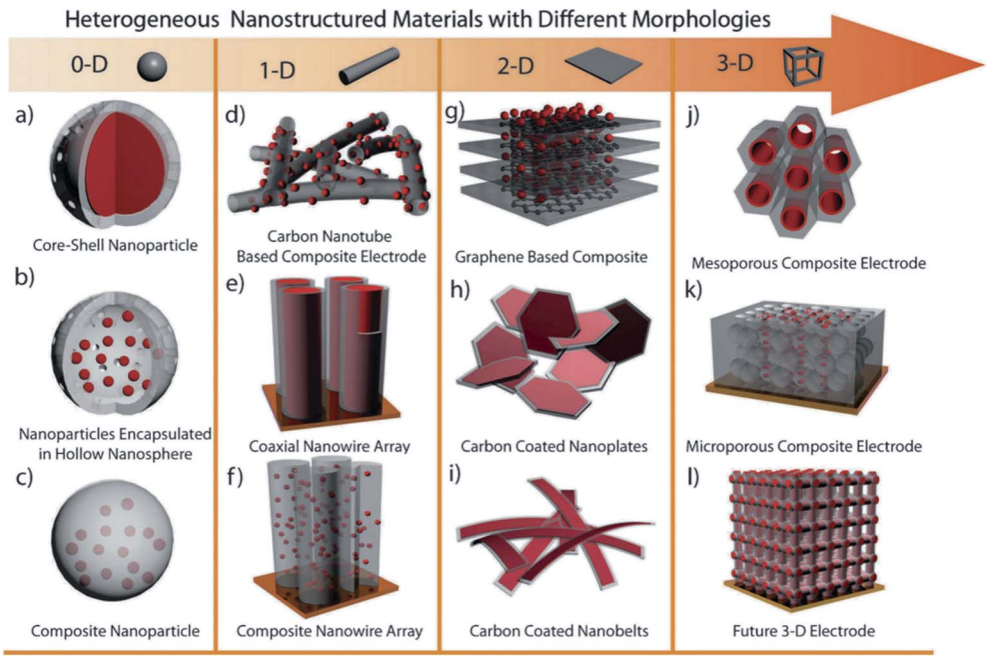

Fig. 18 Schematic illustration of different heterogeneous materials based on structural complexity. This figure has been adapted/reproduced from ref. 259 with permission from the Royal Society of Chemistry.[259]

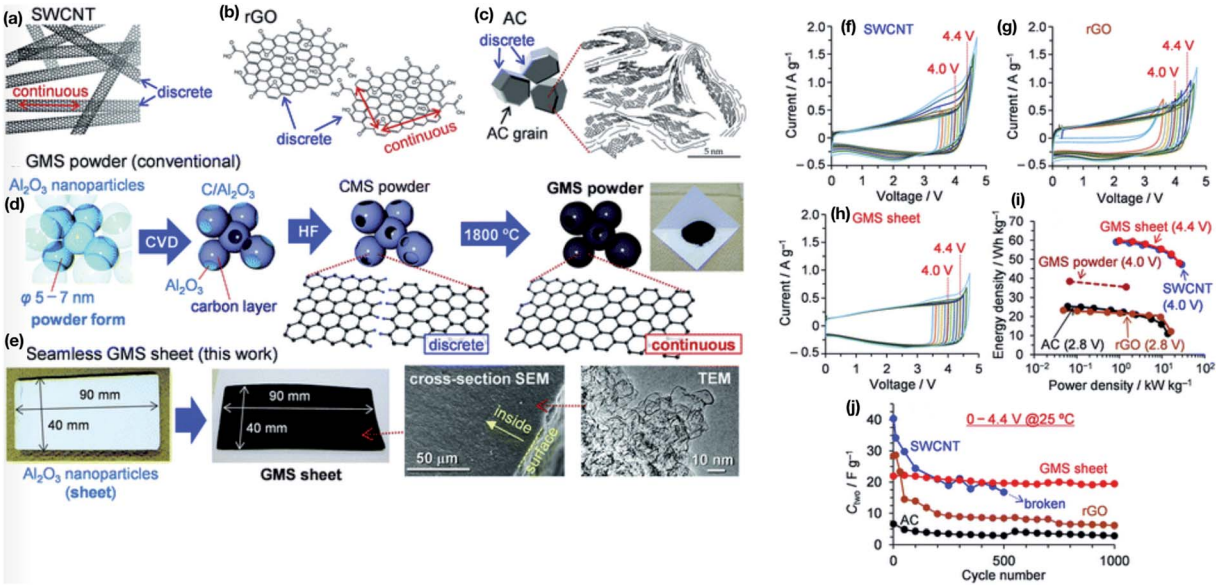

Fig. 19 (a) Carbon materials used in the work of Nomura *et al.* where they have demonstrated a superstable mesoporous carbon sheet made of edge-free graphene walls. The figure depicts (a) SWCNTs (single-walled carbon nanotubes), (b) rGO (reduced graphene oxide), (c) AC (activated carbon), (d) GMS (graphene mesosponge) powder preparation, and (e) sheet-moulded Al_2O_3 nanoparticles and a GMS sheet with cross-sectional SEM and TEM images. (f) Cyclic voltammetric scans of (a) SWCNTs, (g) rGO (reduced graphene oxide) and (h) GMS (graphene mesosponge) performed at 10 mV s^{-1} in 1.5 M TEMA-BF_4/PC. (i) Ragone plot measured at upper limit voltage. (j) Capacitance *vs.* cycle numbers. (a–j) have been adapted/reproduced from ref. 320 with permission from the Royal Society Of Chemistry.[320]

consisting of mesoporous–microporous composite electrodes. Some of the previously reported nanostructures comprising the aforementioned structures have significantly improved the capacitance and storage capabilities for energy storage applications. 0D or quasi-zero-dimensional materials are atomic clusters and nanoparticles which are spatially confined molecular systems possessing an aspect ratio from one to infinity. They can be used as electrode materials with a nanoscale crystalline particle size and show better discharge life due to their high specific surface area eventually improving the power density. Some of the typical examples considering 0D nanoparticles for supercapacitor application include hydrous IrO_2 (ref. 260) (specific capacitance 550 F g^{-1}), SnO_2,[261] and amorphous RuO_2 (ref. 262) (specific capacitance 720 F g^{-1}). He *et al.*[263] found that particle size has an intrinsic effect on reaction kinetics to achieve better cycling stability in 0D nanocrystals. Combining 0D active materials with carbonaceous materials is an effective strategy to improve the efficiency of energy storage.[264] Similarly 1D NSMs are also able to solve the problem of low specific surface area and provide improvisation for electrode active-materials. Zhao *et al.*[265] investigated the nanosizing effects of ultrasmall $FeSe_2$ with a high surface area which exhibits enhanced electrochemical performance with a high capacity of 500 mA h g^{-1}, good rate capability of 250 mA h g^{-1} at 10 A g^{-1}, and superior cycling stability over 400 cycles. 1D nanostructures including metal oxide frameworks,[266–270] carbon-based materials[271–278] and metal chalcogenides[279,280] have distinctive accelerated charge transfer properties. Ou *et al.*[281] synthesized rGO-coated Sb_2Se_3 nanorods that showed a current density of 0.1 A g^{-1}, a good rate capability of 386 mA h g^{-1} at a current density of 2 A g^{-1}, and excellent stability up to 500 cycles. In recent years, 2D nanostructured materials have been a focus in materials research due to their low dimensional characteristics and bulk properties. Their unique shape-dependent characteristics have evolved to their usage in sensors, photocatalysts, energy storage applications, and nanoreactors.[282–284] Hierarchical nanostructures or 3D nanostructures exhibit great cycling stability[259] and reaction kinetics due to their 3D configurations,[285–290] whereas hollow nanostructures owing to their well-defined shell and interior void have versatile features providing extra space for strain and buffering large volume change during reaction improving the cycling stability.[291–306] Owing to the characteristics of nanostructured materials, the performance can be notably differentiated. Hybrid supercapacitors comprising of 3D nanostructures have greater efficiency due to the stoichiometry and arrangement of electrode materials. Li *et al.*[303] fabricated ultrathin MoS_2 nanosheet arrays vertically anchored on bagasse-derived three-dimensional (3D) porous carbon frameworks for an efficient increase in conductivity, high specific capacity and sodium-ion diffusion rates. Gu *et al.*[304] investigated four-layered bismuth oxyhalogens for EDLC's capacitive and pseudo-capacitive behavior. They concluded that due to the faradaic reaction mechanism, BiOI exhibits the highest capacitance among the four bismuth oxyhalogens; due to the high electronegativity of F, BiOF has a higher capacitance than BiOCl and BiOBr and due to the larger interlayer distance, BiOBr has a higher capacitance than BiOCl. Similar work has been proposed for the fine layered structure and properties of Bi_2SiO_5 and $Bi_2O_2CO_3$.[305]

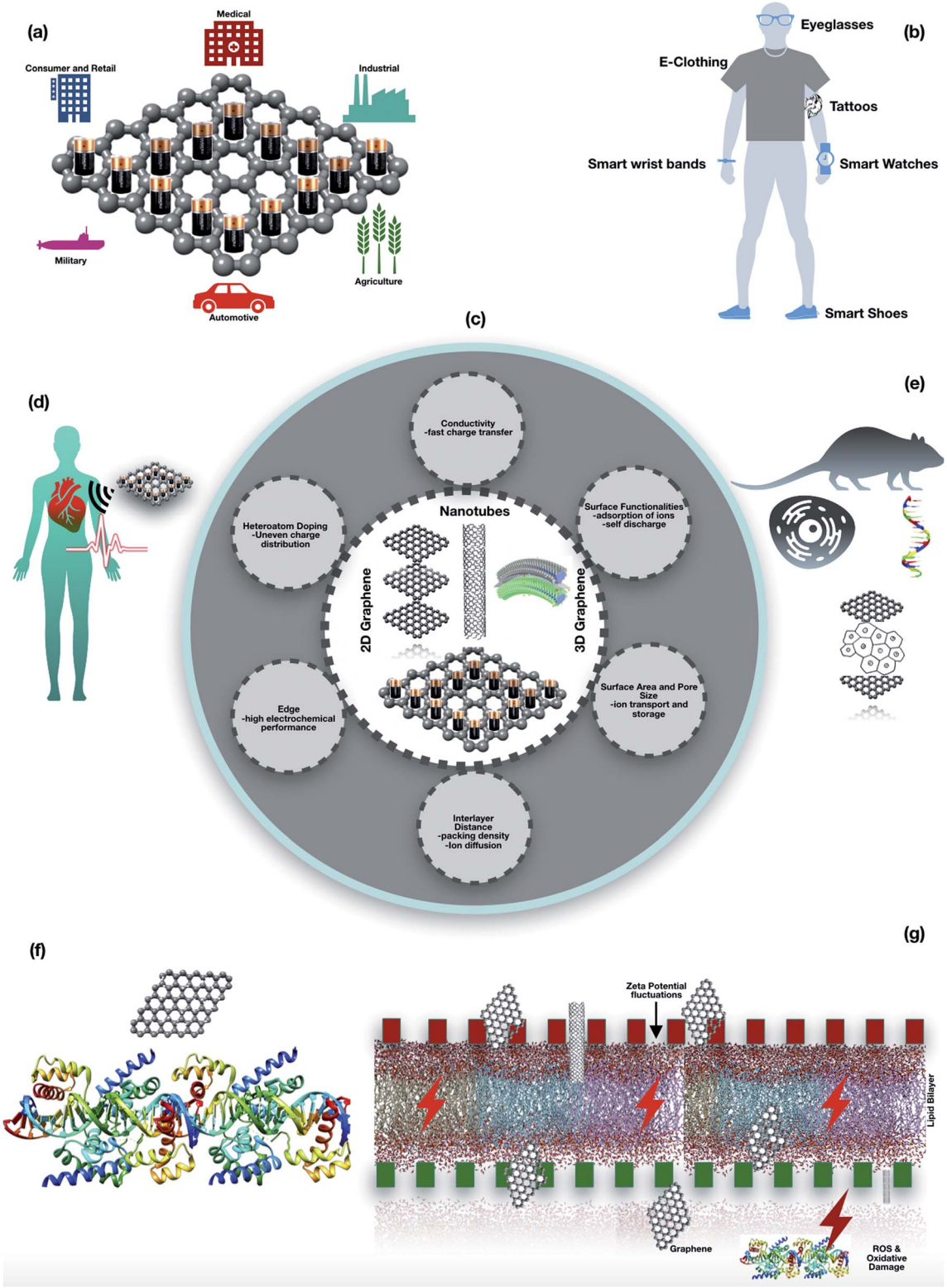

Fig. 20 (a) Application of graphene-based supercapacitors in various sectors. (b) Graphene-based supercapacitors or miniaturized bio-electronics. (c) Properties affecting the synthesis of graphene-based supercapacitors varying from 2D graphene to 3D curved graphene. (d) Improved pacemakers and implantable medical devices. (e) Graphene-based supercapacitors for tissue engineering. (f) Graphene-based supercapacitors for drug-delivery. (g) Antibacterial activity of graphene with altered biological properties.

The imminent fortuity of graphene-based supercapacitors

In this current review, we will now focus on lightweight supercapacitors that have an imminent opportunity to be used widely in the near future, and one such example is graphene where we can expect the scenario of using viable graphene-based supercapacitors using advanced energy storage and recovery solutions.[306,307] Graphene is a thin layer of pure carbon endowed with an abundance of specific features, such as being the best known conductor, environmentally friendly and sustainable, a tightly packed hexagonal honeycomb lattice procuring high strength as it is the thinnest compound with high strength and light absorption characteristics, and it can replace activated carbon in supercapacitors due to its high surface area, light weight and elasticity.[308] Due to its wide range of applicability for instance usage in ultra-fast computers, transforming transportation (cars and aircraft), weaving washable wearables, flexible and transparent solar cells, cleaning up oil spills, desalinating seawater, preventing microbial infections *etc.*, graphene has been considered as potential electrode material for electrochemical energy storage devices.[309] The theoretical upper limit of storing charge previously was estimated to be 550 F g^{-1} based on graphene-based supercapacitors which are compared to current supercapacitors that have a limit of 150 F g^{-1}. One advantage of using graphene as an electrode material is that it doesn't depend on the distribution of pores like other carbon-based materials and has a high surface area that is readily accessible to the electrolytes. Utilizing the intrinsic surface area and surface capacitance, the stacking of graphene layers has been avoided to increase the efficiency of the heterogeneous electron transfer kinetics. For that purpose curved graphene layers were introduced for electrode material preparation where an energy density of 85.6 W h kg^{-1} at room temperature and 136 W h kg^{-1} at 80 °C were measured at a current density of 1 A g^{-1}.[6] Although many approaches have been used to synthesize graphene for supercapacitor applications to prevent agglomerations that tend to restack back to graphite,[200,201,310,311] a novel low temperature based exfoliation of graphene due to unique surface chemistry has been obtained which has a high capacitance rate and good energy storage performance.[312] The restacking and aggregation nature of graphene motivated by strong π-π interaction compromises the capacitance values and leads to reduced conductivity. To overcome the problem of restacking, 3D graphene has attracted a lot of attention .[285,313–319] Conventional supercapacitors use activated carbon as an electrode material whose stability has been compromised for the automobile industry due to instability and high voltage and temperature operations. The typical voltage of single cells using activated carbon is limited to 2.8 V, and the stacking of a large number of cells is thus necessary to achieve 300 to 500 V for automobiles that require high stability and high operating voltage. Single-walled carbon nanotubes (SWCNTs) are superior to ACs in terms of voltage stability and can achieve up to 4.0 V at room temperature. Recently, Nomura *et al.*[320] reported a new electrode material, a seamless mesoporous carbon sheet consisting of continuous graphene walls with a very small number of carbon edge sites (Fig. 19(a–e), which are the origin of corrosion reactions. Using this new material, it is possible to assemble symmetric supercapacitors with excellent stability under 3.5 V@60 °C and 4.4 V@25 °C conditions (Fig. 19(f–j)), even using a conventional organic electrolyte. Moreover, high-voltage operation at 4.4 V makes it possible to achieve 2.7 times higher energy density compared to conventional ACs.

As far as the applications of graphene-based supercapacitors are concerned, several properties modulate the preparation of graphene-based materials to be widely used in different applications that have an intrinsic effect on physical and chemical properties. Properties[321] and characteristics are depicted in Fig. 20(c). An important physical property of supercapacitor electrode materials is electrical conductivity which is imposed by graphene due to fast charge transfer between the electrodes.[26] Another crucial aspect of graphene is surface functionalities where heteroatom doping and introducing functional groups are possible, for instance, oxygen, nitrogen, and sulfur and phenol, keto, ether, and quinone groups respectively.[15,322–324] Other properties such as the edges, surface area, pore size and interlayer distance between the graphene sheets play a major role in increasing capacitance and power density by the mechanism of synthesis for which physicochemical properties have been affected in order to produce better performances.[321] Apart from physicochemical properties, some of the mechanical properties such as stiffness, strength, and toughness affect the multi-functionality of such materials which in turn is a challenge to the industry and scientists to explore further.[325] The development of supercapacitors is driven by their applications (Fig. 20(a)). They include primarily integrated energy sources, especially as a buffer in front of a rechargeable battery. Such use prolongs the battery life and enables fast energy recycling, *e.g.*, from breaking of electric vehicles. Supercapacitors can be made flexible with applications in self-powered (especially piezo and small temperature difference powered devices) and wearable electronics (Fig. 20(b)). The other main aspects of graphene-based biological supercapacitors may enable improved pacemakers and implantable medical devices using ions derived from body fluids which could lead to long-lasting cardiac pacemakers. They work on the principle of graphene layered with a modified human protein as an electrode which is typically 1 μm thick, flexible and twisted inside the body without any mechanical damage while improving the charge storing capacity[326] as depicted in Fig. 20(d). The application is not limited to biomedical applications but has attracted many areas of research such as bioengineering, drug delivery, tissue engineering, biotechnology and bioinformatics[327] (Fig. 20(e)). Another specific example is the antibacterial activity of graphene oxides that have potential effects on therapeutics and disease diagnosis[328] (Fig. 19(f)). Since graphene induces some electrostatic effects the lipid bilayer acts as an electrolyte and graphene as an electrode to induce charge transfer, thereby accelerating the antibacterial activity through reactive oxygen species (ROS) and oxidative stress[329] (Fig. 20(g)). From environmental aspects,

graphene-based materials have additional advantages in addressing global environmental challenges.

Graphene-based materials can be used as a sorbent or photocatalytic material for environmental decontamination for future water treatment and desalination membranes. The exceptional properties of graphene-based materials have also shown progress in the adsorption of several contaminants, metal ions, organic compounds, and gaseous pollutants. Also, graphene-based membranes such as nanoporous graphene membrane sheets and graphene-oxide barriers have an additional advantage in water treatment, water desalination, capacitive deionization, and antimicrobial activity whereas reduced graphene oxide (rGO) is widely used in gas sensing technology (chemical and biological sensing).[330–354] The next important factor influencing EDLC performance is quantum capacitance from electronic structure theory that arises from the limited Density of States (DOS) contribution near the Fermi level due to band filling/emptying during the charging of EDLCs.[355] The effects of quantum capacitance have been firstly observed by Tao *et al.*, on single-layer graphene in an electrochemical cell that showed good agreement with DFT predictions.[356] Later, Ruoff *et al.*[357] studied the layer effect on the capacitance for few-layer graphene electrodes, and Downard *et al.*[358] measured the quantum capacitance of aryldiazonium modified few-layer graphene electrodes. Quantum capacitance can be obtained from the electrode DOS directly[357,359–364] and is relevant for the studies of gated graphene and nanotubes for capacitance–voltage profiling. Ji *et al.*[357] measured the capacitance of one to five-layer graphene in EDLCs where they found that capacitance has been suppressed near neutrality and is abnormally enhanced for thickness below a few layers. Recently, Raha *et al.*[365] investigated a forest-like 3D carbon structure formed from reduced graphene oxide used as an electrode material for high-performance supercapacitors where they validated the effect of quantum capacitance on a graphite sheet based supercapacitor by means of DFT and experimental studies. Zhan *et al.*[366] investigate a novel C_{60}-modified graphene supercapacitor material, which highlights a complex interplay among the surface morphology, electronic structure, and interfacial capacitance, suggesting general improvement strategies for optimizing carbon-based supercapacitor materials. An effective strategy to construct novel electrode materials with high energy storage density has been illustrated by Li *et al.*,[367] using N-doped graphene quantum dots for high-performance flexible supercapacitors. Song *et al.*[368] and many other researchers[369–378] investigated graphene oxide as a supercapacitor electrode material to study the quantum capacitance by means of DFT studies. These observations may shed light on developing new theoretical models based on DFT studies for the improvement of the energy density of carbon-based supercapacitors.

Two-dimensional nanotubular materials for hybrid supercapacitors

Few capacity records are held by nanotube network-based supercapacitors. The reason lies in a generally higher specific surface area of activated carbon materials. However, these structures often lack the required hierarchical morphology. Therefore exceptional capacitances are obtained only at slow voltage scan rates. At about 5 to 10 mV s^{-1} scan rates capacities reach the order of 500 F g^{-1}, which will probably be improved by the time this review is published,[379,380] and the same is true for rationally stacked graphene.[381] Although carbon nanotube network-based supercapacitors so far generally demonstrated slightly lower capacitances, there are some notable exceptions. CVD grown multi-walled CNTs on nickel catalyst particles attached to microfibrous carbon paper and functionalized with carbon aerogel coating yielded 524 F g^{-1} capacitance.[176,381] Here the hierarchical morphology was created from the aerogel to the CNT network and over to microfibers. This result can be 2 to 6 times improved (up to 3000 F g^{-1}) by activating the CNTs, however, at the expense of lower stability.[382] Lower stability with capacitance decreasing with cycling can be understood from self-healing of activated nanotubes, and opening the interior of the tubes with activation provides rate-dependent results. Already in 2011 a polyaniline–MnO_2 nanotube nanocomposite supercapacitor was demonstrated to have 626 F g^{-1} specific capacitance and a corresponding energy density of 17.8 W h kg^{-1}.[383] The way to improve these results is to employ pseudocapacitive charge storage. However, for this purpose the currently used oxide and polymer nanotube networks have an insufficient surface area and conductivity compared to CNTs, graphene and activated carbon.[384] Therefore, it is desirable to develop functionalized carbon nanotube networks suitable for the hybrid storage mechanism. For the first time, the utilization of an ultralight and extremely porous nano-microtubular aerographite tetrapodal network as an electrode interface for electrochemical capacitive energy storage was reported by Parlak *et al.*, in ref. 385. A simple and robust electrode fabrication strategy based on surface functionalized aerographite with optimum selected porosity leads to high specific capacitance (640 F g^{-1}) and high energy (14.2 W h kg^{-1}) and power densities (9.67 $\times$ 10^3 W kg^{-1}). The study also indicates that aerographite shows hybrid capacitive behavior, bearing a double layer and pseudocapacitance simultaneously. Recently Zhou *et al.*[386] showed the fabrication of flexible electrodes based on nanocarbon electronic conductors combined with pseudocapacitive materials for wearable supercapacitors. Novel flexible densified horizontally aligned carbon nanotube arrays (HACNTs) with a controlled nanomorphology for improved ion transport are introduced and combined with a conformally coated poly(3-methylthiophene) (P3MT) conducting polymer to impart pseudocapacitance. The resulting P3MT/HACNT nanocomposite electrodes exhibit a high areal capacitance of 3.1 F cm^{-2} at 5 mA cm^{-2}, with areal capacitance remaining at 1.8 F cm^{-2} even at a current density of 200 mA cm^{-2}. The asymmetric supercapacitor cell also delivers more than 1–2 orders of magnitude improvement in both areal energy and power density over the state-of-the-art cells. Yi *et al.*[387] demonstrated a hybrid supercapacitor constructed from a Si-based anode (with boron doping) and a porous carbon cathode that delivers a capacity of 685 mA Hg^{-1} at a high current density of 6.4 A g^{-1}. The hybrid supercapacitor

Table 4 Progress in nanotubular materials for hybrid supercapacitors

Material	Energy density	Specific/ volumetric capacitance	Cycles	Specific power (W kg^{-1})	Reference
Mo oxide nanotube arrays	—	2000 F cm^{-3}	>10 000	—	450
MoS_2 nanosheets	26 W h kg^{-1}	26.7 F g^{-1}	6000	750 W kg^{-1}	451
Poly(3-oligo(ethylene oxide))thiophene (PD2ET) with SWCNTs	22.5 W h kg^{-1}	399 F g^{-1}	8000	—	452
MnO_{2-x}/MWCNT	—	~259.6 F g^{-1}	>10 000	—	453
(GO)/carbon nanotube (CNT) foams	—	56.69 F g	2000	—	454
POM (polyoxometalate) based inorganic–organic hybrids		986–1611 F g^{-1}	1000		455
CoS_2/NSC-CNT-p	14.1 W h kg^{-1}	544.2 F g^{-1}	2000		456
Bi-metal (Ni wire) organic framework nanosheets Ni@CoNi-MOF/CNT	31.3 mW h cm^{-3}	100 F cm^{-1}	10 000		457
Ag micro/nanoparticles (MNPs) in MWCNTs	—	1083 F g^{-1}	10 000	—	458
Polypyrrole-based hybrid nanostructures		64 F g^{-1}	500		459
TiO_2-VACNT (vertically aligned carbon nanotube) hybrid		16.24 mF cm^{-2}	5000		460
Vertically aligned CNT-TiO_2	0.041 μW h cm^{-2}	6.436 mF cm^{-2}	2000		461
Porous carbon nanotube-graphene hybrid fibers (CNT-GFs)	4.83 mW h cm^{-3}	60.75 F cm^{-1}	10 000		223
Zn–Co–S@HTCSs//Fe_2O_3@PPNTs	85.12 W h kg^{-1}	~149 mA Hg^{-1}	6000	460 W kg^{-1}	462
Carbon nanosheet (CN)/CNT	—	110 mF cm^{-1}	10 000	—	463
Copper hexacyanoferrate (CuHCF)/MWCNT	60.4 W h kg^{-1}	989 F g^{-1}	10 000	0.5 kW kg^{-1}	464
N-Doped carbon nanonet flakes (NCNFs)	—	613 F g^{-1}	20 000	—	465
Copper (Cu) hydroxide nanotube array grafted nickel aluminum layered double hydroxide nanosheets (CH NTAs@NiAl LDH NSs)	24 991.5 μW cm^{-2}	250 μAh cm^{-2}	10 000	—	466
CNT/MnO_2	8.14 mW h cm^{-3}	492 F cm^{-3}	7000	—	467
Ni_6MnO_8@CNTs	58.2 W h kg^{-1}	711 F g^{-1}	5000	831.4 W kg^{-1}	468
Carbon fiber-reinforced cellulose nanofiber/ multiwalled carbon nanotubes (CF-CNF/MWCNT-HAs)	8.93 mW h cm^{-3}	19.4 F cm^{-3}	3000		469
TiO_2 nanotube arrays (TNTAs) TNTAs/C/MnO_2	465 mW h m^{-2}	492 mF cm^{-2}	3000	—	470
Ultrafine tin dioxide (SnO_2)/few-walled carbon nanotubes (FWNTs)	30.63 kW kg^{-1}	220.5 F g^{-1}	1000	512.79 W kg^{-1}	471
Zn_2GeO_4/CNT-O	—	120 F g^{-1}	200 000	—	472

exhibits a high energy density of 128 W h kg^{-1} at 1229 W kg^{-1} with a long cycling life (capacity retention of 70% after 6000 cycles and low self-discharge rate (voltage retention of 82% after 50 hours)). Some of the recent advancements and progress in nanotubular materials for hybrid-based supercapacitors are listed in Table 4.

Metal oxide (MO_x) based nanotube networks for hybrid supercapacitors

The current focus is synthesizing multifunctional materials with ultralow density, a high surface area, and mechanical robustness which are emphasized in energy storage devices.[388] These nanostructured materials have been devised to functionalize in energy storage devices being fabricated on the basis of a high surface area in which electrolyte ions can easily permeate, diffuse with high porosity through these functionalized electrode materials.[389–391] Many efforts have been devoted to incorporating metal oxide frameworks into graphene sheets resulting in 3D composite electrodes[392] as shown in Fig. 21.

We will give some instances where nanostructured metal oxides have been used as a framework for advanced supercapacitors. As reported by Sharma *et al.*,[393] hollow nanostructures of copper oxides with various morphologies have counteracted electrochemical stabilization in their solid counterparts where higher specific capacitance values through cyclic voltammetry and charge–discharge studies have been reported compared to copper oxide-based composites with CNTs, graphene and rGO. The specific capacitance as reported was estimated to be 144 F g^{-1} at a current density of 1.0 A g^{-1} as compared to conventional Cu_2O/rGO,[394] microstructures,[395] and nanoparticle-MWCNTs[396] with capacitance values of 31 F g^{-1}, 173 F g^{-1}, and 132 F g^{-1} at current density values of 0.1 A g^{-1}, 0.1 A g^{-1}, and 2.5 A g^{-1} respectively. The first metal oxides (RuO_2), which brought limelight to pseudo-capacitors with very high specific capacitance values was never used as a framework for energy storage devices,[397] due to high toxicity and cost. Rather alternative approaches *e.g.* hybrid composites were considered. For example, RuO_2/CNT (anode) based composite materials delivered high power with the aim of developing

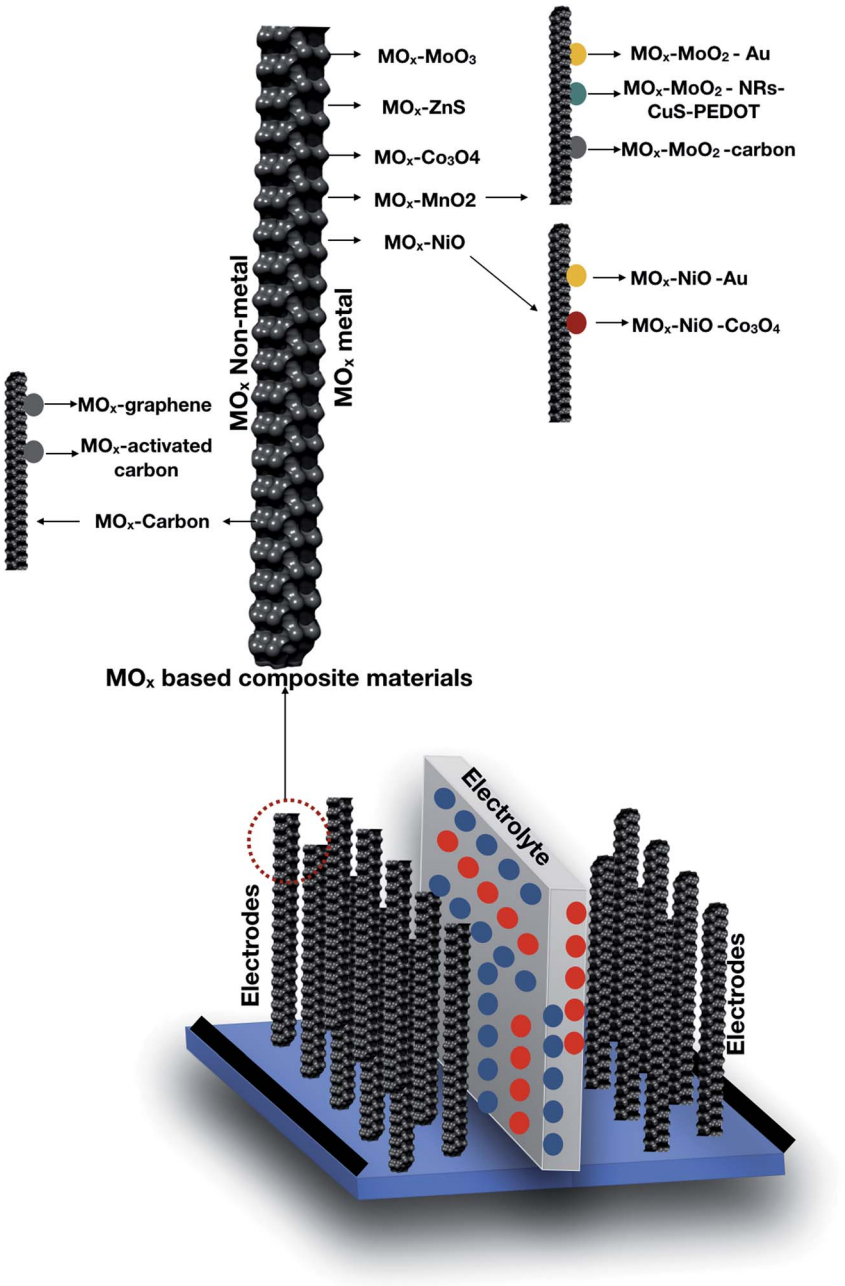

Fig. 21 Metal oxide (MO_x) based composite materials for advanced supercapacitors, including composites doped with metal and nonmetallic materials.

hybrid capacitors in combination with $Co(OH)_2$/CNTs (cathode) without loss of energy where the maximum energy density and specific power density of the cell reach the value of 23.7 W h kg^{-1} and 8.1 kW kg^{-1}, respectively.[398] For a high-performance supercapacitor, MnO_2 as a pseudocapacitive material has been extensively investigated for fabricating fiber shaped supercapacitors in combination with CNTs. Gong *et al.* investigated[399] a fiber shaped supercapacitor with coaxial Ni as the current collector based on a CNT/MnO_2 hybrid nanostructure shell with a capacitance of 231 mF cm^{-1}. It works on the principle of redox interactions and ion intercalation/deintercalation and has vast applications in wearable electronic devices. Recently, vanadium oxide (V_2O_5), a cheap transition metal oxide in combination with CNTs, has become a promising candidate in supercapacitor application.[400] It possesses high porosity and high pore volume that ensures electrolyte deposition on high surface area electrodes within the range of nanometer-scale showing a high specific capacity of 452 mA h g^{-1} and retaining up to 65% of the capacity while discharging. Mandal *et al.*[401] investigated the same with a thin film coating of ~6 nm V_2O_5 that has a high capacity of 680 mA h g^{-1} with a 67% retention rate during discharge cycles. Low-cost zinc oxide (ZnO) based composite materials have a greater impact on advanced supercapacitors due to their viable properties such as good electrochemical

reversibility, eco-friendliness, good cycling stability and simple preparation. Kalpana *et al.* first reported a ZnO/carbon aerogel[402] composite where ZnO electrode porosity improves charge/discharge cycles with the capacitance of the mixed oxide electrode/carbon aerogel being 375 F g^{-1} at 75 mA cm^{-2}. Wu *et al.*[403] successfully synthesized ZnO/rGO compounds with uniform incorporation of RGO sheets into the ZnO matrix and achieved a specific capacitance of up to 308 F g^{-1} at 1 A g^{-1}, and only 6.5% of the available capacity was attenuated after more than 1500 cycles. Du *et al.* reported that a rGO and honeycomb-like ZnO particle mixed material exhibited an improved capacitance of 231 F g^{-1} at 0.1 A g^{-1} due to the presence of spacers and also at the same time flower-like ZnO decorated rGO was reported with a specific capacitance of 149 F g^{-1} at 0.1 A g^{-1}.[404,405] Bi *et al.*[406] demonstrated the molecular dynamics simulation of the structure and performance of conductive metal–organic framework (MOF) electrodes for supercapacitors with room temperature ionic liquids. They applied jump-wise voltages between two identical electrodes and monitored the charge dynamics of applied voltage. They achieved a gravimetric energy density of ~57 W h kg^{-1} at a cell voltage of 4 V. The MOF with the smallest pore diameter (0.81 nm) gives 8.8 μF cm^{-2} at −1.1 and +1.5 V and a pore diameter of 1.57 nm delivers a capacitance of ~10 μF cm^{-2} from −0.5 to +0.5 V. Also, to obtain the best gravimetric performance, they have chosen MOFs with the largest pore size ~2.39 nm that delivered a higher energy of 57 W h kg^{-1} and power density of 135–390 kW kg^{-1} at a cell voltage of 4 V.

Summary & outlook

In this review, we have summarized and systematically outlined the conventional strategies associated with the development of nanotube network-based supercapacitor materials, their properties, and their implications for supercapacitors' performance. CNTs used for supercapacitor electrodes generally provide lower specific capacitance than in the case of activated carbon. Nevertheless, the mesoporous structure of CNTs results in higher electrode conductivity and consequently higher specific power. Functionalization with metallic oxides or conductive polymers in the CNT material results in higher specific capacitance if such a composite is used for supercapacitor electrodes. Composites such as MoS_2 nanosheets anchored on N-doped carbon microspheres with pseudocapacitive properties achieve excellent rate capacity and cycling stability[407] which shows good application potential, along with a maximum energy density of 120 W h kg^{-1} and capacity retention of 85.5% over 4000 cycles. But, with the ever-increasing demand for energy storage applications, lithium-ion batteries cannot meet such requirements due to lack of lithium resources and uneven global distribution. Researchers are now focused on potassium ion storage technology as a promising substitute for energy storage applications. Chen *et al.* proposed disordered, large interlayer spacing and oxygen-rich carbon nanosheets for potassium ion hybrid capacitors which promisingly showed a high energy density of 149 W h kg^{-1}, an ultrahigh power output of 21 kW kg^{-1}, and a long cycling life (80% capacity retention after 5000 cycles).[408] As another such example 3D hierarchical $NiCo_2O_4$ nanosheets/carbon nanotubes/carbon cloth as a flexible electrode material for electrochemical capacitors showed a maximum specific capacitance of 1518 F g^{-1} at a scan rate of 5 mV s^{-1} in 2 mol L^{-1} KOH aqueous solution and excellent stability under the conditions of long term cycling, mechanical bending and twisting conditions.[409] A recent paper on a metal oxide-based supercapacitor using copper oxide nanoparticles with a multi-walled nanotube nanocomposite yielded a specific capacitance of 452.8 F g^{-1} at a 10 mV s^{-1} scan rate. Also, the nanocomposite exhibited good cycling stability with 90% capacity retention over 500 charge–discharge cycles.[410] 3D polyaniline nanothorns on buckypaper as an electrode exhibit a high specific capacitance of 742 F g^{-1} at 1 A g^{-1} in a 1 M H_2SO_4 electrolyte and a capacitance retention of 76% after 2000 cycles.[411] As a supercapacitor electrode material, $NiCo_2S_4$ nanotubes with a unique hollow and spinous structure exhibit a good specific capacitance (630 F g^{-1} at 1 A g^{-1}), low internal resistance R_s (0.68 Ω) and high capacitance retention (91% after 3000 cycles) at 10 A g^{-1}.[412] Some of the recent developments in high-performance supercapacitors using nanotubular networks have opened a new avenue for exploring techniques, specifically electrode characterization and modulations, to achieve high power density, capacity retention, and good cyclability.[215,216,223–227,264,386,413–433] Although the advancements and implementations of nanotubular networks in supercapacitors have significantly achieved better storage capabilities and performance, tailoring and optimization of materials are still in a developmental phase where cost-effectiveness and good performance are some of the key concerns in practical applicability. In an attempt to develop a combination of high power and energy densities, hybrid technology is one of the challenging aspects. For that we need better understanding of surface chemistry between electrode materials and electrolytes to improve the interfacial interactions favorable for enhanced charge transfer. Nanoarchitectures play a vital role in establishing a structure–property synergy between different components such as porous electrode materials. Thus, surface-functionalized engineered materials need to be intensively explored to obtain an optimized supercapacitor which can deal with the energy crisis we are facing today.

Conflicts of interest

There are no conflicts to declare.

Acknowledgements

The authors acknowledge the financial support from the Swedish Research Council.

References

1 R. Kötz and M. Carlen, *Electrochim. Acta*, 2000, **45**, 2483–2498.
2 J. Ho, T. R. Jow and S. Boggs, *IEEE Electr. Insul. Mag.*, 2010, **26**, 20–25.

3 T. Garite, B. Snell, D. Walker and V. Darrow, *Obstet. Gynecol.*, 1995, **86**, 411–416.
4 B. E. Conway, *J. Electrochem. Soc.*, 1991, **138**, 1539.
5 K. Naoi, P. Simon, *J. Electrochem. Soc.*, 2008, **17**, 34–37.
6 C. Liu, Z. Yu, D. Neff, A. Zhamu and B. Z. Jang, *Nano Lett.*, 2010, **10**, 4863–4868.
7 F. Bonaccorso, L. Colombo, G. Yu, M. Stoller, V. Tozzini, A. C. Ferrari, R. S. Ruoff and V. Pellegrini, *Science*, 2015, **347**, 1246501.
8 A. Yu, A. Davies and Z. Chen, in *Electrochemical Technologies for Energy Storage and Conversion*, Wiley-VCH Verlag GmbH & Co. KGaA, Weinheim, Germany, 2012, vol. 1, pp. 317–382.
9 P. Simon and Y. Gogotsi, in *Materials for Sustainable Energy*, Co-Published with Macmillan Publishers Ltd, UK, 2010, pp. 138–147.
10 R. Berenguer, *Bol. Grupo Español Carbón*, 2015, 9–13.
11 A. Lewandowski, A. Olejniczak, M. Galinski and I. Stepniak, *J. Power Sources*, 2010, **195**, 5814–5819.
12 Y. Chen, X. Zhang, D. Zhang, P. Yu and Y. Ma, *Carbon*, 2011, **49**, 573–580.
13 F. Wang, S. Xiao, Y. Hou, C. Hu, L. Liu and Y. Wu, *RSC Adv.*, 2013, **3**, 13059.
14 L. Chang and Y. Hang Hu, *Compr. Energy Syst.*, 2018, **2–5**, 663–695.
15 E. Frackowiak, Q. Abbas and F. Béguin, *J. Energy Chem.*, 2013, **22**, 226–240.
16 F. Béguin and E. Frackowiak, *Supercapacitors*, Wiley-VCH Verlag GmbH & Co. KGaA, Weinheim, Germany, 2013.
17 Z. Tan, G. Chen and Y. Zhu, *Science*, 2015, **1**, 211–225.
18 L. Demarconnay, E. G. Calvo, L. Timperman, M. Anouti, D. Lemordant, E. Raymundo-Piñero, A. Arenillas, J. A. Menéndez and F. Béguin, *Electrochim. Acta*, 2013, **108**, 361–368.
19 G. P. Pandey, Y. Kumar and S. A. Hashmi, *Indian J. Chem., Sect. A: Inorg., Phys., Theor. Anal.*, 2010, **49**, 743–751.
20 G. Feng, S. Li, V. Presser and P. T. Cummings, *J. Phys. Chem. Lett.*, 2013, **4**, 3367–3376.
21 C. Arbizzani, S. Beninati, M. Lazzari, F. Soavi and M. Mastragostino, *J. Power Sources*, 2007, **174**, 648–652.
22 P. T. Ha, H. Moon, B. H. Kim, H. Y. Ng and I. S. Chang, *Biosens. Bioelectron.*, 2010, **25**, 1629–1634.
23 A. Javaid, in *Activated Carbon Fiber and Textiles*, Elsevier, 2017, pp. 281–303.
24 A. Muzaffar, M. B. Ahamed, K. Deshmukh and J. Thirumalai, *Renewable Sustainable Energy Rev.*, 2019.
25 W. Zuo, R. Li, C. Zhou, Y. Li, J. Xia and J. Liu, *Adv. Sci.*, 2017.
26 A. G. Pandolfo and A. F. Hollenkamp, *J. Power Sources*, 2006, **157**, 11–27.
27 P. Gómez-Romero, O. Ayyad, J. Suárez-Guevara and D. Muñoz-Rojas, *J. Solid State Electrochem.*, 2010, **14**, 1939–1945.
28 D. Tie, S. Huang, J. Wang, J. Ma, J. Zhang and Y. Zhao, *Energy Storage Mater.*, 2019, **21**, 22–40.
29 E. S. Kim, E. H. Ahn, T. Dvir and D. H. Kim, *Int. J. Nanomedicine*, 2014, **9**, 1–5.
30 D. P. Dubal, O. Ayyad, V. Ruiz and P. Gómez-Romero, *Chem. Soc. Rev.*, 2015, **44**, 1777–1790.
31 Y. Wang and Y. Xia, *Adv. Mater.*, 2013, **25**, 5336–5342.
32 Y. Huang, Y. Li, Q. Gong, G. Zhao, P. Zheng, J. Bai, J. Gan, M. Zhao, Y. Shao, D. Wang, L. Liu, G. Zou, D. Zhuang, J. Liang, H. Zhu and C. Nan, *ACS Appl. Mater. Interfaces*, 2018, **10**, 16572–16580.
33 H.-C. Wu, Y.-P. Lin, E. Lee, W.-T. Lin, J.-K. Hu, H.-C. Chen and N.-L. Wu, *Mater. Chem. Phys.*, 2009, **117**, 294–300.
34 K. Ku, B. Kim, H. Chung and W. Kim, *Synth. Met.*, 2010, **160**, 2613–2617.
35 Z. Ren, Y. Li and J. Yu, *iScience*, 2018, **9**, 138–148.
36 C. U. Jeong, S.-Y. Lee, J. Kim, K. Y. Cho and S. Yoon, *J. Power Sources*, 2018, **398**, 193–200.
37 L. Tong, K. H. Skorenko, A. C. Faucett, S. M. Boyer, J. Liu, J. M. Mativetsky, W. E. Bernier and W. E. Jones, *J. Power Sources*, 2015, **297**, 195–201.
38 A. Burke, *J. Power Sources*, 2000, **91**, 37–50.
39 A. S. Aricò, P. Bruce, B. Scrosati, J. M. Tarascon and W. Van Schalkwijk, *Nat. Mater.*, 2005, **4**, 366–377.
40 A. Chu and P. Braatz, *J. Power Sources*, 2002, **112**, 236–246.
41 G. Z. Chen, *Int. Mater. Rev.*, 2017, **62**, 173–202.
42 M. Salanne, B. Rotenberg, K. Naoi, K. Kaneko, P.-L. Taberna, C. P. Grey, B. Dunn and P. Simon, *Nat. Energy*, 2016, **1**, 16070.
43 Y. Shao, M. F. El-Kady, J. Sun, Y. Li, Q. Zhang, M. Zhu, H. Wang, B. Dunn and R. B. Kaner, *Chem. Rev.*, 2018, **118**, 9233–9280.
44 J. R. Miller and A. F. Burke, *Electrochem. Soc. Interface*, 2008, **17**, 53–57.
45 B. E. Conway, V. Birss and J. Wojtowicz, *J. Power Sources*, 1997, **66**, 1–14.
46 T. Brousse, D. Bélanger and J. W. Long, *J. Electrochem. Soc.*, 2015, **162**, A5185–A5189.
47 Y. Zhang, X. Cui, L. Zu, X. Cai, Y. Liu, X. Wang and H. Lian, *Materials*, 2016, **9**, 734.
48 J. R. Miller and A. F. Burke, *Electrochem. Soc. Interface*, 2008, **17**, 53–57.
49 D. Shin, Y. Kim, J. Seo, N. Chang, Y. Wang and M. Pedram, in *Proceedings Design, Automation and Test in Europe*, Date, 2011.
50 Cadex Electronics Inc., *How Does a Supercapacitor Work*, 2019.
51 R. A. Dougal, S. Liu and R. E. White, *IEEE Trans. Compon. Packag. Technol.*, 2002, **25**, 120–131.
52 E. Frackowiak and F. Béguin, *Carbon*, 2001, **39**, 937–950.
53 E. Frackowiak, K. Metenier, V. Bertagna and F. Beguin, *Appl. Phys. Lett.*, 2000, **77**, 2421–2423.
54 C. Niu, E. K. Sichel, R. Hoch, D. Moy and H. Tennent, *Appl. Phys. Lett.*, 1997, **70**, 1480–1482.
55 K. H. An, W. S. Kim, Y. S. Park, H. J. Jeong, Y. C. Choi, J. M. Moon, D. J. Bae, S. C. Lim and Y. H. Lee, *AIP Conf. Proc.*, 2001, **590**, 241–244.
56 C. Du, J. Yeh and N. Pan, *Nanotechnology*, 2005, **16**, 350–353.
57 B. J. Yoon, S. H. Jeong, K. H. Lee, H. Seok Kim, C. Gyung Park and J. Hun Han, *Chem. Phys. Lett.*, 2004, **388**, 170–174.
58 A. Muhulet, F. Miculescu, S. I. Voicu, F. Schütt, V. K. Thakur and Y. K. Mishra, *Mater. Today Energy*, 2018, **9**, 154–186.

59 H. Yang, S. Kannappan, A. S. Pandian, J.-H. Jang, Y. S. Lee and W. Lu, *Nanotechnology*, 2017, **28**, 445401.
60 K. Yu, Z. Wen, H. Pu, G. Lu, Z. Bo, H. Kim, Y. Qian, E. Andrew, S. Mao and J. Chen, *J. Mater. Chem. A*, 2013, **1**, 188–193.
61 Y. Gogotsi, A. Nikitin, H. Ye, W. Zhou, J. E. Fischer, B. Yi, H. C. Foley and M. W. Barsoum, *Nat. Mater.*, 2003, **2**, 591–594.
62 J. Chmiola, G. Yushin, Y. Gogotsi, C. Portet, P. Simon and P. L. Taberna, *Science*, 2006, **313**, 1760–1763.
63 C. Kjølseth, H. Fjeld, Ø. Prytz, P. I. Dahl, C. Estournès, R. Haugsrud and T. Norby, *Solid State Ionics*, 2010, **181**, 268–275.
64 A. J. Chmiola, G. Yushin, Y. Gogotsi, C. Portet, P. Simon and P. L. Taberna, *Science*, 2006, **313**, 1760–1763.
65 R. de Levie and A. Vogt, *J. Electroanal. Chem.*, 1992, **341**, 353–360.
66 J. Dzubiella and J.-P. Hansen, *J. Chem. Phys.*, 2005, **122**, 234706.
67 J. Marañón Di Leo and J. Marañón, *J. Mol. Struct.: THEOCHEM*, 2005, **729**, 53–57.
68 M. Carrillo-Tripp, H. Saint-Martin and I. Ortega-Blake, *Phys. Rev. Lett.*, 2004, **93**, 168104.
69 T. Ohkubo, T. Konishi, Y. Hattori, H. Kanoh, T. Fujikawa and K. Kaneko, *J. Am. Chem. Soc.*, 2002, **124**, 11860–11861.
70 Q. Lu, J. G. Chen and J. Q. Xiao, *Angew. Chem., Int. Ed.*, 2013, **52**, 1882–1889.
71 J. Gamby, P. L. Taberna, P. Simon, J. F. Fauvarque and M. Chesneau, *J. Power Sources*, 2001, **101**, 109–116.
72 K. Kiyohara, T. Sugino and K. Asaka, *J. Chem. Phys.*, 2010, **132**, 144705.
73 A. A. Kornyshev, *Faraday Discuss.*, 2013, **164**, 117.
74 H. Itoi, H. Nishihara and T. Kyotani, *Langmuir*, 2016, **32**, 11997–12004.
75 L. Han, K. G. Karthikeyan, M. A. Anderson and K. B. Gregory, *J. Colloid Interface Sci.*, 2014, **430**, 93–99.
76 S. M. Jung, D. L. Mafra, C. Te Lin, H. Y. Jung and J. Kong, *Nanoscale*, 2015, **7**, 4386–4393.
77 K. Urita, C. Urita, K. Fujita, K. Horio, M. Yoshida and I. Moriguchi, *Nanoscale*, 2017, **9**, 15643–15649.
78 X. Gao, S. Porada, A. Omosebi, K. L. Liu, P. M. Biesheuvel and J. Landon, *Water Res.*, 2016, **92**, 275–282.
79 H. L. K. S. Mosch, O. Akintola, W. Plass, S. Höppener, U. S. Schubert and A. Ignaszak, *Langmuir*, 2016, **32**, 4440–4449.
80 M. Sevilla and A. B. Fuertes, *ChemSusChem*, 2016, **9**, 1880–1888.
81 J.-G. Li, Y.-F. Ho, M. M. M. Ahmed, H.-C. Liang and S.-W. Kuo, *Chem.–Eur. J.*, 2019, **18**, 6208–6216.
82 H. Itoi, H. Nishihara and T. Kyotani, *Langmuir*, 2016, **32**, 11997–12004.
83 C. Lian, X. Kong, H. Liu and J. Wu, *J. Phys.: Condens. Matter*, 2016, **28**, 464008.
84 A. Aldalbahi, M. Rahaman, M. Almoigli, A. Meriey and K. Alharbi, *Nanomaterials*, 2018, **8**, 19.
85 S. M. Jung, D. L. Mafra, C. Te Lin, H. Y. Jung and J. Kong, *Nanoscale*, 2015, **7**, 4386–4393.
86 Y. Lee, S. Noh, M. S. Kim, H. J. Kong, K. Im, O. S. Kwon, S. Kim and H. Yoon, *Nanoscale*, 2016, **8**, 11940–11948.
87 M. Seredych, E. Rodríguez-Castellõn and T. J. Bandosz, *ChemSusChem*, 2015, **8**, 1955–1965.
88 G. Wu, Y. Hu, Y. Liu, J. Zhao, X. Chen, V. Whoehling, C. Plesse, G. T. M. Nguyen, F. Vidal and W. Chen, *Nat. Commun.*, 2015, **6**, 7258.
89 A. Pramanik, S. Maiti and S. Mahanty, *Dalton Trans.*, 2015, **44**, 14604–14612.
90 K. Lee, H. Song, K. H. Lee, S. H. Choi, J. H. Jang, K. Char and J. G. Son, *ACS Appl. Mater. Interfaces*, 2016, **8**, 22516–22525.
91 R. K. Kalluri, M. M. Biener, M. E. Suss, M. D. Merrill, M. Stadermann, J. G. Santiago, T. F. Baumann, J. Biener and A. Striolo, *Phys. Chem. Chem. Phys.*, 2013, **15**, 2309–2320.
92 C. Song and B. Corry, *J. Phys. Chem. B*, 2009, **113**, 7642–7649.
93 K. Tai, S. Haider, A. Grottesi and M. S. P. Sansom, *Eur. Biophys. J.*, 2009, **38**, 347–354.
94 L. Yang, B. H. Fishbine, A. Migliori and L. R. Pratt, *J. Am. Chem. Soc.*, 2009, **131**, 12373–12376.
95 Y. Shim and H. J. Kim, *ACS Nano*, 2009, **3**, 1693–1702.
96 H. Sui, J. Yao and L. Zhang, *Computation*, 2015, **3**, 687–700.
97 M. Holmboe and I. C. Bourg, *J. Phys. Chem. C*, 2014, **118**, 1001–1013.
98 J. Geske and M. Vogel, *Mol. Simul.*, 2017, **43**, 13–18.
99 D. Liu, C. Zheng, Q. Yang and C. Zhong, *J. Phys. Chem. C*, 2009, **113**, 5004–5009.
100 S. Wang, Q. Feng, F. Javadpour, T. Xia and Z. Li, *Int. J. Coal Geol.*, 2015, **147–148**, 9–24.
101 A. Boţan, B. Rotenberg, V. Marry, P. Turq and B. Noetinger, *J. Phys. Chem. C*, 2011, **115**, 16109–16115.
102 A. Özgür Yazaydin and R. W. Thompson, *Microporous Mesoporous Mater.*, 2009, **123**, 169–176.
103 L. Connelly, H. Jang, F. Teran Arce, S. Ramachandran, B. L. Kagan, R. Nussinov and R. Lal, *Biochemistry*, 2012, **51**, 3031–3038.
104 M. L. Fernández, M. Risk, R. Reigada and P. T. Vernier, *Biochem. Biophys. Res. Commun.*, 2012, **423**, 325–330.
105 A. Sharma, S. Namsani and J. K. Singh, *Mol. Simul.*, 2015, **41**, 414–422.
106 J. Vatamanu, D. Bedrov and O. Borodin, *Mol. Simul.*, 2017, **43**, 838–849.
107 R. Capone, H. Jang, S. A. Kotler, B. L. Kagan, R. Nussinov and R. Lal, *Biochemistry*, 2012, **51**, 776–785.
108 A. V. Korchuganov, V. M. Chernov, K. P. Zolnikov, D. S. Kryzhevich and S. G. Psakhie, *Inorg. Mater. Appl. Res.*, 2016, **7**, 648–657.
109 Y. Hu, D. Devegowda, A. Striolo, A. Phan, T. A. Ho, F. Civan and R. F. Sigal, *SPE J.*, 2014, **20**, 112–124.
110 Y. Ichikawa, K. Kawamura, N. Theramast and K. Kitayama, *Mech. Mater.*, 2004, **36**, 487–513.
111 J. Azamat, A. Khataee and F. Sadikoglu, *RSC Adv.*, 2016, **6**, 94911–94920.
112 Y. Tao, Q. Xue, Z. Liu, M. Shan, C. Ling, T. Wu and X. Li, *ACS Appl. Mater. Interfaces*, 2014, **6**, 8048–8058.

113 V. Karanikola, A. F. Corral, H. Jiang, A. Eduardo Sáez, W. P. Ela and R. G. Arnold, *J. Membr. Sci.*, 2015, **483**, 15–24.
114 D. Dubbeldam and R. Q. Snurr, *Mol. Simul.*, 2007, **33**, 305–325.
115 I. C. Bourg and C. I. Steefel, *J. Phys. Chem. C*, 2012, **116**, 11556–11564.
116 F. Y. Jiang, Y. Bouret and J. T. Kindt, *Biophys. J.*, 2004, **87**, 182–192.
117 C. L. Rountree, R. K. Kalia, E. Lidorikis, A. Nakano, L. Van Brutzel and P. Vashishta, *Annu. Rev. Mater. Res.*, 2002, **32**, 377–400.
118 A. O. Imdakm and T. Matsuura, *J. Membr. Sci.*, 2005, **262**, 117–128.
119 M. M. A. Shirazi, A. Kargari, A. F. Ismail and T. Matsuura, *Desalination*, 2016, **377**, 73–90.
120 A. O. Imdakm and T. Matsuura, *J. Membr. Sci.*, 2004, **237**, 51–59.
121 A. A. Lee, S. Kondrat and A. A. Kornyshev, *Phys. Rev. Lett.*, 2014, **113**, 048701.
122 C. Largeot, C. Portet, J. Chmiola, P.-L. Taberna, Y. Gogotsi and P. Simon, *J. Am. Chem. Soc.*, 2008, **130**, 2730–2731.
123 G. Feng and P. T. Cummings, *J. Phys. Chem. Lett.*, 2011, **2**, 2859–2864.
124 S. Wang, H. Li, H. Sawada, C. S. Allen, A. I. Kirkland, J. C. Grossman and J. H. Warner, *Nanoscale*, 2017, **9**, 6417–6426.
125 H. Zhou, X. Chen, L. Wang, X. Zhong, G. Zhuang, X. Li, D. Mei and J. Wang, *Phys. Chem. Chem. Phys.*, 2015, **17**, 24420–24426.
126 Z. Jin, *Fluid Phase Equilib.*, 2018, **458**, 177–185.
127 L. Zhu, Y. Jin, Q. Xue, X. Li, H. Zheng, T. Wu and C. Ling, *J. Mater. Chem. A*, 2016, **4**, 15015–15021.
128 B. Jin, X. Zhang, F. Li, N. Zhang, Z. Zong, S. Cao, Z. Li and X. Chen, *Phys. Chem. Chem. Phys.*, 2019, **21**, 6126–6132.
129 L. Zhang, Y. Xiong, Y. Li, M. Wei, W. Jiang, R. Lei and Z. Wu, *Fuel*, 2017, **204**, 1–11.
130 C. R. Clarkson, J. Wood, S. Burgis, S. Aquino and M. Freeman, *SPE Reservoir Eval. Eng.*, 2013, **15**, 648–661.
131 A. V. Neimark and P. I. Ravikovitch, 2000, pp. 51–60.
132 Z. Li, Z. Jin and A. Firoozabadi, *SPE J.*, 2014, **19**, 1096–1109.
133 M. Thommes, R. Guillet-Nicolas and K. A. Cychosz, in *Mesoporous Zeolites: Preparation, Characterization and Applications*, 2015, pp. 349–384.
134 R. Zaleski, A. Kierys, M. Dziadosz, J. Goworek and I. Halasz, *RSC Adv.*, 2012, **2**, 3729–3734.
135 F. Béguin, K. Kierzek, M. Friebe, A. Jankowska, J. Machnikowski, K. Jurewicz and E. Frackowiak, *Electrochim. Acta*, 2006, **51**, 2161–2167.
136 D. Henderson, *J. Colloid Interface Sci.*, 2012, **374**, 345–347.
137 J. P. Olivier, *J. Porous Mater.*, 1995, **2**, 9–17.
138 S. Yorgun and D. Yildiz, *J. Taiwan Inst. Chem. Eng.*, 2015, **53**, 122–131.
139 C. M. Lastoskie and K. E. Gubbins, *Adv. Chem. Eng.*, 2000, **128**, 41–50.
140 J. Landers, G. Y. Gor and A. V. Neimark, *Colloids Surf., A*, 2013, **437**, 3–32.
141 J. Fu, Y. Liu, Y. Tian and J. Wu, *J. Phys. Chem. C*, 2015, **119**, 5374–5385.
142 V. R. Cooper, L. Kong and D. C. Langreth, *Phys. Procedia*, 2010, **3**, 1417–1430.
143 T. Yamamoto, A. Endo, Y. Inagi, T. Ohmori and M. Nakaiwa, *J. Colloid Interface Sci.*, 2005, **284**, 614–620.
144 M. Thommes and K. A. Cychosz, *Adsorption*, 2014, **20**, 233–250.
145 C. Cazorla and S. A. Shevlin, *Dalton Trans.*, 2013, **42**, 4670–4676.
146 M. Thommes, K. A. Cychosz and A. V. Neimark, in *Novel Carbon Adsorbents*, 2012, pp. 107–145.
147 J. Landers, G. Y. Gor and A. V. Neimark, *Colloids Surf., A*, 2013, **437**, 3–32.
148 P. I. Ravikovitch, G. L. Haller and A. V. Neimark, *Adv. Colloid Interface Sci.*, 1998, **76–77**, 203–226.
149 S. Zhou and A. Bongiorno, *Acc. Chem. Res.*, 2014, **47**, 3331–3339.
150 D. W. Oxtoby, *Annu. Rev. Mater. Res.*, 2002, **32**, 39–52.
151 P. I. Ravikovitch, A. Vishnyakov, R. Russo and A. V. Neimark, *Langmuir*, 2000, **16**, 2311–2320.
152 S. Lowell, J. E. Shields, M. A. Thomas and M. Thommes, *Characterization of porous solids and powders: surface area, pore size and density*, Springer Science & Business Media, 2012, vol. 16.
153 D. Saha, S. Deng and Z. Yang, *J. Porous Mater.*, 2009, **16**, 141–149.
154 J. N. Caguiat, D. W. Kirk and C. Q. Jia, *Carbon*, 2014, **72**, 47–56.
155 M. Matena, J. Björk, M. Wahl, T.-L. Lee, J. Zegenhagen, L. H. Gade, T. A. Jung, M. Persson and M. Stöhr, *Phys. Rev. B: Condens. Matter Mater. Phys.*, 2014, **90**, 125408.
156 M. Thommes, *Chem.-Ing.-Tech.*, 2010, **82**, 1059–1073.
157 S. Figueroa-Gerstenmaier, J. B. Avalos, L. D. Gelb, K. E. Gubbins and L. F. Vega, *Langmuir*, 2003, **19**, 8592–8604.
158 C. G. Van De Walle and A. Janotti, *Phys. Status Solidi B*, 2011, **248**, 19–27.
159 N. A. Seaton, J. P. R. B. Walton and N. Quirke, *Carbon*, 1989, **27**, 853–861.
160 C. Lastoskie, K. E. Gubbins and N. Quirke, *J. Phys. Chem.*, 1993, **97**, 4786–4796.
161 X. Chen, R. Paul and L. Dai, *Natl. Sci. Rev.*, 2017, **4**, 453–489.
162 J. Yi, Z. Huo, A. M. Asiri, K. A. Alamry and J. Li, *Prog. Chem.*, 2018, **30**, 1624–1633.
163 C. Zhong, Y. Deng, W. Hu, J. Qiao, L. Zhang and J. Zhang, *Chem. Soc. Rev.*, 2015, **44**, 7484–7539.
164 L. L. Zhang and X. S. Zhao, *Chem. Soc. Rev.*, 2009, **38**, 2520–2531.
165 F. Schütt, S. Signetti, H. Krüger, S. Röder, D. Smazna, S. Kaps, S. N. Gorb, Y. K. Mishra, N. M. Pugno and R. Adelung, *Nat. Commun.*, 2017, **8**, 1215.
166 T. Sekino, *Inorganic and Metallic Nanotubular Materials*, Springer Berlin Heidelberg, Berlin, Heidelberg, 2010, vol. 117.
167 V. V. N. Obreja, *Phys. E*, 2008, **40**, 2596–2605.

168 M. F. Mousavi, M. Hashemi, M. S. Rahmanifar and A. Noori, *Electrochim. Acta*, 2017, **228**, 290–298.
169 R. Saito, G. Dresselhaus and M. S. Dresselhaus, *Chem. Phys. Lett.*, 1992, **195**, 537–542.
170 R. Saito, G. Dresselhaus and M. S. Dresselhaus, *Physical Properties of Carbon Nanotubes*, Imperial College Press and Distributed by World Scientific Publishing Co., 1998.
171 R. H. Baughman, *Science*, 2002, **297**, 787–792.
172 A. L. Elías, N. Perea-López, L. P. Rajukumar, A. McCreary, F. López-Urías, H. Terrones and M. Terrones, in *Nanotube Superfiber Materials*, Elsevier, 2014, pp. 457–493.
173 E. L. Gui, L.-J. Li, K. Zhang, Y. Xu, X. Dong, X. Ho, P. S. Lee, J. Kasim, Z. X. Shen, J. A. Rogers and Mhaisalkar, *J. Am. Chem. Soc.*, 2007, **129**, 14427–14432.
174 C. Y. Lee, H. M. Tsai, H. J. Chuang, S. Y. Li, P. Lin and T. Y. Tseng, *J. Electrochem. Soc.*, 2005, **152**, A716.
175 J. Y. Lee, K. Liang, K. H. An and Y. H. Lee, *Synth. Met.*, 2005, **150**, 153–157.
176 T. Bordjiba, M. Mohamedi and L. H. Dao, *Adv. Mater.*, 2008, **20**, 815–819.
177 M. Seifert, *Angew. Chem., Int. Ed.*, 2017, **56**, 7351.
178 H. Pan, J. Li and Y. P. Feng, *Nanoscale Res. Lett.*, 2010, **5**, 654–668.
179 H. Zhang, G. P. Cao and Y. S. Yang, *Nanotechnology*, 2007, **18**, 195607.
180 Y. Soneda, J. Yamashita, M. Kodama, H. Hatori, M. Toyoda and M. Inagaki, *Appl. Phys. A*, 2006, **82**, 575–578.
181 Y. Soneda, M. Toyoda, Y. Tani, J. Yamashita, M. Kodama, H. Hatori and M. Inagaki, *J. Phys. Chem. Solids*, 2004, **65**, 219–222.
182 G. Agar, *Johnson Matthey Technol. Rev.*, 2014, **58**, 221–223.
183 C. G. Liu, M. Liu, F. Li and H. M. Cheng, *Appl. Phys. Lett.*, 2008, **92**, 143108.
184 X. Xiao, T. Li, Z. Peng, H. Jin, Q. Zhong, Q. Hu, B. Yao, Q. Luo, C. Zhang, L. Gong, J. Chen, Y. Gogotsi and J. Zhou, *Nano Energy*, 2014, **6**, 1–9.
185 D. N. Futaba, K. Hata, T. Yamada, T. Hiraoka, Y. Hayamizu, Y. Kakudate, O. Tanaike, H. Hatori, M. Yumura and S. Iijima, *Nat. Mater.*, 2006, **5**, 987–994.
186 H. Pan, C. K. Poh, Y. P. Feng and J. Lin, *Chem. Mater.*, 2007, **19**, 6120–6125.
187 D. Pankratov, Z. Blum, D. B. Suyatin, V. O. Popov and S. Shleev, *ChemElectroChem*, 2014, **1**, 343–346.
188 M. N. Hyder, S. W. Lee, F. Ç. Cebeci, D. J. Schmidt, Y. Shao-Horn and P. T. Hammond, *ACS Nano*, 2011, **5**, 8552–8561.
189 X. Wang, M. Falk, R. Ortiz, H. Matsumura, J. Bobacka, R. Ludwig, M. Bergelin, L. Gorton and S. Shleev, *Biosens. Bioelectron.*, 2012, **31**, 219–225.
190 P. Bollella, R. Ludwig and L. Gorton, *Appl. Mater. Today*, 2017.
191 M. Kaempgen, J. Ma, G. Gruner, G. Wee and S. G. Mhaisalkar, *Appl. Phys. Lett.*, 2007, **90**, 264104.
192 C. L. Pint, N. W. Nicholas, S. Xu, Z. Sun, J. M. Tour, H. K. Schmidt, R. G. Gordon and R. H. Hauge, *Carbon*, 2011, **49**, 4890–4897.
193 L. Gao, A. Peng, Z. Y. Wang, H. Zhang, Z. Shi, Z. Gu, G. Cao and B. Ding, *Solid State Commun.*, 2008, **146**, 380–383.
194 R. Reit, J. Nguyen and W. J. Ready, *Electrochim. Acta*, 2013, **91**, 96–100.
195 S. Dörfler, I. Felhösi, T. Marek, S. Thieme, H. Althues, L. Nyikos and S. Kaskel, *J. Power Sources*, 2013, **227**, 218–228.
196 B.-H. Kim, K. S. Yang, Y. A. Kim, Y. J. Kim, B. An and K. Oshida, *J. Power Sources*, 2011, **196**, 10496–10501.
197 S. Talapatra, S. Kar, S. K. Pal, R. Vajtai, L. Ci, P. Victor, M. M. Shaijumon, S. Kaur, O. Nalamasu and P. M. Ajayan, *Nat. Nanotechnol.*, 2006, **1**, 112–116.
198 B. Kim, H. Chung and W. Kim, *Nanotechnology*, 2012, **23**, 155401.
199 Y.-K. Hsu, Y.-C. Chen, Y.-G. Lin, L.-C. Chen and K.-H. Chen, *J. Mater. Chem.*, 2012, **22**, 3383.
200 K. Kakaei, M. D. Esrafili and A. Ehsani, *Interface Sci. Technol.*, 2019, 339–386.
201 M. A. Pope, S. Korkut, C. Punckt and I. A. Aksay, *J. Electrochem. Soc.*, 2013, **160**, A1653–A1660.
202 C. Tran and V. Kalra, *J. Power Sources*, 2013, **235**, 289–296.
203 L.-F. Chen, Z.-H. Huang, H.-W. Liang, H.-L. Gao and S.-H. Yu, *Adv. Funct. Mater.*, 2014, **24**, 5104–5111.
204 F. Miao, C. Shao, X. Li, K. Wang and Y. Liu, *J. Mater. Chem. A*, 2016, **4**, 4180–4187.
205 T. Hiraoka, A. Izadi-Najafabadi, T. Yamada, D. N. Futaba, S. Yasuda, O. Tanaike, H. Hatori, M. Yumura, S. Iijima and K. Hata, *Adv. Funct. Mater.*, 2010, **20**, 422–428.
206 B.-H. Kim, K. S. Yang, H.-G. Woo and K. Oshida, *Synth. Met.*, 2011, **161**, 1211–1216.
207 C. Du and N. Pan, *Nanotechnology*, 2006, **17**, 5314–5318.
208 Y. Jiang, J. Yan, X. Wu, D. Shan, Q. Zhou, L. Jiang, D. Yang and Z. Fan, *J. Power Sources*, 2016, **307**, 190–198.
209 Y. Qiu, G. Li, Y. Hou, Z. Pan, H. Li, W. Li, M. Liu, F. Ye, X. Yang and Y. Zhang, *Chem. Mater.*, 2015, **27**, 1194–1200.
210 T. Kim, G. Jung, S. Yoo, K. S. Suh and R. S. Ruoff, *ACS Nano*, 2013, **7**, 6899–6905.
211 L.-F. Chen, X.-D. Zhang, H.-W. Liang, M. Kong, Q.-F. Guan, P. Chen, Z.-Y. Wu and S.-H. Yu, *ACS Nano*, 2012, **6**, 7092–7102.
212 X. Yang, J. Zhu, L. Qiu and D. Li, *Adv. Mater.*, 2011, **23**, 2833–2838.
213 Q. Cheng, J. Tang, J. Ma, H. Zhang, N. Shinya and L.-C. Qin, *Phys. Chem. Chem. Phys.*, 2011, **13**, 17615.
214 W. Lu, L. Qu, K. Henry and L. Dai, *J. Power Sources*, 2009, **189**, 1270–1277.
215 P. Lu, X. Wang, L. Wen, X. Jiang, W. Guo, L. Wang, X. Yan, F. Hou, J. Liang, H.-M. Cheng and S. X. Dou, *Small*, 2019, **15**, e1805064.
216 S. N. Ansari, M. Saraf, A. K. Gupta and S. M. Mobin, *Chem.–Asian J.*, 2019, **14**, 3566–3571.
217 C. R. Chen, H. Qin, H. P. Cong and S. H. Yu, *Adv. Mater.*, 2019, **31**, e1900573.
218 M. Tahir, L. He, W. A. Haider, W. Yang, X. Hong, Y. Guo, X. Pan, H. Tang, Y. Li and L. Mai, *Nanoscale*, 2019, **11**, 7761–7770.
219 Y. Zhou, Y. Zhu, B. Xu and X. Zhang, *Chem. Commun.*, 2019, **55**, 4083–4086.

220 C. Pereira, R. S. Costa, L. Lopes, B. Bachiller-Baeza, I. Rodriguez-Ramos, A. Guerrero-Ruiz, P. B. Tavares, C. Freire and A. M. Pereira, *Nanoscale*, 2019, **11**, 3397.
221 X. Guan, D. Kong, Q. Huang, L. Cao, P. Zhang, H. Lin, Z. Lin and H. Yuan, *Polymers*, 2019, **11**, 178.
222 Y. Chen, B. Xu, J. Gong, J. Wen, T. Hua, C. W. Kan and J. Deng, *ACS Appl. Mater. Interfaces*, 2019, **11**, 2120–2129.
223 H. Park, R. B. Ambade, S. H. Noh, W. Eom, K. H. Koh, S. B. Ambade, W. J. Lee, S. H. Kim and T. H. Han, *ACS Appl. Mater. Interfaces*, 2019, **11**, 9011–9022.
224 W. Zhou, Y. Du, J. Zeng, F. Liu and Y. Zhu, *Nanoscale*, 2019, **11**, 7624–7633.
225 F. Daneshvar, A. Aziz, A. M. Abdelkader, T. Zhang, H.-J. Sue and M. E. Welland, *Nanotechnology*, 2019, **30**, 015401.
226 H. Niu, Y. Zhang, Y. Liu, N. Xin and W. Shi, *J. Colloid Interface Sci.*, 2019, **539**, 545–552.
227 X. Fu, A. Chen, Y. Yu, S. Hou and L. Liu, *Chem.–Asian J.*, 2019, **14**, 634–639.
228 X. Guan, L. Cao, Q. Huang, D. Kong, P. Zhang, H. Lin, W. Li, Z. Lin and H. Yuan, *Polymers*, 2019, **11**, 973.
229 M. K. Jha, K. Hata and C. Subramaniam, *ACS Appl. Mater. Interfaces*, 2019, **11**, 18285–18294.
230 Z. Chang, X. Sang, Y. Song, X. Sun and X. X. Liu, *Dalton Trans.*, 2019, **48**, 6812–6816.
231 E. P. Gilshteyn, D. Amanbayev, A. S. Anisimov, T. Kallio and A. G. Nasibulin, *Sci. Rep.*, 2017, **7**, 17449.
232 Q. Wang, J. Yan and Z. Fan, *Energy Environ. Sci.*, 2016, **9**, 729–762.
233 M. Huang, Y. Zhang, F. Li, L. Zhang, R. S. Ruoff, Z. Wen and Q. Liu, *Sci. Rep.*, 2015, **4**, 3878.
234 T. Chen and L. Dai, *Mater. Today*, 2013, **16**, 272–280.
235 Y. K. Mishra, S. Kaps, A. Schuchardt, I. Paulowicz, X. Jin, D. Gedamu, S. Freitag, M. Claus, S. Wille, A. Kovalev, S. N. Gorb and R. Adelung, *Part. Part. Syst. Charact.*, 2013, **30**, 775–783.
236 J. Marx, A. Brouschkin, S. Roth, D. Smazna, Y. K. Mishra, H. Wittich, K. Schulte, R. Adelung and B. Fiedler, *Synth. Met.*, 2018, **235**, 145–152.
237 K. Shehzad, Y. Xu, C. Gao and X. Duan, *Chem. Soc. Rev.*, 2016, **45**, 5541–5588.
238 M. D. Slater, D. Kim, E. Lee and C. S. Johnson, *Adv. Funct. Mater.*, 2013, **23**, 947–958.
239 S. W. Kim, D. H. Seo, X. Ma, G. Ceder and K. Kang, *Adv. Energy Mater.*, 2012, **2**, 710–721.
240 A. K. Shukla and T. Prem Kumar, *Wiley Interdiscip. Rev.: Energy Environ.*, 2013, **2**, 14–30.
241 X. Hu, W. Zhang, X. Liu, Y. Mei and Y. Huang, *Chem. Soc. Rev.*, 2015, **44**, 2376–2404.
242 Y. Fang, X.-Y. Yu and X. W. (David) Lou, *Matter*, 2019, **1**, 90–114.
243 J. N. Tiwari, R. N. Tiwari and K. S. Kim, *Prog. Mater. Sci.*, 2012, **57**, 724–803.
244 Y.-T. Kim, J. H. Han, B. H. Hong and Y.-U. Kwon, *Adv. Mater.*, 2010, **22**, 515–518.
245 T. Okada, K. Kawashima, Y. Nakata and X. Ning, *Jpn. J. Appl. Phys.*, 2005, **44**, 688–691.
246 H. Xia, J. Feng, H. Wang, M. O. Lai and L. Lu, *J. Power Sources*, 2010, **195**, 4410–4413.
247 G.-R. Li, Z.-P. Feng, J.-H. Zhong, Z.-L. Wang and Y.-X. Tong, *Macromolecules*, 2010, **43**, 2178–2183.
248 J.-M. Park, K. S. Nalwa, W. Leung, K. Constant, S. Chaudhary and K.-M. Ho, *Nanotechnology*, 2010, **21**, 215301.
249 L. M. Cao, H. Tian, Z. Zhang, X. Y. Zhang, C. X. Gao and W. K. Wang, *Nanotechnology*, 2004, **15**, 139–142.
250 B. B. Nayak, D. Behera and B. K. Mishra, *J. Am. Ceram. Soc.*, 2010, **93**, 3080–3083.
251 A. K. P. Mann and S. E. Skrabalak, *Chem. Mater.*, 2011, **23**, 1017–1022.
252 P. F. Siril, A. Lehoux, L. Ramos, P. Beaunier and H. Remita, *New J. Chem.*, 2012, **36**, 2135.
253 S. Vizireanu, S. D. Stoica, C. Luculescu, L. C. Nistor, B. Mitu and G. Dinescu, *Plasma Sources Sci. Technol.*, 2010, **19**, 034016.
254 S.-H. Jung, E. Oh, K.-H. Lee, Y. Yang, C. G. Park, W. Park and S.-H. Jeong, *Cryst. Growth Des.*, 2008, **8**, 265–269.
255 L. Wang and Y. Yamauchi, *Chem. Mater.*, 2009, **21**, 3562–3569.
256 J. N. Wang, L. F. Su and Z. P. Wu, *Cryst. Growth Des.*, 2008, **8**, 1741–1747.
257 J. Liu, J. Essner and J. Li, *Chem. Mater.*, 2010, **22**, 5022–5030.
258 W. Lei, D. Liu, P. Zhu, X. Chen, J. Hao, Q. Wang, Q. Cui and G. Zou, *CrystEngComm*, 2010, **12**, 511–516.
259 R. Liu, J. Duay and S. B. Lee, *Chem. Commun.*, 2011, **47**, 1384–1404.
260 H. Elzanowska, E. Miasek and V. I. Birss, *Electrochim. Acta*, 2008, **53**, 2706–2715.
261 J. Mu, B. Chen, Z. Guo, M. Zhang, Z. Zhang, C. Shao and Y. Liu, *J. Colloid Interface Sci.*, 2011, **356**, 706–712.
262 T. P. Gujar, V. R. Shinde, C. D. Lokhande, W.-Y. Kim, K.-D. Jung and O.-S. Joo, *Electrochem. Commun.*, 2007, **9**, 504–510.
263 M. He, K. Kravchyk, M. Walter and M. V. Kovalenko, *Nano Lett.*, 2014, **14**, 1255–1262.
264 Q. Xu, W. Li, L. Ding, W. Yang, H. Xiao and W.-J. Ong, *Nanoscale*, 2019, **11**, 1475–1504.
265 F. Zhao, S. Shen, L. Cheng, L. Ma, J. Zhou, H. Ye, N. Han, T. Wu, Y. Li and J. Lu, *Nano Lett.*, 2017, **17**, 4137–4142.
266 R. S. Devan, R. A. Patil, J. H. Lin and Y. R. Ma, *Adv. Funct. Mater.*, 2012, **22**, 3326–3370.
267 M. Ge, C. Cao, J. Huang, S. Li, Z. Chen, K. Q. Zhang, S. S. Al-Deyab and Y. Lai, *J. Mater. Chem. A*, 2016, **4**, 6772–6801.
268 J. Tian, Z. Zhao, A. Kumar, R. I. Boughton and H. Liu, *Chem. Soc. Rev.*, 2014, **43**, 6920–6937.
269 G. Zhang, X. Xiao, B. Li, P. Gu, H. Xue and H. Pang, *J. Mater. Chem. A*, 2017, **5**, 8155–8186.
270 T. Zhu, H. Bin Wu, Y. Wang, R. Xu and X. W. Lou, *Adv. Energy Mater.*, 2012, **2**, 1497–1502.
271 S. Peng, G. Jin, L. Li, K. Li, M. Srinivasan, S. Ramakrishna and J. Chen, *Chem. Soc. Rev.*, 2016, **45**, 1225–1241.
272 S. Zhai, L. Wei, H. E. Karahan, X. Chen, C. Wang, X. Zhang, J. Chen, X. Wang and Y. Chen, *Energy Storage Mater.*, 2019, **19**, 102–123.

273 Y. Liang, D. Wu and R. Fu, *Sci. Rep.*, 2013, **3**, 1119.
274 C. Cheng and H. J. Fan, *Nano Today*, 2012, **7**, 327–343.
275 Q. Wei, F. Xiong, S. Tan, L. Huang, E. H. Lan, B. Dunn and L. Mai, *Adv. Mater.*, 2017, **29**, 1602300.
276 J. Le Xie, C. X. Guo and C. M. Li, *Energy Environ. Sci.*, 2014, **7**, 2559–2579.
277 Z. Yin and Q. Zheng, *Adv. Energy Mater.*, 2012, **2**, 179–218.
278 B. I. Kharisov, O. V. Kharissova, B. O. García, Y. P. Méndez and I. G. De La Fuente, *RSC Adv.*, 2015, **5**, 105507–105523.
279 W. Zhao, C. Zhang, F. Geng, S. Zhuo and B. Zhang, *ACS Nano*, 2014, **8**, 10909–10919.
280 E. Lhuillier, S. Pedetti, S. Ithurria, B. Nadal, H. Heuclin and B. Dubertret, *Acc. Chem. Res.*, 2015, **48**, 22–30.
281 X. Ou, C. Yang, X. Xiong, F. Zheng, Q. Pan, C. Jin, M. Liu and K. Huang, *Adv. Funct. Mater.*, 2017, **27**, 1606242.
282 X. Wang, J. Feng, Y. Bai, Q. Zhang and Y. Yin, *Chem. Rev.*, 2016, **116**, 10983–11060.
283 C. Marichy, M. Bechelany and N. Pinna, *Adv. Mater.*, 2012, **24**, 1017–1032.
284 L. Yu, H. Hu, H. Bin Wu and X. W. D. Lou, *Adv. Mater.*, 2017, **29**.
285 H. Jiang, P. S. Lee and C. Li, *Energy Environ. Sci.*, 2013, **6**, 41–53.
286 P. Yu, X. Zhang, D. Wang, L. Wang and Y. Ma, *Cryst. Growth Des.*, 2009, **9**, 528–533.
287 X.-Y. Yu, L. Yu and X. W. D. Lou, *Adv. Energy Mater.*, 2016, **6**, 1501333.
288 J. Wang, Y. Cui and D. Wang, *Adv. Mater.*, 2019, **31**, 1801993.
289 P. Tartaj and J. M. Amarilla, *Chem. Commun.*, 2014, **50**, 2077–2088.
290 H. Hu, B. Y. Guan and X. W. Lou, *Chem*, 2016, **1**, 102–113.
291 J. Hong, J. Y. Han, H. Yoon, P. Joo, T. Lee, E. Seo, K. Char and B. S. Kim, *Nanoscale*, 2011, **3**, 4515–4531.
292 G. Zhang, L. Yu, H. E. Hoster and X. W. Lou, *Nanoscale*, 2013, **5**, 877–881.
293 P. Liu and L. Zhang, *Crit. Rev. Solid State Mater. Sci.*, 2009, **34**, 75–87.
294 C. K. Ranaweera, Z. Wang, E. Alqurashi, P. K. Kahol, P. R. Dvornic, B. K. Gupta, K. Ramasamy, A. D. Mohite, G. Gupta and R. K. Gupta, *J. Mater. Chem. A*, 2016, **4**, 9014–9018.
295 Y. E. Miao, W. Fan, D. Chen and T. Liu, *ACS Appl. Mater. Interfaces*, 2013, **5**, 4423–4428.
296 B. Y. Guan, X. Y. Yu, H. Bin Wu and X. W. D. Lou, *Adv. Mater.*, 2017, **29**.
297 Z. A. Qiao, B. Guo, A. J. Binder, J. Chen, G. M. Veith and S. Dai, *Nano Lett.*, 2013, **13**, 207–212.
298 B. T. Zhu, Z. Wang, S. Ding, J. S. Chen and X. W. Lou, *RSC Adv.*, 2011, **1**, 397–400.
299 C. Y. Cao, W. Guo, Z. M. Cui, W. G. Song and W. Cai, *J. Mater. Chem.*, 2011, **21**, 3204–3209.
300 F. Xu, Z. Tang, S. Huang, L. Chen, Y. Liang, W. Mai, H. Zhong, R. Fu and D. Wu, *Nat. Commun.*, 2015, **6**, 7221.
301 C. Liu, J. Wang, J. Li, R. Luo, J. Shen, X. Sun, W. Han and L. Wang, *ACS Appl. Mater. Interfaces*, 2015, **7**, 18609–18617.
302 L. Yu, L. Zhang, H. Bin Wu and X. W. D. Lou, *Angew. Chem., Int. Ed.*, 2014, **53**, 3711–3714.
303 Y. Li, H. Wang, B. Huang, L. Wang, R. Wang, B. He, Y. Gong and X. Hu, *J. Mater. Chem. A*, 2018, **6**, 14742–14751.
304 W. Gu, L. Yang, F. Teng, Z. U. Abiden and F. Zhao, *Energy Technol.*, 2019, **7**, 1900460.
305 W. Gu, F. Teng, Z. Liu, Z. Liu, W. Hao, A. Zhang and Y. Teng, *J. Electroanal. Chem.*, 2017, **804**, 185–191.
306 A. K. Geim and K. S. Novoselov, *Nat. Mater.*, 2007, **6**, 183–191.
307 D. C. Marcano, D. V. Kosynkin, J. M. Berlin, A. Sinitskii, Z. Sun, A. Slesarev, L. B. Alemany, W. Lu and J. M. Tour, *ACS Nano*, 2010, **4**, 4806–4814.
308 R. Mertens, *Graphene Supercapacitors Introd*, News, https://www.graphene-info.com/graphene-supercapacitors.
309 T. Pallone, https://www.globalspec.com, 2018.
310 A. S. Aricò, P. Bruce, B. Scrosati, J. M. Tarascon and W. Van Schalkwijk, *Nat. Mater.*, 2005, **4**, 366–377.
311 Z. S. Iro, C. Subramani and S. S. Dash, *Int. J. Electrochem. Sci.*, 2016, **11**, 10628–10643.
312 W. Lv, D. M. Tang, Y. B. He, C. H. You, Z. Q. Shi, X. C. Chen, C. M. Chen, P. X. Hou, C. Liu and Q. H. Yang, *ACS Nano*, 2009, **3**, 3730–3736.
313 S. He and W. Chen, *Nanoscale*, 2015, **7**, 6957–6990.
314 L. Manjakkal, C. G. Núñez, W. Dang and R. Dahiya, *Nano Energy*, 2018, **51**, 604–612.
315 X. H. Xia, D. L. Chao, Y. Q. Zhang, Z. X. Shen and H. J. Fan, *Nano Today*, 2014, **9**, 785–807.
316 B. G. Choi, M. Yang, W. H. Hong, J. W. Choi and Y. S. Huh, *ACS Nano*, 2012, **6**, 4020–4028.
317 X. Dong, J. Wang, J. Wang, M. B. Chan-Park, X. Li, L. Wang, W. Huang and P. Chen, *Mater. Chem. Phys.*, 2012, **134**, 576–580.
318 H. Sun, L. Mei, J. Liang, Z. Zhao, C. Lee, H. Fei, M. Ding, J. Lau, M. Li, C. Wang, X. Xu, G. Hao, B. Papandrea, I. Shakir, B. Dunn, Y. Huang and X. Duan, *Science*, 2017, **356**, 599–604.
319 X. Dong, X. Wang, L. Wang, H. Song, H. Zhang, W. Huang and P. Chen, *ACS Appl. Mater. Interfaces*, 2012, **4**, 3129–3133.
320 K. Nomura, H. Nishihara, N. Kobayashi, T. Asada and T. Kyotani, *Energy Environ. Sci.*, 2019, **12**, 1542–1549.
321 W. Yang, M. Ni, X. Ren, Y. Tian, N. Li, Y. Su and X. Zhang, *Curr. Opin. Colloid Interface Sci.*, 2015, **20**, 416–428.
322 F. Béguin, V. Presser, A. Balducci and E. Frackowiak, *Adv. Mater.*, 2014, **26**, 2219–2251.
323 D. W. Wang and D. Su, *Energy Environ. Sci.*, 2014, **7**, 576–591.
324 D. Hulicova-Jurcakova, M. Seredych, G. Q. Lu and T. J. Bandosz, *Adv. Funct. Mater.*, 2009, **19**, 438–447.
325 D. G. Papageorgiou, I. A. Kinloch and R. J. Young, *Prog. Mater. Sci.*, 2017, **90**, 75–127.
326 I. M. Mosa, A. Pattammattel, K. Kadimisetty, P. Pande, M. F. El-Kady, G. W. Bishop, M. Novak, R. B. Kaner, A. K. Basu, C. V. Kumar and J. F. Rusling, *Adv. Energy Mater.*, 2017, **7**, 1700358.

327 T. P. Dasari Shareena, D. McShan, A. K. Dasmahapatra and P. B. Tchounwou, *Nano-Micro Lett.*, 2018, **10**.
328 S. K. Verma, E. Jha, P. K. Panda, J. K. Das, A. Thirumurugan, M. Suar and S. K. S. Parashar, *Nanomedicine*, 2018, **13**, 43–68.
329 X. Zou, L. Zhang, Z. Wang and Y. Luo, *J. Am. Chem. Soc.*, 2016, **138**, 2064–2077.
330 F. Perreault, A. Fonseca De Faria and M. Elimelech, *Chem. Soc. Rev.*, 2015, **44**, 5861–5896.
331 Y. Wang, Z. Li, J. Wang, J. Li and Y. Lin, *Trends Biotechnol.*, 2011, **29**, 205–212.
332 Z. Wang and B. Mi, *Environ. Sci. Technol.*, 2017, **51**, 8229–8244.
333 G. Lalwani, M. D'Agati, A. M. Khan and B. Sitharaman, *Adv. Drug Delivery Rev.*, 2016, **105**, 109–144.
334 K. Lü, G. X. Zhao and X. K. Wang, *Chin. Sci. Bull.*, 2012, **57**, 1223–1234.
335 S. Wang, H. Sun, H. M. Ang and M. O. Tadé, *Chem. Eng. J.*, 2013, **226**, 336–347.
336 K. Hu, D. D. Kulkarni, I. Choi and V. V. Tsukruk, *Prog. Polym. Sci.*, 2014, **39**, 1934–1972.
337 B. Luo, S. Liu and L. Zhi, *Small*, 2012, **8**, 630–646.
338 A. B. Seabra, A. J. Paula, R. De Lima, O. L. Alves and N. Durán, *Chem. Res. Toxicol.*, 2014, **27**, 159–168.
339 A. Kamyshny and S. Magdassi, *Small*, 2014, **10**, 3515–3535.
340 C. Ameta, R. Ameta and S. Kothari, in *Microwave-Assisted Organic Synthesis*, A Green Chemical Approach, 2014, pp. 253–286.
341 V. C. Sanchez, A. Jachak, R. H. Hurt and A. B. Kane, *Chem. Res. Toxicol.*, 2012, **25**, 15–34.
342 M. S. Mauter and M. Elimelech, *Environ. Sci. Technol.*, 2008, **42**, 5843–5859.
343 S. C. Ray, *Applications of Graphene and Graphene-Oxide Based Nanomaterials*, 2015.
344 R. Leary and A. Westwood, *Carbon*, 2011, **49**, 741–772.
345 H. Wang, H. S. Casalongue, Y. Liang and H. Dai, *J. Am. Chem. Soc.*, 2010, **132**, 7472–7477.
346 A. Chavez-Valdez, M. S. P. Shaffer and A. R. Boccaccini, *J. Phys. Chem. B*, 2013, **117**, 1502–1515.
347 M. Holzinger, A. Le Goff and S. Cosnier, *Front. Chem.*, 2014, **2**, 63.
348 M. Pumera, *Chem. Soc. Rev.*, 2010, **39**, 4146–4157.
349 W. Hu, C. Peng, W. Luo, M. Lv, X. Li, D. Li, Q. Huang and C. Fan, *ACS Nano*, 2010, **4**, 4317–4323.
350 X. Chen and S. S. Mao, *Chem. Rev.*, 2007, **107**, 2891–2959.
351 S. Goenka, V. Sant and S. Sant, *J. Controlled Release*, 2014, **173**, 75–88.
352 M. Pumera, *Energy Environ. Sci.*, 2011, **4**, 668–674.
353 J. Bai and B. Zhou, *Chem. Rev.*, 2014, **114**, 10131–10176.
354 M. Hu, Z. Yao and X. Wang, *Ind. Eng. Chem. Res.*, 2017, **56**, 3477–3502.
355 C. Zhan, C. Lian, Y. Zhang, M. W. Thompson, Y. Xie, J. Wu, P. R. C. Kent, P. T. Cummings, D. E. Jiang and D. J. Wesolowski, *Adv. Sci.*, 2017, **4**.
356 J. Xia, F. Chen, J. Li and N. Tao, *Nat. Nanotechnol.*, 2009, **4**, 505–509.
357 H. Ji, X. Zhao, Z. Qiao, J. Jung, Y. Zhu, Y. Lu, L. L. Zhang, A. H. MacDonald and R. S. Ruoff, *Nat. Commun.*, 2014, **5**, 3317.
358 P. A. Brooksby, A. K. Farquhar, H. M. Dykstra, M. R. Waterland and A. J. Downard, *J. Phys. Chem. C*, 2015, **119**, 25778–25785.
359 S. Luryi, *Appl. Phys. Lett.*, 1988, **52**, 501–503.
360 S. Dröscher, P. Roulleau, F. Molitor, P. Studerus, C. Stampfer, K. Ensslin and T. Ihn, *Phys. Scr.*, 2012, **T146**, 014009.
361 E. Paek, A. J. Pak and G. S. Hwang, *J. Electrochem. Soc.*, 2013, **160**, A1–A10.
362 M. D. Stoller, C. W. Magnuson, Y. Zhu, S. Murali, J. W. Suk, R. Piner and R. S. Ruoff, *Energy Environ. Sci.*, 2011, **4**, 4685–4689.
363 L. Li, C. Richter, S. Paetel, T. Kopp, J. Mannhart and R. C. Ashoori, *Science*, 2011, **332**, 825–828.
364 A. A. Shylau, J. W. Kłos and I. V. Zozoulenko, *Phys. Rev. B: Condens. Matter Mater. Phys.*, 2009, **80**, 205402.
365 H. Raha, B. Manna, D. Pradhan and P. K. Guha, *Nanotechnology*, 2019, **30**, 435404.
366 C. Zhan, T. A. Pham, M. R. Cerón, P. G. Campbell, V. Vedharathinam, M. Otani, D. E. Jiang, J. Biener, B. C. Wood and M. Biener, *ACS Appl. Mater. Interfaces*, 2018, **10**, 36860–36865.
367 Z. Li, X. Liu, L. Wang, F. Bu, J. Wei, D. Pan and M. Wu, *Small*, 2018, **14**, 1801498.
368 C. Song, J. Wang, Z. Meng, F. Hu and X. Jian, *ChemPhysChem*, 2018, **19**, 1579–1583.
369 M. Mousavi-Khoshdel, E. Targholi and M. J. Momeni, *J. Phys. Chem. C*, 2015, **119**, 26290–26295.
370 S. Ratha, S. R. Marri, N. A. Lanzillo, S. Moshkalev, S. K. Nayak, J. N. Behera and C. S. Rout, *J. Mater. Chem. A*, 2015, **3**, 18874–18881.
371 B. SanthiBhushan, M. S. Khan, V. K. Bohat and A. Srivastava, *IEEE Trans. Nanotechnol.*, 2018, **17**, 205–211.
372 Y. Liu, J. Li, W. Li, Y. Li, F. Zhan, H. Tang and Q. Chen, *Int. J. Hydrogen Energy*, 2016, **41**, 10354–10365.
373 P. Hirunsit, M. Liangruksa and P. Khanchaitit, *Carbon*, 2016, **108**, 7–20.
374 Y. Zhao, S. Huang, M. Xia, S. Rehman, S. Mu, Z. Kou, Z. Zhang, Z. Chen, F. Gao and Y. Hou, *Nano Energy*, 2016, **28**, 346–355.
375 S. Gupta, B. Aberg, S. Carrizosa and N. Dimakis, *Materials*, 2016, **9**, 615.
376 Y. Xu, Y. Feng, X. Li, G. Hu, Y. Luo, L. Sun, T. Tang, J. Wen, H. Wang and M. Li, *Int. J. Electrochem. Sci.*, 2017, **12**, 8820–8831.
377 C. Qu, L. Zhang, W. Meng, Z. Liang, B. Zhu, D. Dang, S. Dai, B. Zhao, H. Tabassum, S. Gao, H. Zhang, W. Guo, R. Zhao, X. Huang, M. Liu and R. Zou, *J. Mater. Chem. A*, 2018, **6**, 4003–4012.
378 A. Pathak, A. S. Gangan, S. Ratha, B. Chakraborty and C. S. Rout, *J. Phys. Chem. C*, 2017, **121**, 18992–19001.
379 J. Kim, J. H. Jeon, H. J. Kim, H. Lim and I. K. Oh, *ACS Nano*, 2014, **8**, 2986–2997.

380 Z. Li, Z. Xu, H. Wang, J. Ding, B. Zahiri, C. M. B. Holt, X. Tan and D. Mitlin, *Energy Environ. Sci.*, 2014, **7**, 1708–1718.
381 Z.-S. Wu, K. Parvez, A. Winter, H. Vieker, X. Liu, S. Han, A. Turchanin, X. Feng and K. Müllen, *Adv. Mater.*, 2014, **26**, 4552–4558.
382 G. Wang, R. Liang, L. Liu and B. Zhong, *Electrochim. Acta*, 2014, **115**, 183–188.
383 Jaidev, R. I. Jafri, A. K. Mishra and S. Ramaprabhu, *J. Mater. Chem.*, 2011, **21**, 17601.
384 S. Saha, P. Samanta, N. C. Murmu and T. Kuila, *J. Energy Storage*, 2018, **17**, 181–202.
385 O. Parlak, Y. Kumar Mishra, A. Grigoriev, M. Mecklenburg, W. Luo, S. Keene, A. Salleo, K. Schulte, R. Ahuja, R. Adelung, A. P. F. Turner and A. Tiwari, *Nano Energy*, 2017, **34**, 570–577.
386 Y. Zhou, X. Wang, L. Acauan, E. Kalfon-Cohen, X. Ni, Y. Stein, K. K. Gleason and B. L. Wardle, *Adv. Mater.*, 2019, e1901916.
387 R. Yi, S. Chen, J. Song, M. L. Gordin, A. Manivannan and D. Wang, *Adv. Funct. Mater.*, 2014, **24**, 7433–7439.
388 K. L. Stano, S. Faraji, R. Hodges, O. Yildiz, B. Wells, H. I. Akyildiz, J. Zhao, J. Jur and P. D. Bradford, *Small*, 2016, **12**, 2432–2438.
389 C. D. Lokhande, D. P. Dubal and O.-S. Joo, *Curr. Appl. Phys.*, 2011, **11**, 255–270.
390 F. Shi, L. Li, X. Wang, C. Gu and J. Tu, *RSC Adv.*, 2014, **4**, 41910–41921.
391 M. Zhi, C. Xiang, J. Li, M. Li and N. Wu, *Nanoscale*, 2013, **5**, 72–88.
392 X. Huang, X. Qi, F. Boey and H. Zhang, *Chem. Soc. Rev.*, 2012, **41**, 666–686.
393 V. Sharma, I. Singh and A. Chandra, *Sci. Rep.*, 2018, **8**, 1307.
394 B. Li, H. Cao, G. Yin, Y. Lu and J. Yin, *J. Mater. Chem.*, 2011, **21**, 10645–10648.
395 L. Chen, Y. Zhang, P. Zhu, F. Zhou, W. Zeng, D. D. Lu, R. Sun and C. Wong, *Sci. Rep.*, 2015, **5**, 9672.
396 M. A. S. M. Haniff, S. M. Hafiz, K. A. Wahid, Z. Endut, M. I. Syono, N. M. Huang, S. A. Rahman and I. A. Azid, *J. Mater. Sci.*, 2017, **52**, 6280–6290.
397 V. Subramanian, S. C. Hall, P. H. Smith and B. Rambabu, *Solid State Ionics*, 2004, **175**, 511–515.
398 X. F. Wang, Z. You and D. B. Ruan, *Chin. J. Chem.*, 2006, **24**, 1126–1132.
399 W. Gong, B. Fugetsu, Z. Wang, I. Sakata, L. Su, X. Zhang, H. Ogata, M. Li, C. Wang, J. Li, J. Ortiz-Medina, M. Terrones and M. Endo, *Commun. Chem.*, 2018, **1**, 16.
400 J. S. Sakamoto and B. Dunn, *J. Electrochem. Soc.*, 2002, **149**, A26.
401 S. Mandal, J. M. Amarilla, J. Ibáñez and J. M. Rojo, *J. Electrochem. Soc.*, 2002, **148**, A24.
402 D. Kalpana, K. S. Omkumar, S. S. Kumar and N. G. Renganathan, *Electrochim. Acta*, 2006, **52**, 1309–1315.
403 H. Wu, S. Lin, C. Chen, W. Liang, X. Liu and H. Yang, *Mater. Res. Bull.*, 2016, **83**, 434–441.
404 G. Du, Y. Li, L. Zhang, X. Wang, P. Liu, Y. Feng and X. Sun, *Mater. Lett.*, 2014, **128**, 242–244.
405 A. Meng, J. Shao, X. Fan, J. Wang and Z. Li, *RSC Adv.*, 2014, **4**, 60300–60305.
406 S. Bi, M. Chen, R. Wang, J. Feng, M. Dinca, A. A. Kornyshev and G. Feng, 2019, **1–19**, arXiv:1903.00279 [cond-mat.mtrl-sci].
407 J. Jiang, Y. Zhang, Y. An, L. Wu, Q. Zhu, H. Dou and X. Zhang, *Small Methods*, 2019, 1900081.
408 J. Chen, B. Yang, H. Hou, H. Li, L. Liu, L. Zhang and X. Yan, *Adv. Energy Mater.*, 2019, **9**, 1803894.
409 J. N. Zhang, P. Liu, L. N. Jin, C. Jin and S. W. Bian, *ChemistrySelect*, 2017, **2**, 8618–8624.
410 R. Paulose and M. Raja, *J. Nanosci. Nanotechnol.*, 2019, **19**, 8151–8156.
411 X. Wang, H. Wei, X. Liu, W. Du, X. Zhao and X. Wang, *Nanotechnology*, 2019, **30**, 325401.
412 W. Huang, A. Zhang, H. Liang, R. Liu, J. Cai, L. Cui and J. Liu, *J. Colloid Interface Sci.*, 2019, **549**, 140–149.
413 B. Liang, Z. Zheng, M. Retana, K. Lu, T. Wood, Y. Ai, X. Zu and W. Zhou, *Nanotechnology*, 2019, **30**, 295401.
414 L.-P. Lv, C. Zhi, Y. Gao, X. Yin, Y. Hu, D. Crespy and Y. Wang, *Nanoscale*, 2019, **11**, 13996–14009.
415 S. Cho, I. Jung, L. Zhang, S. Yoo, J. H. Won, S. B. Jung, L. Liu and S. Park, *Nanotechnology*, 2019, **30**, 425401.
416 Y. Yang, S.-W. Ng, D. Chen, J. Chang, D. Wang, J. Shang, Q. Huang, Y. Deng and Z. Zheng, *Small*, 2019, e1902071.
417 X. Wang, Y. Zhang, J. Zheng, X. Liu and C. Meng, *J. Colloid Interface Sci.*, 2019, **554**, 191–201.
418 B. Zhang, J. Li, F. Liu, T. Wang, Y. Wang, R. Xuan, G. Zhang, R. Sun and C. Wong, *Chem.–Eur. J.*, 2019, **25**, 11715–11724.
419 M. Hu, C. Cui, C. Shi, Z.-S. Wu, J. Yang, R. Cheng, T. Guang, H. Wang, H. Lu and X. Wang, *ACS Nano*, 2019, **13**, 6899–6905.
420 Z. Yang and Z. Chen, *Nanotechnology*, 2019, **30**, 245402.
421 C. Zhang, H. Li, A. Huang, Q. Zhang, K. Rui, H. Lin, G. Sun, J. Zhu, H. Peng and W. Huang, *Small*, 2019, **15**, e1805493.
422 L. Wu, K. Zhang, X. Zhu, S. Cao, D. Niu and X. Feng, *Langmuir*, 2019, **35**, 5125–5129.
423 J. Liu and P. Liu, *J. Colloid Interface Sci.*, 2019, **542**, 1–7.
424 S. Ramesh, K. Karuppasamy, H. M. Yadav, J.-J. Lee, H.-S. Kim, H.-S. Kim and J.-H. Kim, *Sci. Rep.*, 2019, **9**, 6034.
425 U. Kamran, Y. J. Heo, J. W. Lee and S. J. Park, *Micromachines*, 2019, 234.
426 W. Ma, M. Li, X. Zhou, J. Li, Y. Dong and M. Zhu, *ACS Appl. Mater. Interfaces*, 2019, **11**, 9283–9290.
427 B. Cheng, R. Cheng, F. Tan, X. Liu, J. Huo and G. Yue, *Nanoscale Res. Lett.*, 2019, **14**, 66.
428 K. Trzcinski, M. Szkoda, A. P. Nowak, M. Lapinski and A. Lisowska-Oleksiak, *Beilstein J. Nanotechnol.*, 2019, **10**, 483–493.
429 S. C. Dhanabalan, B. Dhanabalan, X. Chen, J. S. Ponraj and H. Zhang, *Nanoscale*, 2019, **11**, 3046–3101.
430 F. Hekmat, S. Shahrokhian and S. Rahimi, *Nanoscale*, 2019, **11**, 2901–2915.
431 M. Manoj, C. Muhamed Ashraf, M. Jasna, K. M. Anilkumar, B. Jinisha, V. S. Pradeep and S. Jayalekshmi, *J. Colloid Interface Sci.*, 2019, **535**, 287–299.

432 Z. Zhang, Z. Yao, Y. Meng, D. Li, Q. Xia and Z. Jiang, *Inorg. Chem.*, 2019, **58**, 1591–1598.
433 H. Li, Z. Li, Z. Wu, M. Sun, S. Han, C. Cai, W. Shen, X. Liu and Y. Fu, *J. Colloid Interface Sci.*, 2019, **549**, 105–113.
434 Z. Tan, G. Chen and Y. Zhu, *Nanocarbons Adv. Energy Storage*, 2015, **1**, 211–225.
435 Y. Kou, Y. Xu, Z. Guo and D. Jiang, *Angew. Chem., Int. Ed.*, 2011, **50**, 8753–8757.
436 A. Izadi-Najafabadi, T. Yamada, D. N. Futaba, M. Yudasaka, H. Takagi, H. Hatori, S. Iijima and K. Hata, *ACS Nano*, 2011, **5**, 811–819.
437 Z. Tang, C. Tang and H. Gong, *Adv. Funct. Mater.*, 2012, **22**, 1272–1278.
438 K. Naoi, W. Naoi, S. Aoyagi, J. Miyamoto and T. Kamino, *Acc. Chem. Res.*, 2013, **46**, 1075–1083.
439 H. C. Chien, W. Y. Cheng, Y. H. Wang and S. Y. Lu, *Adv. Funct. Mater.*, 2012, **22**, 5038–5043.
440 X. Yang, C. Cheng, Y. Wang, L. Qiu and D. Li, *Science*, 2013, **341**, 534–537.
441 L. Mai, H. Li, Y. Zhao, L. Xu, X. Xu, Y. Luo, Z. Zhang, W. Ke, C. Niu and Q. Zhang, *Sci. Rep.*, 2013, **3**, 1718.
442 L. Zhang, F. Zhang, X. Yang, G. Long, Y. Wu, T. Zhang, K. Leng, Y. Huang, Y. Ma, A. Yu and Y. Chen, *Sci. Rep.*, 2013, **3**, 1408.
443 Z. S. Wu, X. Feng and H. M. Cheng, *Natl. Sci. Rev.*, 2014, **1**, 277–292.
444 R. Signorelli, D. C. Ku, J. G. Kassakian and J. E. Schindall, *Proc. IEEE*, 2009, **97**, 1837–1847.
445 C. Wang, M. Osada, Y. Ebina, B. W. Li, K. Akatsuka, K. Fukuda, W. Sugimoto, R. Ma and T. Sasaki, *ACS Nano*, 2014, **8**, 2658–2666.
446 M. F. El-Kady, M. Ihns, M. Li, J. Y. Hwang, M. F. Mousavi, L. Chaney, A. T. Lech and R. B. Kaner, *Proc. Natl. Acad. Sci.*, 2015, **112**, 4233–4238.
447 Z. Peng, J. Lin, R. Ye, E. L. G. Samuel and J. M. Tour, *ACS Appl. Mater. Interfaces*, 2015, **7**, 3414–3419.
448 N. Choudhary, C. Li, H.-S. Chung, J. Moore, J. Thomas and Y. Jung, *ACS Nano*, 2016, **10**, 10726–10735.
449 C. Arbizzani, M. Mastragostino and F. Soavi, *J. Power Sources*, 2001, **100**, 164–170.
450 J. Bowen, H. Seyedsina, C. Hongqi, M. Shiva, N. T. Nguyen, Y. Min, A. Marco and S. Patrik, *Appl. Mater. Today*, 2019, **17**, 227–235.
451 S. García-Dalí, J. I. Paredes, J. M. Munuera, S. Villar-Rodil, A. Adawy, A. Martínez-Alonso and J. M. D. Tascón, *ACS Appl. Mater. Interfaces*, 2019, **0**, acsami.9b13484.
452 M. Zhou, Y. Li, Q. Gong, Z. Xia, Y. Yang, X. Liu, J. Wang and Q. Gao, *ChemElectroChem*, 2019, **6**, 4595–4607.
453 D. Shin, H. Hwang, T. Yeo, S. Park, T. Kim, J. Lee and W. Choi, *Carbon*, 2019, **152**, 746–754.
454 Y.-R. Son and S.-J. Park, *Chem. Eng. J.*, 2019, **373**, 1020–1029.
455 N. Du, L. Gong, L. Fan, K. Yu, H. Luo, S. Pang, J. Gao, Z. Zheng, J. Lv and B. Zhou, *ACS Appl. Nano Mater.*, 2019, **2**, 3039–3049.
456 K. Lei, J. Ling, J. Zhou, H. Zou, W. Yang and S. Chen, *Mater. Res. Bull.*, 2019, **116**, 59–66.
457 M. Hong, C. Zhou, S. Xu, X. Ye, Z. Yang, L. Zhang, Z. Zhou, N. Hu and Y. Zhang, *J. Power Sources*, 2019, **423**, 80–89.
458 T. Yeo, J. Lee, D. Shin, S. Park, H. Hwang and W. Choi, *J. Mater. Chem. A*, 2019, **7**, 9004–9018.
459 L. Wang, C. Zhang, X. Jiao and Z. Yuan, *Nano Res.*, 2019, **12**, 1129–1137.
460 P. Avasthi, A. Kumar and V. Balakrishnan, *ACS Appl. Nano Mater.*, 2019, **2**, 1484–1495.
461 P. Avasthi and V. Balakrishnan, *Adv. Mater. Interfaces*, 2019, **6**, 1801842.
462 F. Hekmat, H. Hosseini, S. Shahrokhian and H. E. Unalan, *Energy Storage Mater.*, DOI: 10.1016/j.ensm.2019.09.022.
463 P. He, Z. Ding, X. Zhao, J. Liu, Q. Huang, J. Peng and L.-Z. Fan, *Carbon*, 2019, **155**, 453–461.
464 F. Song, D. Huo, J. Hu, H. Huang, J. Yuan, J. Shen and A.-J. Wang, *Nanotechnology*, 2019, **30**, 505401.
465 D. Xia, J. Quan, G. Wu, X. Liu, Z. Zhang, H. Ji, D. Chen, L. Zhang, Y. Wang, S. Yi, Y. Zhou, Y. Gao and R. Jin, *Nanomaterials*, 2019, **9**, 1225.
466 S. Chandra Sekhar, G. Nagaraju, B. Ramulu, S. K. Hussain, D. Narsimulu and J. S. Yu, *Nano Res.*, 2019, **12**, 2597–2608.
467 W. Gong, B. Fugetsu, Z. Wang, T. Ueki, I. Sakata, H. Ogata, F. Han, M. Li, L. Su, X. Zhang, M. Terrones and M. Endo, *Carbon*, 2019, **154**, 169–177.
468 J. Liu, T. Xiong, T. Liu, C. Yang, H. Jiang and X. Li, *Electrochim. Acta*, 2019, **320**, 134627.
469 L. Xia, X. Li, Y. Wu, S. Hu, Y. Liao, L. Huang, Y. Qing and X. Lu, *Chem. Eng. J.*, 2020, **379**, 122325.
470 Z. Zhang, Z. Xu, Z. Yao, Y. Meng, Q. Xia, D. Li and Z. Jiang, *J. Alloys Compd.*, 2019, **805**, 396–403.
471 J. Chen, *Int. J. Electrochem. Sci.*, 2019, 7293–7302.
472 P. Liu, Q. Ru, P. Zheng, Z. Shi, Y. Liu, C. Su, X. Hou, S. Su and F. Chi-Chung Ling, *Chem. Eng. J.*, 2019, **374**, 29–38.
473 P. Simon and Y. Gogotsi, *Nat. Mater.*, 2008, **7**, 845–854.
474 Battery UniversityTM sponsored by Cadex Electronics Inc., Copyr. ©2003–2018 Cadex Electron. Inc.
475 R. R. Salunkhe, Y. Kamachi, N. L. Torad, S. M. Hwang, Z. Sun, S. X. Dou, J. H. Kim and Y. Yamauchi, *J. Mater. Chem. A*, 2014, **2**, 19848–19854.
476 Z. Yu, L. Tetard, L. Zhai and J. Thomas, *Energy Environ. Sci.*, 2015, **8**, 702–730.
477 C. Péan, C. Merlet, B. Rotenberg, P. A. Madden, P. L. Taberna, B. Daffos, M. Salanne and P. Simon, *ACS Nano*, 2014, **8**, 1576–1583.
478 T. Sekino, *Inorganic and Metallic Nanotubular Materials*, Springer Berlin Heidelberg, Berlin, Heidelberg, 2010, vol. 117.
479 M. Carbone, L. Gorton and R. Antiochia, *Electroanalysis*, 2015.
480 A. Schuchardt, T. Braniste, Y. K. Mishra, M. Deng, M. Mecklenburg, M. A. Stevens-Kalceff, S. Raevschi, K. Schulte, L. Kienle, R. Adelung and I. Tiginyanu, *Sci. Rep.*, 2015, **5**, 8839.
481 S. Garlof, M. Mecklenburg, D. Smazna, Y. K. Mishra, R. Adelung, K. Schulte and B. Fiedler, *Carbon*, 2017, **111**, 103–112.

